Nanoparticles delivery to the central nervous system in-vivo: PVP nanoparticles for brain drug delivery and neuroprotection with siRNA-caspase-3

Thesis

for the degree of

doctor rerum naturalum (Dr. rer. nat.)

approved by the Faculty of Natural Sciences of Otto von Guericke University Magdeburg

by BSc, Dipl.-Pharm. Mohamed Tawfik

born on 27.06.1990 in Cairo

Examiner: Prof. Dr. Bernhard A Sabel

Prof. Dr. Hagen von Briesen

submitted on: 17.09.2020

defended on: 06.05.2021

Abstract

Neurological disorders are on the rise and they represent the second largest category of life-threatening diseases. Although significant achievements have been attained in the brain anatomy and pathology, many potential drug treatments aimed at the central nervous system (CNS)' diseases are limited in their ability to improve clinical outcomes. This is due to the blood-neural barriers, such as the blood-brain barrier (BBB), which separates the vascular system from the CNS parenchyma. But functionalized nanoparticles have successfully overcome these barriers, offering new strategies for brain drug delivery when loaded with diagnostic or therapeutic agents. However, none has achieved the market approval to date. At the same time, neuronal cell death (apoptosis) after a CNS trauma is problematic, because post-apoptosis induces irreversible neuronal damage. Hence, an important objective is to prevent or stop the apoptosis process to protect the lesioned neurons from dying. In the same context, siRNA-based gene therapy holds a great promise to induce neuroprotection by targeting the genes responsible for the execution of the apoptosis process. Yet, siRNA-based therapies are mainly devoted for the treatment of liver diseases and few authors studied it for neuroprotection *in-vivo*.

In this study I investigated two polymeric nano-carriers platform to target the CNS. The first was to study functionalized polyvinylpyrrolidone nanoparticles (PVP-NPs) to cross the blood-retina barrier (BRB)- which can reflect the situation at the BBB- using a rat model of *in-vivo* imaging of the retina. The second was to study the poly (butyl-cyanoacrylate) nanoparticles (PBCA NPs) as nano-carriers for caspase-3-siRNA for delivery to the retina and investigate its ability *in-vivo* to stop the apoptosis of retinal ganglion cells after damage using *in-vivo* imaging to the retina.

PVP NPs were loaded with hydrophobic fluorescent markers (Dil and FITC) as a surrogate for hydrophobic drugs and injected intravenously into the tail vein of rats. PVP-Dil-CFSE NPs had a particle size of 344 nm, a polydispersity index (PDI) of 0.26 and a negative zeta potential of -15 mv. My results indicate that linking the hydrophobic fluorescence marker (Carboxyfluorescein-succinimidyl-ester) CFSE to the surface of the PVP NPs can induce their passage into the retina tissue. In addition, I observed a substantial internalization of the modified NPs into blood cells which was revealed by the *ex-vivo* wholemount retina imaging.

On the other hand, caspase-3 siRNA encapsulated in PBCA NPs (CaspNPs) was produced with a particle size of 143 nm, a polydispersity index (PDI) of 0.26 and a negative zeta potential of -9.87 mv. Specification of blank PBCA NPs was 124.08 nm, 0.26 PDI and -11.96 mv. To test the effects *in-vivo*, a rat optic nerve crush (ONC) model was employed in

this study. Lesioned cells were treated with CaspNPs and blank PBCA NPs which were delivered into the eye by intravitreal injection. Longitudinal, repeated retinal ganglion cell counts using confocal neuroimaging showed that post-traumatic cell loss after CaspNPs injection was only 36.1% versus 63.4% in controls.

In sum, the results of the first study indicate PVP NPs to be a potential new nano-carrier platform to target the brain while hidden in the blood cells. The second study results suggest that CaspNPs can serve as a potential therapeutic tool to reduce/stop neurons cell death, which may be valuable for neuroprotection or neuromodulation of central nervous system dysfunction in neurological disorders. Though my *in-vivo* experiments with rats show promising results that NPs can deliver drugs and genes to the CNS, more pre-clinical and clinical studies are needed to verify these conclusions.

Zusammenfassung

Neurologische Erkrankungen nehmen zu und stellen die zweitgrößte Kategorie der lebensbedrohlichen Krankheiten dar. Obwohl auf dem Gebiet der Anatomie und Pathologie des Gehirns bedeutende Entwicklungsfortschritte erzielt wurden, sind viele potenzielle medikamentöse Behandlungen von Erkrankungen des Zentralnervensystems (ZNS) in ihrer Eignung begrenzt, die klinischen Ergebnisse zu verbessern. Dies ist auf Blut-neurale Barrieren zurückzuführen, wie z.B. die Blut-Hirn-Schranke (BHS), die das Gefäßsystem vom ZNS-Parenchym trennt.

Funktionalisierte Nanopartikel haben diese Barrieren jedoch erfolgreich überwunden und bieten neue Strategien für die Verabreichung von Medikamenten in das Gehirn, wenn sie mit Diagnostika/Therapeutika beladen sind. Bislang hat jedoch noch kein Arzneimittel mit Nanopartikeln die Marktzulassung erreicht. Außerdem ist der neuronale Zelltod (Apoptose) nach einem ZNS-Trauma problematisch, da die Post-Apoptose irreversible, neuronale Schäden induziert. Ein wichtiges Ziel ist es daher, den Apoptoseprozess zu verhindern oder zu stoppen, um die geschädigten Nervenzellen vor dem Absterben zu bewahren. In diesem Kontext hat die siRNA-basierte Gentherapie ein großes Potenzial zur Induktion von Neuroprotektion, indem sie auf Gene abzielt, die für Apoptoseprozesse verantwortlich sind. Allerdings werden siRNA-basierte Therapien hauptsächlich für die Behandlung von Lebererkrankungen eingesetzt und nicht für die *in-vivo* Neuroprotektion.

Im Rahmen dieser Arbeit wurden zwei polymere Nano-Trägerplattformen mit dem Ziel untersucht, das ZNS zu erreichen. Ziel der ersten Studie war zunächst, funktionalisierte Polyvinylpyrrolidon-Nanopartikel (PVP-NPs) zur Überwindung der Blut-Retina-Schranke - die die Situation an der BHS widerspiegelt - anhand eines Rattenmodells für die in-vivo-Netzhautdarstellung untersucht. In der zweiten Studie wurden Poly(butylcyanoacrylat)-Nanopartikel (PBCA-NPs) als Nanocarrier für die Verabreichung von Caspase-3-siRNA in der in vivo Retina untersucht. Ziel dieses Ansatzes war es, die Apoptose von retinalen Ganglienzellen nach Schädigung durch in vivo Bildgebung der Netzhaut zu hemmen.

PVP-NPs wurden mit hydrophoben Fluoreszenzmarkern (Dil und FITC) als Surrogat für hydrophobe Medikamente beladen und intravenös in die Schwanzvene von Ratten injiziert. PVP-Dil-CFSE-NPs hatten eine Partikelgröße von 344 nm und ein negatives Zetapotential von -15 mv. Die Ergebnisse des Experiments deuten darauf hin, dass die Bindung des hydrophoben Fluoreszenzmarkers (Carboxyfluoresceinsuccinimidylester) CFSE an die Oberfläche von PVP-NPs ihre Passage in das retinale Gewebe induzieren kann. Darüber hinaus wurde eine signifikante Internalisierung der modifizierten NPs in Blutzellen beobachtet. Diese wurden durch eine ex-vivo Ganzkörper-Retina-Visualisierung sichtbar gemacht.

Andererseits wurde in PBCA NPs (CaspNPs) verkapselte Caspase-3 siRNA mit einer Partikelgröße von 143 nm, einem Polydispersitätsindex (PDI) von 0,26 und einem negativen Zetapotential von -9,87 mv produziert. Die Spezifikation der leeren PBCA-NPs betrug 124,08 nm, 0,26 PDI und -11,96 mv.

Um die Auswirkungen *in-vivo* zu testen, wurde in dieser Studie ein Modell zur Quetschung des Sehnervs der Ratte (ONC) verwendet. Lädierte Zellen wurden entweder mit CaspNPs oder mit leeren PBCA-NPs behandelt, die durch intravitreale Injektion in das Auge eingebracht worden waren. Wiederholte Zählungen der retinalen Ganglienzellen durch konfokales Neuroimaging hat ergeben, dass der posttraumatische Zellverlust nach der CaspNPs-Injektion nur 36,1 % betrug gegenüber 63,4% bei den Kontrollgruppen.

Zusammenfassend kann festgestellt werden, dass PVP NPs eine potentielle Nano-Carrier-Plattform darstellen, die es ermöglicht, das Gehirn getarnt durch Blutzellen zu erreichen. Die Ergebnisse der zweiten Studie deuten darauf hin, dass CaspNPs als potenzielles therapeutisches Mittel zur Verringerung des Zelltods von Neuronen der Retina dienen können, was neue Perspektiven für die Neuroprotektion oder Neuromodulation von Funktionsstörungen des Zentralnervensystems bei neurologischen Erkrankungen eröffnet.

Obwohl die vivo-Experimente mit Ratten vielversprechende Beweise dafür liefern, dass NPs Medikamente und Gene in das ZNS transportieren können, sind weitere präklinische und klinische Studien notwendig, um diese Ergebnisse zu verifizieren.

Table of Contents

List of abbreviations

AIF	Apoptosis inducing factor
APAF1	Apoptotic protease activating factor 1
ATP/dATP	Deoxyadenosine triphosphate
AGO2	Argonaute RISC catalytic component 2
BBB	Blood-brain barrier
Bcl-2	B-cell lymphoma 2
BCRP	ATP-binding cassette super-family G member 2
BCSFB	Blood-cerebrospinal fluid barrier
BRB	Blood-retina barrier
CaspNPs	Caspase-3 siRNA loaded poly (butyl cyanoacrylate) nanoparticles
CNS	Central nervous system
CSF	Cerebrospinal fluid
DISC	Death-inducing signaling complex
DNA	Deoxyribonucleic acid
dsRNA	Double-stranded RNA
ECF	Extracellular fluid
FadD	Fas-associated protein with death domain
Fasl	First apoptosis signal ligand
FDA	Food and drug administration
GLUT1	Glucose transporter 1
ICON	*In-vivo* confocal neuroimaging
IOP	Intraocular pressure
ISF	Interstitial fluid
LAT1	Large neutral amino acid transporter
Ldopa	Levodopa
MDR1	Multidrug resistance protein 1

miRNA	microRNA
mRNA	messenger RNA
ONC	Optic nerve crush
PACA	Poly (alkyl-cyanoacrylate)
PBCA	Poly (butyl-cyanoacrylate)
PBS	Phosphate-buffered saline
PEG	Polyethylene glycol
PLA	Polylactic acid
PLGA	Poly (lactic-co-glycolic acid)
PVP	Poly-vinyl-pyrrolidone
RES	Reticuloendothelial system
RGCs	Retinal ganglion cells
RISC	RNA-induced silencing complex
RNS	Reactive nitric species
ROS	Reactive oxygen species
RPE	Retinal pigment epithelium
shRNA	short hairpin RNA
siRNA	small interfering RNA
SLNs	Solid lipid nanoparticles
SMAC	Second mitochondria-derived activator of caspases
TEM	Transmission electron microscopy
TFR	Transferrin receptor
TNF-α	Tumor necrosis factor

List of figures and tables

1. General introduction

Central nervous system studies are the frontline of the medical research because for most pathologies successful therapies are missing. Even with the numerous studies performed to achieve an efficient treatment for CNS diseases such Alzheimer's, traumatic brain injury and retinal diseases, hardly any effective treatment has been developed yet. This could be attributed to two main obstacles. Firstly, the programmed cell death / "apoptosis" (from the Greek, falling away) and secondly the blood-neural barriers. Apoptosis is a genetically regulated mechanism which is homeostatic and vital to the development and maintenance of tissues and organs' functions. However, imbalance in apoptosis is associated with different pathologies such as cancer, neurodegenerative diseases and neurodegenerative diseases neurodegenerative diseases (1). Moreover, apoptosis can have devastating consequences when it affects CNS neurons, as they hardly regenerate, and they are lost irreversibly. For example, a trauma in the optic nerve may lead to retinal ganglion cell (RGC) death, and patients suffer from the vision deterioration acutely as well as chronically (2). In this context - as the apoptosis depends on gene expression - gene therapy could be an approach to inhibit neuronal cell death. siRNA is a common therapeutic tool for gene therapy used for its high efficacy and specificity in gene silencing. Hence, siRNA that blocks caspase-3, a key molecule that induces apoptosis, could be used to achieve neuroprotective effect on injured neurons by silencing the gene expression responsible for neuronal apoptosis (3). siRNA cause a gene silencing effect called RNA interference which was discovered in 1998 (4). To date, different siRNA products have been synthesized and applied for gene therapy (5). Still, the current gene therapy approaches possess some disadvantages such as: unwanted gene expression, poor therapeutic effect and the innate immune response if the used carrier is a virus (6). Therefore, there is a need for a carrier to load the siRNA, protect it from premature degradation and overcome these limitations (7). The second main obstacle for CNS therapy is the blood-neural barriers. Most widely known is the blood-brain barrier (BBB) which is an unsurmountable barrier that separates the blood circulation from the cerebral parenchyma preventing 98% of drugs from penetrating the brain to protect CNS tissue, halt neuronal degeneration or to restore brain function (8). Nano-carriers with specific surface modifications have attained a great success in this context by crossing the blood-neural barriers, including the BBB or the blood-retina barrier (BRB), because they can deliver drugs (nucleic acids and macromolecules) to the brain tissues (9,10). This was accomplished using different types of nanoparticles, such as organic NPs like liposomes, PBCA and chitosan, or inorganic NPs such as gold and magnetic NPs (11,12). However, no nanoparticulate system for the treatment of CNS disorders to achieve neuroprotection have reached the drug market. Therefore, the discovery of new nanoparticles to cross the BBB will increase the chance to obtain a new universal nano carrier which can deliver

drugs to the CNS, efficiently and safely. As aforementioned, the finding of siRNA loaded nanoparticles to inhibit post-mitotic neuronal apoptosis, would also be an opportunity to find a new therapy for neurodegenerative diseases.

In light of these considerations, I have conducted two studies using two different kinds of polymeric NPs to target the CNS. The first was to investigate the ability of the new poly-vinyl-pyrrolidone nanoparticles (PVP NPs) to pass the BRB which is a surrogate model for the BBB and to study the pharmacokinetics and distribution of the BRB passage using the *in-vivo* confocal neuroimaging (ICON). The second was to observe the anti-apoptosis effect induced by caspase-3 siRNA-PBCA (polybutyl-cyanoacrylate) NPs on retinal ganglion cells' (RGCs) survival for more than a month post optic nerve crush (ONC) using ICON as well.

As the following sections show, the study builds upon a large body of prior technological state of the art, the elements of which are now discussed.

2. Technology state of the art

2.1. Gene therapy

Basically, gene therapy arose as a potential solution few decades ago to replace, repair or regulate genes to treat inherited or acquired diseases (13). It is a disease treatment approach to deliver exogenous nucleic acids into the body to encode/inhibit specific gene expression and manipulate cellular signaling pathways (14). Current therapeutic nucleic acids used for this approach are DNA, miRNA, mRNA, shRNA, antisense oligonucleotides and siRNA. This approach has become easier after the completion of the human genome project to better understand the genetic roots of many different diseases such as cancer and Morbus Parkinson. Thus, gene therapy could offer higher therapeutic potential rather than the current two major structural classes of FDA approved drugs i.e., small molecules and proteins (15-20). The history of gene therapy can be tracked to 1953 when the DNA structure was defined (21). Afterwards, since 1989, many clinical trials of gene therapy have been conducted (22). However, the success was delayed because extracellular and intracellular barriers exist which are a problem for nucleic acids, the problems of targeting specific cells, endosomal escape and serum stability (23). Thereafter, viral vectors appeared as a solution to overcome the mentioned barriers, but this approach is not favored due to their major drawbacks such as toxicity, limited capacity to load nucleic acids and immunogenicity (24,25). Therefore, researchers also shifted towards the usage of liposomes and polymeric carriers instead due to the advantages they could offer regarding the safety, higher loading capacity into nanoscale and, finally, protecting the loaded nucleic acid from degradation. Nevertheless, none has passed the clinical trial stages for the treatment of neurological disorders (26-28).

2.1.1. Ribonucleic acid

Deoxyribonucleic acids (DNA) and ribonucleic acids (RNA) are holders of genetic information. Ribonucleotide is the basic unit of RNA, which consists of a ribose, a nitrogenous base and a phosphate group. When polymerizing each other via phosphodiester bond, ribonucleotides are turned into an RNA strand (Fig. 1). Unlike the other bio-macromolecules, such as proteins and carbohydrates, RNA has the ability to process genetic information because of the different nitrogenous bases: A, G, C, and U in each ribonucleotide (adenine, guanine, cytosine and uracil), respectively.

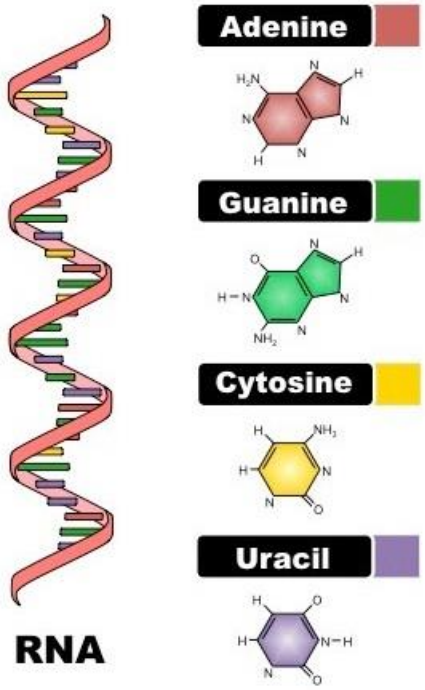

Fig. 1: the structure of RNA. Left: There are 4 types of nitrogenous base for ribonucleotide: adenine (A), guanine (G), cytosine (C) and uracil (U); Right: Their correspondent chemical structures. Taken from reference (29).

According to the base pair complementarity principle, these ribonucleotides are grouped together following their DNA template. The step is called “transcription”, where the RNA is synthesized using a DNA template in the nucleus. This is achieved by gathering and recording the genetic information by the coding sequence from these nitrogenous bases. The subsequent step is termed “translation”. Here the RNA containing the genetic information - named messenger RNA (mRNA) - is delivered from nucleus to ribosome, which is the site of protein synthesis in the cytoplasm. Finally, the whole process which synthesizes a protein according to its DNA template is called “gene expression”. RNA is essential in nature for the synthesis of proteins. It is not just a carrier of genetic information as described above but also a manager of the gene expression (30-32).

2.1.2. RNA interference

RNA interference was discovered first by Fire and Mello in 1998. They found that at the protein production process, a tuning at post-transcription level has a potential as the mRNA can be intervened before binding to ribosomes in the cytoplasm. This was elaborated by silencing the par-1 gene expression using double-stranded RNA (dsRNA) (4). Thereafter, Elbashir et al. proved the

ability to silence a specific fragment of a gene using small interfering RNA (siRNA) (33) and diverse modifications of siRNA have been attained for a variety of genes to silence (34).

Twenty years after the work of Fire and Mello, the RNA interference mechanism is now better understood. Briefly, RNAi is an essential path in eukaryotic cells, in which specific siRNA can target and then split the complementary mRNA. Principally, the double stranded RNA (dsRNA), whether exogenous or endogenous, is processed by a ribonuclease (RNase) III-like enzyme called DICER to smaller molecules in the cytoplasm. This small dsRNA molecule is the siRNA made of 21-23 nucleotides long. Every siRNA then interacts with RNA-induced silencing complex (RISC) which will separate the double stranded siRNA resulting into two siRNAs different strands called passenger (or sense) and guide (or antisense) strand. The passenger strand is the cleaved by the endonuclease argonaute 2 (AGO2) enzymes while the guide strand complementary to target messenger RNA (mRNA) remains with RISC. The guide strand then pairs fully with the mRNA and degrades it to small fragments achieving the post transcriptional gene silencing (knock-down effect) (35,36). (Fig. 2)

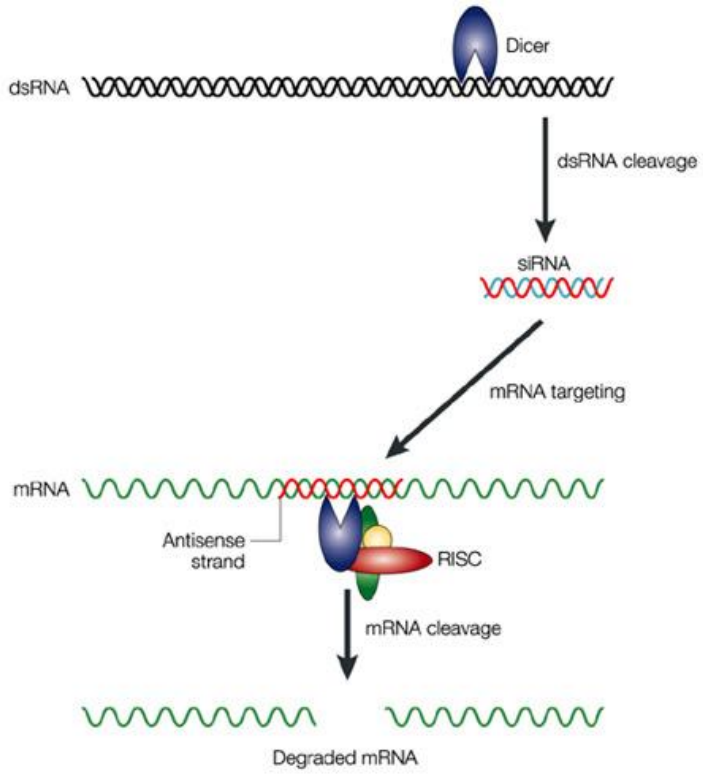

Fig. 2: Scheme of RNA interference. dsRNA chains are cut by Dicer resulting into siRNAs. The antisense strand of the siRNA is used by an RNA-induced silencing complex (RISC) to guide messenger RNA (mRNA) cleavage, promoting mRNA degradation. Consequently, protein expression is terminated. Taken from reference (37).

2.2. Apoptosis

Apoptosis is one of the main mechanisms leading to neuronal death after central nervous system damage. It is a unique mode of "Programmed Cell Death", which was first discovered in 1972 (38). It was described as a natural process to guide cell death in processes of development, degeneration, and regeneration in the mammalian body (39). Mainly, it is needed to preserve the size and function of proliferative tissues in parallel with the death of older cells to make a space for new cells (40). The distinctive biochemical sequence and morphological change permit the cells' death without affecting its neighbors. However, inappropriate regulation of this process can lead to different diseases (41,42). For example, resistance of cells to apoptosis could be the reason behind many types of cancers. Concerning the morphology, a lack of cell swelling accompanied with preservation of organelles (endoplasmic reticulum and mitochondria) is typical. This is different from the other main forms of cell death called necrosis, where cell organelles swell and lysis of plasma membrane can be observed. Because the neurons' death is the primary feature of neurogenerative diseases and as neurons will not be replaced, their loss is usually associated with irreversible functional damage. Cell death can be caused by different factors such as misfolded proteins, reactive oxygen species (ROS) and reactive nitrogen species (RNS), calcium entry and death receptor activation (43-47). The apoptotic response is launched by two pathways: intrinsic (mitochondrial) and extrinsic (death receptor). The intrinsic pathway is activated by the mitochondria. Consequently, different proteins are released from the mitochondria to the cytoplasm. These proteins include: Cytochrome C, SMAC, DIABLO and AIF. Cytochrome C could be the most famous and special one of these proteins which binds to and activates the protein APAF1 leading to the binding of APAF1 to ATP/dATP forming the apoptosome which activate in turn caspase-9 triggering a cascade of caspase activation.

The extrinsic pathway happens when an extracellular death ligand such FasL binds to its death receptor, such as Fas, which then leads to recruitment of more cytosolic factors such as FADD ad caspase-8 resulting into the formation of DISC. Afterwards, caspase-8 is activated which in turn activates caspase-3 (48). Hence, it is logical to describe the caspase family, as the crucial family for apoptosis induction. The caspase family is divided into two sub groups: the initiators caspases including caspase 1,2,4,5,8,9,10,11 and 12 which activates the executioner caspases 3,6,7 and 14. However, not all of them are involved in the apoptosis process and have some other tasks such as immune regulation and spermatogenesis. Still, caspase-3 is the main executor of the apoptosis mechanism as it is present at the last step in both pathways (49,50) (Fig. 3). The relevance of caspase-3 in neuroscience is most obvious, as it is a problem in many neurodegenerative diseases such as brain stroke, focal cerebral

ischemia, Alzheimer's or glaucoma (51-55). As these diseases affect the CNS, the next section will discuss the CNS anatomy and physiology.

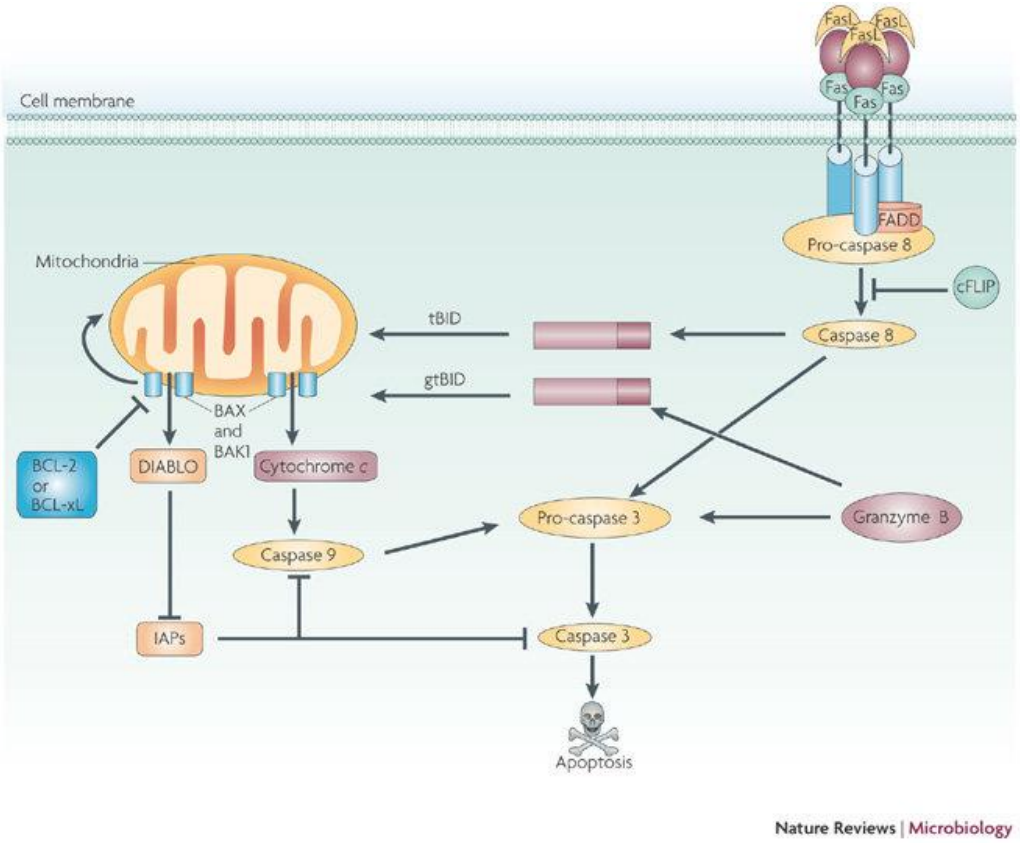

Fig. 3: Caspase dependent apoptosis. Apoptosis initiated by both intrinsic and extrinsic pathways. Different proteins are interacting in both two pathways. No matter what the pathway is, caspase-3 is the apoptosis executor. Taken from reference (56).

2.3. The central nervous system

The central nervous system consists of the brain and the spinal cord. They are the control centers of the body, which organize sensory input and motor output while integrating the activities of the peripheral organs and tissues. Neurons are the primary components cells of the CNS. They use chemical and electrical signals for communication. To achieve this, accurate ionic movements across their membranes is needed. This is a censorious step specially at central synapses using all-or-none action potentials. Moreover, this accurate mechanism is called homeostasis, which is very critical for neuronal signaling and integration inside the CNS environment. The CNS complex structure is separated from the blood by cellular barriers. These barriers exist at the interfaces between the blood and the CNS parenchyma. They act as restrictive sites, which control the ion and molecular flux inside and outside the CNS. Meanwhile, the resident cells of the CNS such as neurons, the macroglia

(astrocytes and oligodendrocytes) and microglia participate in the regulation of the production of the interstitial and extracellular fluid (ISF, ECF). The ionic and molecular flux controlled by the CNS barriers covers the passage of mandatory nutrients from the blood to the CNS tissues, removal of waste products and prohibiting the entry of possible toxic agents or pathogens (57-60). There are five CNS barrier sites which can be recognized: the endothelium of the brain micro vessels or the blood-brain barrier (BBB), the choroid plexus epithelium which secrete the cerebrospinal fluid (CSF) into the cerebral ventricles and the epithelium of the arachnoid matter. Both the choroid plexus and the arachnoid together form the blood-CSF barrier (BCSFB). The blood-retinal barrier (BRB) separates the blood from the retina tissue and possess tight junctions between the retinal pigment epithelium cells and retinal capillary endothelial cells. The blood-spinal cord barrier (BSCB) consists of differentiated micro-vessels enclosed by pericytes and astrocytic end feet and finally, the arachnoid barrier. All together with a variable degree of permeability form what is called the blood-neural barriers (BNBs) (61-63). (Fig. 4)

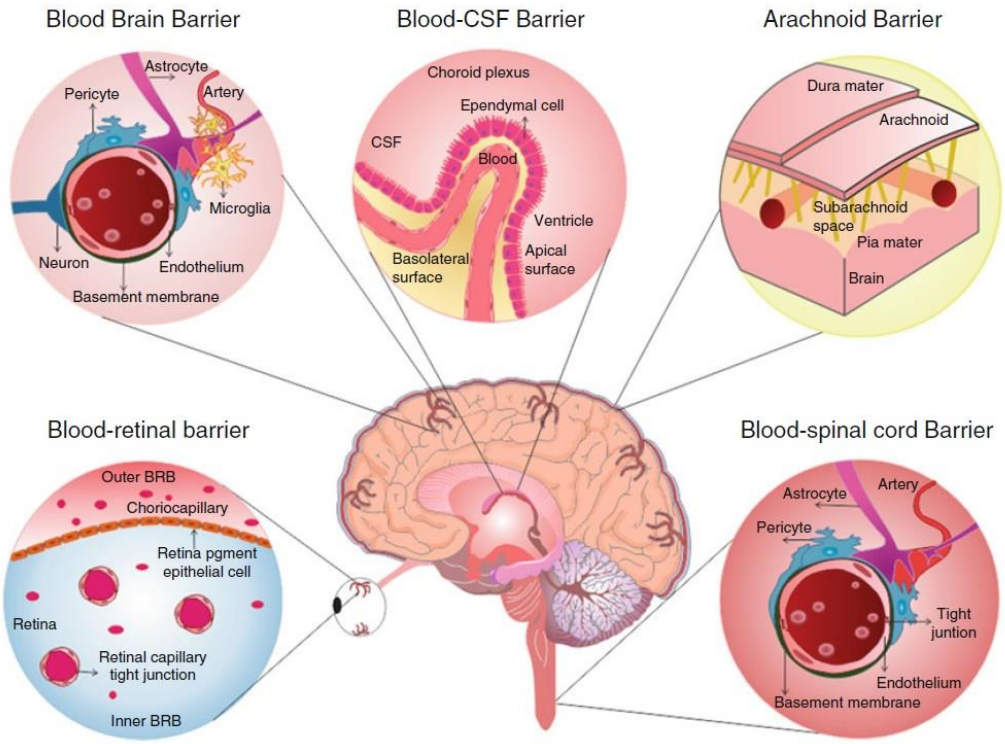

Fig. 4: BNBs at different sites in the brain including the blood-brain barrier, blood-CSF barrier, blood-retinal barrier, blood-spinal cord barrier and arachnoid barrier. Taken from reference (61).

2.3.1. The blood-brain barrier

In 1885, Paul Ehrlich discovered the blood-brain barrier. After injecting intravenously dyes into research animals, he found that all organs were stained except the brain. In contrast, when injected locally into the brain, successful staining was achieved. During the following 100 years, researchers have actively worked to unravel the biological mechanisms that underline the BBB. So far, the most studied and investigated barrier among the BNBs is the BBB. This is due to its capillary's length (650 km) and large surface area (20 m^2) where the main site for molecular exchange and the target of drug delivery happens. Because its complex structure and restricted passage across it, BBB also represents the major drawback against the development of CNS drugs, which can explain the failure of CNS disorders treatment despite the presence of traditional therapies. The BBB is present at the choroid plexus epithelium and controls the molecular exchange between the blood and the CSF. It consists of tight junctions of endothelial cells, astrocytes end feet at the basal lamina, the capillary basement membrane, pericytes in the abluminal side of the endothelial cell between the capillary wall and astrocyte end feet. Tight junctions are non-fenestrated, made of proteins such as occludin and claudins and they exhibit a high electrical resistance with a specialized transport system. The promoted electrical resistance of the tight junctions between the endothelial cells was found to be 1500-2000 Ω cm^2 in the brain while it is only 3.3 Ω cm^2 in other body tissues. Consequently, BBB prohibits the passage of 98% of molecules and 100% of macromolecules (64-68). (Fig. 5)

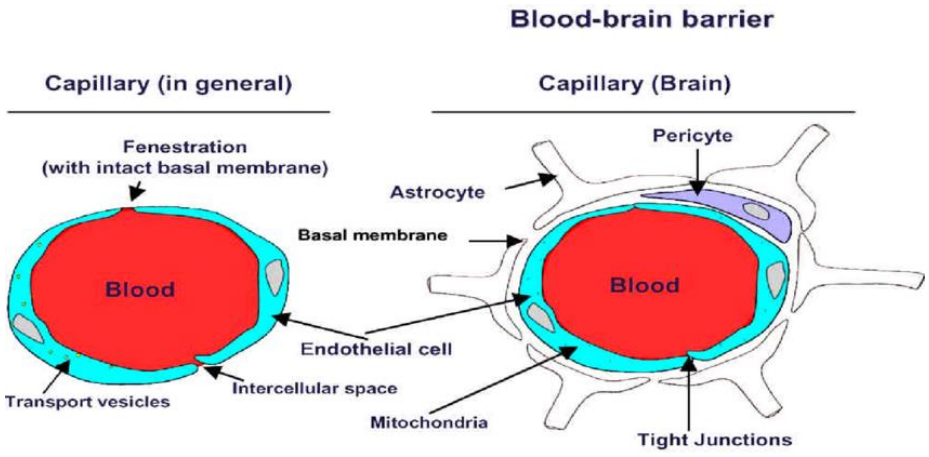

Fig. 5: Difference between capillaries from peripheral organs (left) and brain capillary endothelial cells that build blood brain barrier (right). Taken from reference (69).

2.3.2. Passage mechanisms of the BBB

As a matter of fact, only lipophilic molecules < 500 Da could pass the BBB. On the other hand, the BBB prevents the passage of large sized hydrophilic drugs such as peptides and antibiotics. Nevertheless, the BBB still facilitates the passage of essential endogenous compounds in order to maintain the brain homeostasis using different transport mechanisms which can be used for the development of strategies for drug delivery. Small molecules such as O_2 and CO_2 which are lipophilic and have a small molecular weight and a low protein binding are transported by passive transport mechanism. Active transport mechanisms include transport mediated transcytosis and receptor mediated endocytosis. The former is responsible for the influx of small hydrophilic compounds through a carrier situated on the endothelial cell membranes. For example, glucose binds to its carrier GLUT1 and amino acid binds to its carrier which is LAT1. The latter is responsible for the transport of transferrin, insulin and lipoprotein. This is achieved by binding to the receptors on the endothelial cell's membrane such as TfR for transferrin. The other mechanism to allow BBB passage is called adsorptive endocytosis. This mechanism happens by the interaction between a ligand such as a macromolecule or protein and the cell surface. This is initiated by an electrostatic interaction between the positive charge of the ligand and the plasma membrane negative charge. Moreover, active efflux transporters exist in the BBB such P-glycoprotein, also known as MDR1 and BCRP. Their task is to control the efflux of metabolites and hydrophobic molecules from the brain back to the blood circulation, explaining why many therapeutics have previously failed to pass the BBB and why the current strategies for brain drug delivery are inefficient (70-74). (Fig. 6)

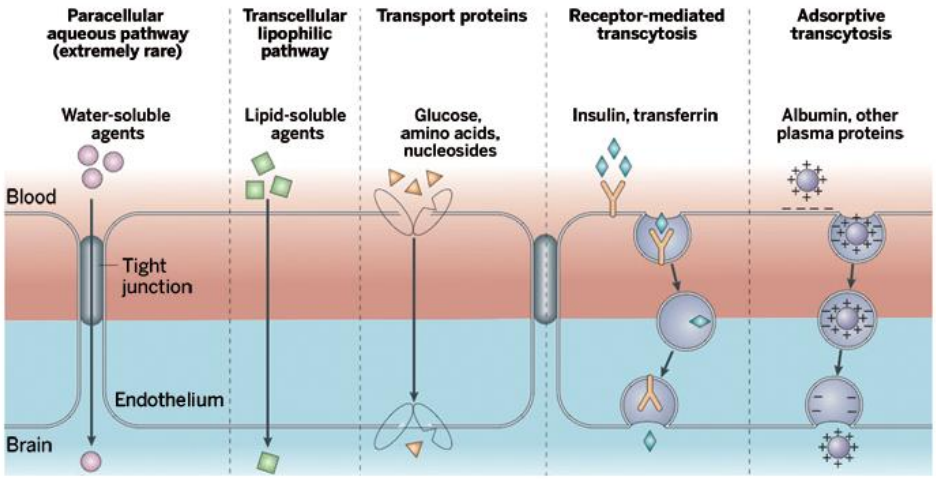

Fig. 6: Schematic representation of transport mechanisms at the BBB site for endogenous and/or exogenous substrates. 1) Some small hydrophilic molecules can be transported via paracellular route 2) transcellular pathway: Lipid-soluble small substrates are able to diffuse across the membrane. 3) Transport protein or Carrier-mediated transport machineries (e.g., Lat1) are responsible for small endogenous molecules. 4) Receptor-mediated endocytosis/transcytosis where larger molecules (e.g., Ins-R=Insulin receptor) are transported using vesicular trafficking towards the brain parenchyma. 5) Adsorptive-mediated endocytosis/transcytosis where large proteins (e.g., albumin) are transported across the BBB. Taken from reference (75).

2.3.3. Brain drug delivery

Principally, there are two strategies to deliver drugs across the BBB, which are, invasive and non-invasive. Invasive techniques such as opening the BBB using a hyperosmotic solution like 25% mannitol by an intra-arterial injection which results in opening the tight junctions for few hours, but it also can cause seizures, bradycardia and hypotension. Another strategy is the direct injection of the drug to the brain parenchyma or to the CSF filled lateral ventricle of the brain using an intracerebral or intracerebroventricular injection, respectively. Because the opening of the skull is essential for these injections, these routes suffer from causing brain tissue damage, bleeding and chance of infection. As for non-invasive methods, they range from chemical modification of drugs taking advantage of the carrier mediated transport mechanism, or using the trojan horse concept (prodrug), by attaching the drug to BBB-permeable molecules taking advantage of the receptor mediated transport mechanism. Such an example is the anti-Parkinson drug L-DOPA acting on the L-amin acid transport system, which, unfortunately, suffers from adverse pharmacokinetics drawback and increase in the molecular weight of the drug itself. Finally, the intranasal route is used as it can reach the brain bypassing the BBB. Still, it faces a limited surface of adsorption of the olfactory bulb

compared to the BBB surface area, delivering a decreased amount of the drug (76-79). In the same perspective, the BRB represents a major drawback for the retina drug delivery, which will be discussed in the next three sections.

2.3.4. Retina

The retina is a part of the embryonic diencephalon, and therefore it is a part of the central nervous system. It represents the innermost layer tissue of the eye and contains different number of neurons cells like photoreceptors, bipolar cells and retinal ganglion cells which transform the light to electrical impulses. These impulses are sent to the brain via the optic nerve, where they are transformed into images. The retina is divided into seven different layers of tissues: (i) retinal ganglion layer, (ii) inner plexiform layer, (iii) inner nuclear layer, (iv) outer plexiform layer, (v) outer nuclear layer, (vi) photoreceptor layer, and (vii) pigment epithelium.

Diseases affecting the neural retina ranges from glaucoma, retinal degeneration and diabetic neuropathy. However, no effective treatment has been found for these neurodegenerative diseases. This is partly due to the isolation of the retina from the blood circulation by the blood-retina barrier, which is analogous to the blood-brain barrier. It is composed of inner and outer parts which allow only lipophilic and small molecules, such as O_2 and CO_2 to cross. Therefore, it is a challenge for a drug to reach the retina tissue and deliver the drug into retinal cells when administrated systemically (80-83). (Fig. 7)

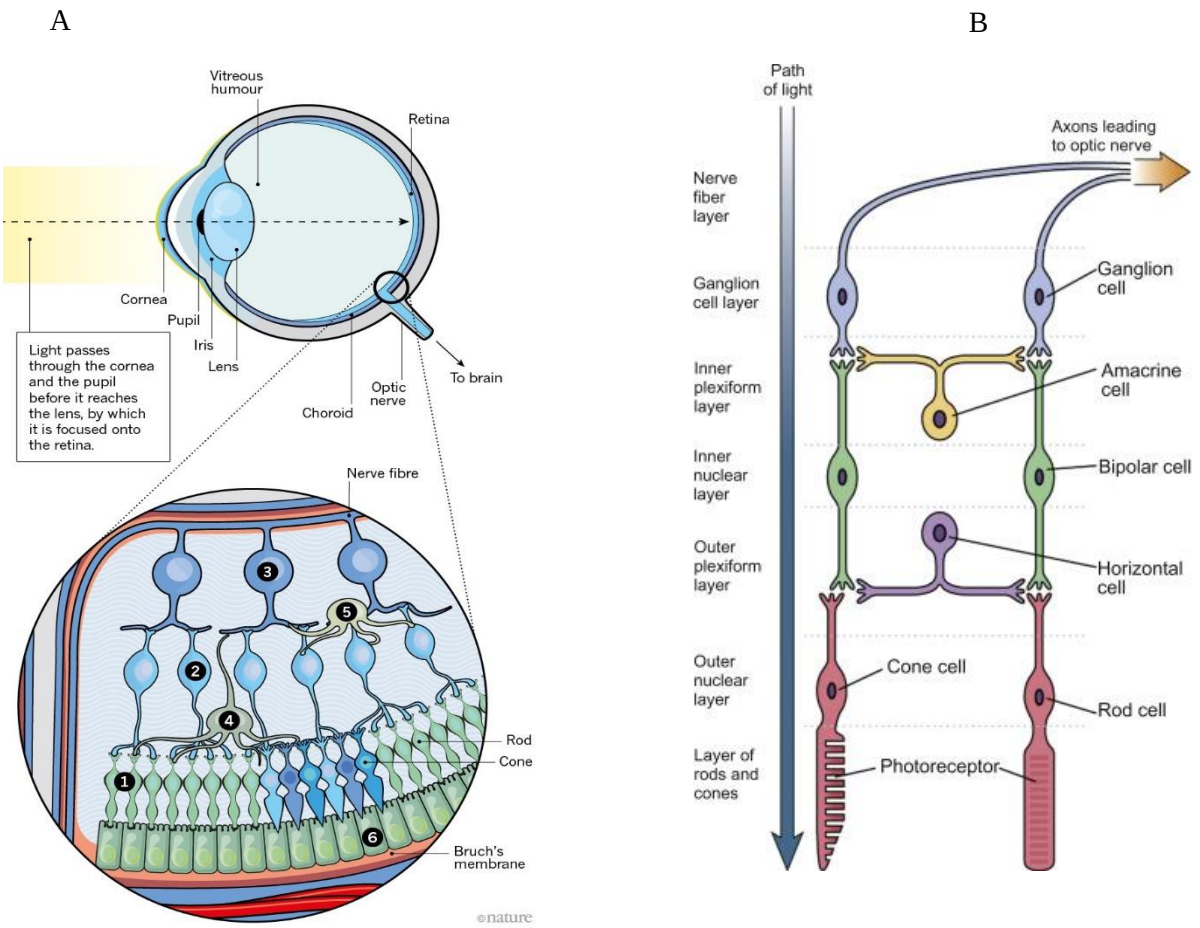

Fig. 7: Retina structure. A: retina neural cell types, 1. Photoreceptors, 2. Bipolar cell, 3. Retinal ganglion cell, 4. Horizontal cell, 5. Amacrine cell and 6. Retinal pigment epithelium (RPE). B: different cellular and synaptic retinal layers. Taken from reference (84,85).

2.3.5. The blood-retina barrier

Blood-retina barrier is the main barrier preventing the drug delivery to the retina for the treatment of posterior eye diseases like optic neuropathies. The BRB lays at the posterior part of the eye. It is formed by nonleaky tight junctions between the retinal capillary endothelial cells (inner blood-retinal barrier) and retinal pigment epithelium (outer blood-retinal barrier). Retinal capillaries prevent the passage of molecules with a diameter of 2 nm or above such as carbon nanoparticles (20 nm), horseradish peroxidase (4 nm) and micro-peroxidase (2 nm). It allows small molecules to permeate such as mannitol. The outer barrier is situated between the photoreceptors and choroid. Being the outer BRB, it has the mandatory function of maintaining the homeostasis of neural retina. It was found that the microperoxidase cannot permeate the RPE *in-vivo* in monkeys. However, the permeation in the RPE was dependent on the lipophilicity. While it was 2 x10 $^{-6}$ cm/s for nadolol (a drug for hypertension treatment), it

was $16x10^{-6}$ for betaxolol (a drug for glaucoma treatment) and FITC-Dextran 77,000 was only 0.027×10^{-6} cm/s (12.8 nm) showing also the size dependent permeation for the RPE. Their task is to limit the entry of drug from blood into the posterior segment of the eye. Besides, the BRB is specifically permeable to lipophilic substances. The intercellular tight junction exists in the retinal capillary endothelial cells, causing a poor permeability of small hydrophilic molecules such as sodium fluorescein and horse radish peroxidase due to the restricted paracellular transport. Moreover, the retinal pigment epithelium also has tight junctions which isolates the outer surface of the multilayer neural retina from the choroid, allowing only the exchange of selected nutrients. Transcellular and paracellular pathways across the retina is impermissible. It must be mentioned that the concentration of systemic administered drugs in the vitreous body of the eye are usually 1-2 % that of plasma level due to the restriction's mechanisms of the BRBs (86-93). (Fig. 8)

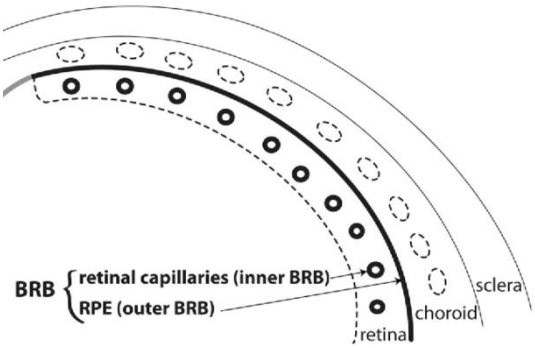

Fig. 8: Schematic representation for the blood-retina barrier. Thick line indicates tight endothelium/epithelium. Dashed ones indicate leaky endothelium/epithelium. Taken from reference (93).

2.3.6. Retina drug delivery

The eye is divided in two parts, anterior segment, which is the front portion that consists mainly of the cornea, pupil, conjunctiva and lens. The posterior segment, the portion behind the lens, consists of vitreous humor, choroid and retina. Therefore, ocular diseases are characterized according to this division. Retina diseases such as glaucoma are considered among posterior eye diseases. Therefore, blinding diseases are associated with posterior segment. There are different routes to target the posterior segment, including the systemic administration, intravitreal and periocular. Systemic administration lacks the efficiency to deliver the drug due to the inner and outer BRB which separates the retina from the blood circulation. Besides, frequent administration will induce risks of systemic side effects.

Systemic treatment of glaucoma with acetazolamide, the carbonic anhydrase inhibitor, causes toxic effects like depression, weight loss and paresthesia. Intravitreal injections are invasive with a high change of side effects such retinal detachment and retina hemorrhage, especially when frequent injections into the vitreous through the pars plana are performed. Periocular applications are used as well, but they can cause an increase in IOP, a strabismus and corneal decomposition. To date, when compared to each other, intravitreal injection is the best concerning the efficacy and the worst in terms of safety (94-98). Therefore, despite its side effects, it is the preferred drug delivery route for the treatment of the posterior eye segment (63). However, in the search for the appropriate route of administration, the existing methods to study the drug pharmacokinetic parameters need to be considered.

2.3.7. Methods to study the brain drug passage

There are different common methods that exist to study the pharmacokinetic parameters of the brain passage. Such methods are: the brain/plasma ratio, brain uptake index, in-situ brain perfusion, and micro-dialysis. However, besides being complex and costly, these techniques have some limitations like the considerable adsorptive effect of plastic tubing in micro-dialysis. The very short capillary transit time which is one second in brain uptake index method, makes the brain extraction procedure a complicated one. Moreover, the limited time for in-situ perfusion (more than 20 min) narrows the time scale for the study. Finally, the cranial window to study the BBB for long-term imaging is a traumatic method risking the contamination because of the bleeding and the chance of infection (103-105).

Thereby, I chose the *in-vivo* neuroimaging system as a method to study the passage of NPs into brain tissue. The ICON method has several advantages over the before-mentioned methods such as (i) ICON can avoid specific artefacts of in-vitro BBB models (high permeability), (ii) detect the rate and the amount of NPs' passage into the brain in one experiment, (iii) indicate the spatial distribution of the carrier in tissue, (iv) analyses particle-induced neuronal death and, (v) most advantageous for my experiment, it can be applied to live animals with experimental brain lesions. Moreover, it provides the usage of the BRB as a surrogate model to the BBB in my study.

2.3.8. Correlation between the BBB and the BRB

Because of the peripheral position of the eye, retina is the only brain tissue available for non-invasive *in-vivo* neuroimaging. Therefore, the retina can be used as a window to the brain

regarding the entry of NPs into a central nervous tissue with live imaging (99). Steuer et al. have investigated the similarities between the BBB and the BRB. Their results revealed that there is a correspondence between the BBB and BRB regarding the expression of efflux proteins and the permeability for many drugs (100,101). In addition, concerning the passage of the NPs into a brain tissue, You et al. proved that the BRB model is valid to reflect the BBB passage after comparing the entry of NPs in *in-vivo* retina micrographs and *ex-vivo* brain slices (102). (Fig. 9)

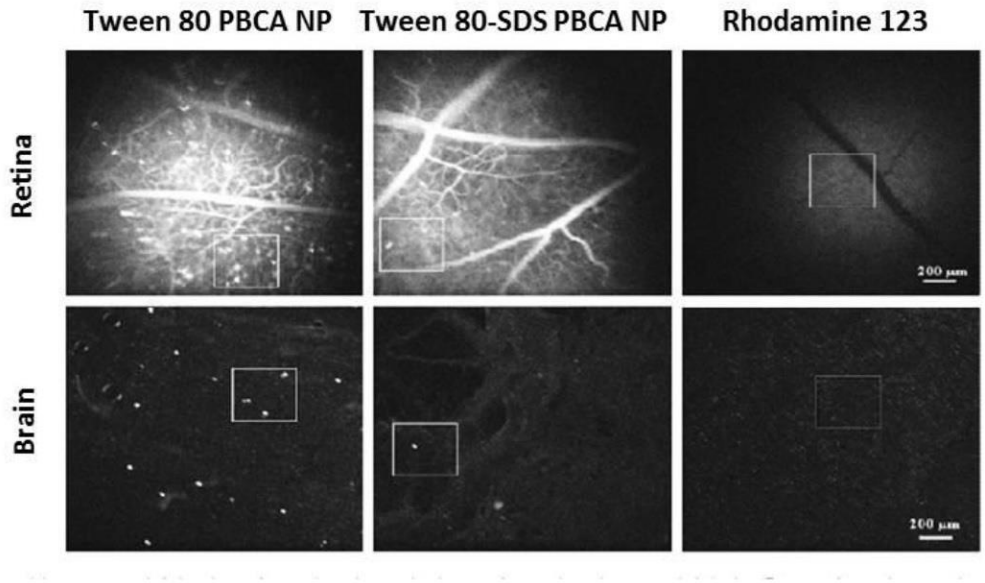

Fig. 9: BBB *vs* BRB. Comparing *in-vivo* retina (upper row) and *ex-vivo* brain slice images (lower row) after injection of fluorescent NPs. The high-permeable Tween 80 PBCA NPs, low-permeable Tween 80-SDS PBCA NPs and Rhodamine 123 (fluorescent marker without NP as control group) showed comparable fluorescence signals between retina and brain tissue. Taken from reference (102).

2.4. Nanomedicine

Nanomedicine is the application of nanotechnology to the medical field in the form of nanoparticles. Nanoparticles for medical purposes are solid colloidal systems that categorize in size from 1 to 1000 nm and contain an active compound (dissolved, entrapped, or encapsulated, or to which, the active compound is adsorbed or attached) (106). They can be produced from different substances, including lipids, polymers and metals. The medical applications of nanoparticles range from tissue regeneration, drug and cell therapy, diagnosis and imaging (107). They were extensively studied and approved by the FDA for different delivery routes like oral (Gastromark), local (DepoCyt), topical (Estrasorb) and systemic (Doxil) (108). Because different drugs have been fabricated for the purpose of CNS treatment

and showed insufficient *in-vivo* characteristics such as rapid enzymatic degradation and inadequate release profile from their galenic formulation, NPs have been developed to manipulate and cross the BBB while conserving these compounds and render them efficient for therapy in brain tissues (109).

2.5. Nanoparticles delivery to the CNS

For decades, different types of NPs have been studied to deliver drugs or nucleic acids to the central nervous system to provide a leverage against the used current strategies mentioned before. However, because of the delicate situation of the brain and the retina, there is a criterion that needs to be followed before investigating a kind of NPs to target the CNS. i] Biocompatibility, which means no induction of negative effects in the body and to avoid the accumulation of unwanted metabolites in the body. ii] Good stability in blood. iii] Avoid being taken up by the RES and immune cells to provide a long circulation time in the blood. iv] Ability to load and deliver different cargos (nucleic acids, proteins, and small molecules). v] to specifically target, which means to only target cells (109-112). To date, many types of NPs have been developed for CNS drug delivery. This includes lipid-based NPs, polymeric NPs and inorganic NPs. (Fig. 10)

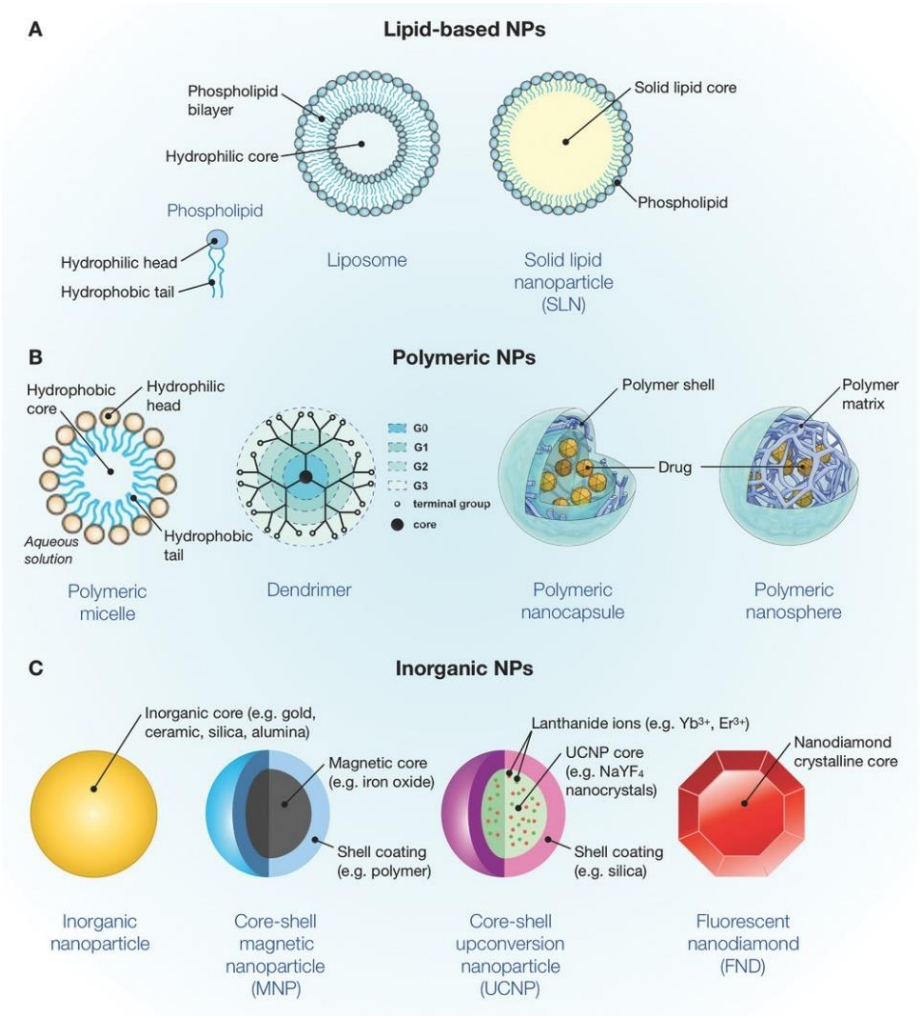

Fig. 10: Schematic representation of different NPs. Lipid-based NPs (A), polymeric NPs (B) and inorganic NPs (C). Taken from reference (110).

2.5.1. Liposomes

A liposome is a spherical small vesicle fabricated from one or more phospholipid bilayers (lamellae) surrounding internal aqueous space. Commonly, they are composed of amphiphilic phospholipids. Albeit, cholesterol could be also included to improve the stability *in-vivo*. Smaller uni-lamellar vesicles are composed of one lipid bilayer and a size of 10 to 100 nm. Larger uni-lamellar vesicles are composed of one bilayer and larger than 100 nm and multi-lamellar vesicles are composed of several bilayers and larger than 500 nm. Usually they have the ability to incorporate both hydrophilic and hydrophobic compounds. Moreover, their physicochemical properties could be manipulated in order to have a controllable drug release and enhance the tissue uptake of the loaded compound. Therefore, when applied as a drug carrier, liposomes have the abilities to improve bio-distribution of drugs in target tissues *in-vivo* (113-115). However, because of the number of excipients and complicated fabrication

method linked to their formulations, they have consequently low physical stability and constraints against controlling and sustaining their drug release (109-115).

2.5.2. Solid lipid nanoparticles

Solid lipid nanoparticles (SLNs) are spherical nanocarriers. Their size ranges from 1-100 nm and they possess a monolayer of phospholipid surrounding a solid hydrophobic core consists of biocompatible lipids such as triglycerides and fatty acids to solubilize lipophilic compounds. The phospholipid layer is composed of biological membrane lipids such as cholesterol or bile salts. SLNs are biodegradable and can load both hydrophobic and hydrophilic drugs. They can as well be used for controlled and targeted drug delivery after functionalization with polymeric coating (to avoid the RES) or ligand attachment (to increase the distribution of the drug within the brain). This was previously achieved using polysorbate 80, where SLNs delivered resveratrol, a neuroprotective agent to the brain (116-118). Still, several limitations of these nano-carriers have been detected such as the poor drug loading capacity, high water content of the dispersions and drug eviction during storage after polymeric transition (119).

2.5.3. Inorganic nanoparticles

Inorganic NPs possess different physical properties which can be utilized for brain drug delivery. They vary from gold NPs, magnetic (iron oxide core), ceramic, silver NPs and silica NPs which have a simple structure: an inorganic core and/or functionalized coating. Each of these particles have been used for different biomedical applications. However, their cytotoxicity is still questioned. For example, silver NPs when administrated showed BBB disruption and brain oedema formation. They can also cause a BBB destruction and astrocyte swelling besides neuronal degeneration. Iron oxide as well can induce the formation of ROS leading to cell apoptosis. Silica NPs can bring foreign materials into the brain and is not absorbed efficiently in the body even after oral administration and titanium dioxide could lead to brain injury and some glia deformation (120-122).

2.5.4. Polymeric nanoparticles

In the last five decades, polymeric NPs have been investigated for different drug delivery routes. Owing to their best combinations of characteristics, polymeric nanoparticles are more favored and consequently more investigated. Because their biodegradable, compatible and bio-adhesive features, they have been also studied for CNS delivery and different routes of

administration such invasive intracranial injection in the brain and intranasal route have been explored. For intravenous administration, polymeric NPs can increase the bio-availability of the drug by enhancing the *in-vivo* half-life and preventing drug degradation. It was found that surface modification with a targeting ligand mediating transport such as transferrin or polysorbate 80 is the main criteria to cross the BBB (123). Polymeric nano-carriers are fabricated from homopolymers or co-polymers. Their types are micelles, dendrimers, nano capsules and nanospheres and they have been all successfully applied for brain drug delivery. Nevertheless, nanospheres have been extensively studies more than any other candidates. Polymeric nanospheres constitute of dense polymer matrix allowing the dispersion, adsorption or covalently bond to the drugs. Polymeric nano capsules are composed of a core and shell mixture which typically consists of a polymer that surrounds a hydrophilic or hydrophobic core. Both types have been and still are investigated in the context of brain drug delivery where a variety of polymers are used. Both exhibit a size of 10-1000 nm, for example natural polymers like the chitosan, gelatin, albumin or synthetic like the polylactic-co-glycolic acid (PLGA), polylactic acid (PLA), polyalkyl-cyanoacrylate (PACA), polyethylene glycol (PEG) and polybutyl-cyanoacrylate (PBCA). It is well known that the biodegradation of polymeric NPs can be controlled depending on the type of polymer used and its concentration as well as its surface modifications. Furthermore, polymeric nanospheres offer the ability to sustain drug release for long periods of time while protecting the unreleased drug from the surrounding environment (124-126).

2.5.5. The choice of Polymeric NPs

Poly-vinyl-pyrrolidone

One of the polymers which has not yet drawn attention is the poly-vinyl-pyrrolidone (PVP). PVP is a non-toxic, non-ionic and bulky polymer with C=O, C–N and CH_2 functional groups that is widely used as a stabilizer in metallic NPs synthesis. Additionally, it is an amphiphilic polymer that contains a hydrophilic component (the pyrrolidone moiety) and a hydrophobic group (the alkyl group) rendering the water and non-aqueous liquids excellent solvents for it (127).

PVP-mescaline was reported to be the first polymer drug conjugate in 1950s (128). Some decades after, crosslinked PVP NPs with methylene-bis-acrylamide were able to entrap vaccines, peptide drugs, other hydrophilic drugs, and DNA (129). Moreover, the findings of Kamada et al. showed that the conjugation of PVP with TNFα led to an antitumor effect 200-fold higher than native TNFα with much longer blood circulation time (130,131).

Later, Kuskov et al. produced nanoparticles synthesized from PVP by an emulsion method. The particles have a hydrophobic core with a hydrophilic surface which renders them easy for surface modification and ideal for delivering hydrophobic drugs. They can carry, for example, the anti-inflammatory, hydrophobic drug indomethacin with a loading efficiency of up to 95% combined with high indomethacin content (35%). Hemolysis and cytotoxicity tests showed no significant or acute toxicity. Furthermore, PVP-NPs showed an exceptionally good stability for at least up to 3 months in saline or in freeze-dried status (132,133).

Poly-butyl-cyanoacrylate

The biocompatible and biodegradable polymeric PBCA NPs have been investigated intensively since 1995 (123,134,135). Cyanoacrylates have been widely used in drug delivery because of their favorable properties such as stability, biodegradability, biocompatibility and targetability (136,137). Moreover, PBCA NPs as promising polymeric drug carriers, as they have a well-characterized, good safety profile and have already been used in patient studies (138,139). Owing to its past in gene therapy as a nano-carrier for DNA or RNA, PBCA NPs could be a promising approach to inhibit neurons death' when loaded with siRNA to silence caspase-3 (140,141). This was recently proven *in-vitro* and *ex-vivo* by Zhang et al. (142). He demonstrated that the respective NPs down regulated caspase-3 expression by a western blot assay in C6 glioma cells with safe cytotoxicity test results. The *ex-vivo* imaging demonstrated that the respective NPs lowered retinal capsase-3 immunofluorescence by 57.9% in rats two days post-optic nerve crush. Because the neuroprotection ability of PBCA NPs was never studied to deliver siRNA *in-vivo* to the CNS, I chose these NPs to deliver caspase-3 siRNA and investigated the possibility of the neuroprotective effect of *in-vivo* caspase-3 silencing after an ONC trauma for more than one month using the *in-vivo* confocal neuroimaging system developed in our lab.

2.5.6. *In-vivo* confocal neuroimaging

The *in-vivo* confocal neuroimaging (ICON) technique has been widely used in our lab to study the distribution of polymeric NPs in the retina after intravenous injection as well as tracking the survival of stained retinal ganglion cell (143-151). It is simply a non-invasive imaging technique that detects the fluorescent signal, using a laser with an appropriate wavelength sent into the eye, and the fluorescent markers are excited and emit a fluorescent light which is captured by a detector (Fig. 11). Consequently, the signals can be detected in the retinal structures (Fig. 12).

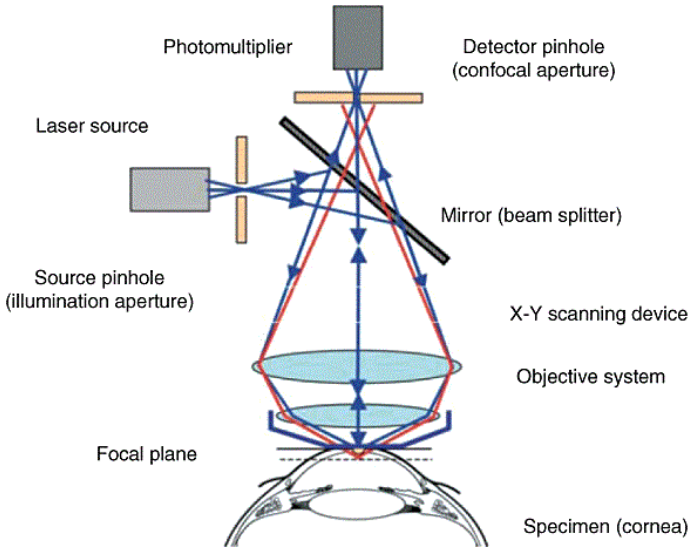

Fig. 11: Schematic representation of *in-vivo* confocal microscopy. The system is adapted so far as a plan-concave lens placed on the cornea, which guides the laser beam to the retina. Taken from reference (152).

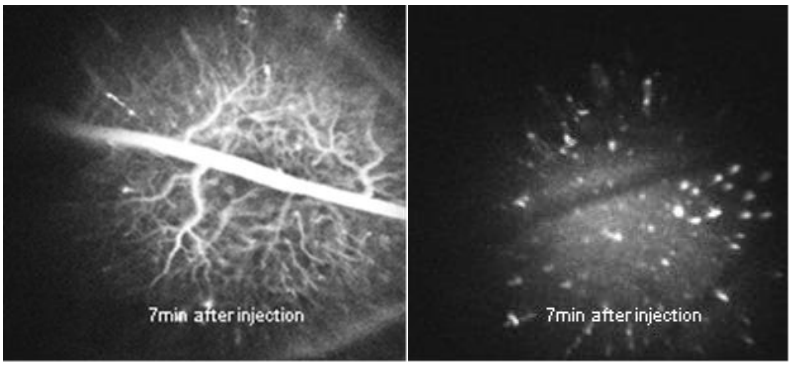

Fig. 12: Images of *in-vivo* confocal neuroimaging for fluorescent dye and fluorescent NPs. A fluorescent dye is injected intravenously and the signal is detected in blood vessel only (left), but the passage of the blood-retina barrier is demonstrated after intravenous injection of fluorescence-labelled NPs (right), as signal dots are localized outside of blood vessels. Taken from reference (149).

2.6. Aim of the dissertation

My PhD thesis has mainly two questions with two objectives to be attained.

Concerning study 1, the PVP project, I wanted firstly to study the behavior of plain PVP NPs (no surfactants or cross-linkers) regarding their ability to target the brain after intravenous administration using the BRB as a model for the blood-brain-barrier (BBB). Second, to investigate the behavior of PVP-Dil NPs (1,1'-Dioctadecyl-3,3,3',3'-Tetramethylindocarbocyanine Perchlorate), PVP-FITC (Fluorescein 5-isothiocyanate) at the BRB was compared to FITC-Dextran as control. The findings have led to the next step which is the modification of NPs' surface by linking the NPs with a lipophilic fluorescent marker CFSE (Carboxyfluorescein succinimidyl ester) and loaded with Dil (production and characterization of PVP-NPs was performed by my partners Amphion group from Moscow). Furthermore, analysis of *ex-vivo* wholemount retina was performed to ascertain the *in-vivo* results. 3D videos of *ex-vivo* wholemount-retina, fluorescence co-localization test and quantitative analysis was achieved using Arivis 4D software (executed by Steffen Hadlak from Arivis AG).

As for study 2, the PBCA project, I have investigated the anti-apoptotic effect induced by PBCA NPs loaded with Casp3-siRNA (CaspNPs), by observing the RGCs survival after optic nerve crush and treatment with two intravitreal injections of CaspNPs over a period of 21- and 35-days post ONC. Furthermore, *ex-vivo* whole mount retina analysis was successfully performed to study the RGCs morphology and survival with higher magnification and cellular resolution. Qualitative results were confirmed by ICON and *ex-vivo* wholemount-retina and achieved by manual counting of RGCs.

3. PVP-CFSE NPs as a new carrier system for drug delivery to the brain: An *In-vivo* and *Ex-vivo* study

3.1. Introduction

Central nervous system diseases are on the rise and they represent the second largest category of life-threatening diseases (154,155). Amongst them, retinal diseases, such as glaucoma, age related macular degeneration (AMD) and diabetic retinopathy, are the main cause of irreversible blindness (82). The conventional therapies like eye drops, are ineffective and they can hardly reach the retina, leading to < 5% of drug bioavailability. Alternatively, the invasive intravitreal injection is more preferred due to the drug concentration level it can provide to the retina. Still, frequent injections are required to maintain the therapeutic efficiency which will results eventually in a poor patient acceptance and complications such as retinal detachment and endophthalmitis (156,157). Therefore, a less invasive and more effective route such as the intravenous administration is needed which can target the disease site more specifically, enhance the biodistribution to the target and reduce the dosage frequencies. (158). However, systemic administration targeting the back of the eye is hampered by a major obstacle, the blood-retina barrier (BRB). Hence, nanotechnology-based drug delivery systems hold a great potential to overcome the limitations for brain and retina drug delivery, especially when injected intravenously (159,160).

In the same perspective, polymeric NPs have emerged as a safe nano-carrier system to target the brain because of their biocompatibility and biodegradability (161,162). However, the selection of an appropriate surfactant is the crucial step to enable the passage of these NPs through the BBB/BRB (148). Yet, unlike unmodified NPs, these surfactants could provoke an immune response (163). Nanoparticles based on polyvinyl-pyrrolidone (PVP) revealed a great potential for drug delivery. PVP is a known component of numerous pharmaceutical and medical products. Additionally, it was previously investigated as artificial vitreous substance, scaffold for lens regeneration and sustainable drug delivery system for anti-glaucoma drugs (131,132,164-166).

Based on these considerations, I have now investigated PVP NPs loaded with fluorescent markers as drug carriers to target the posterior segment of the eye and followed their distribution in different compartments at the BRB, i.e., blood cells, vessel lining and retina tissue. In addition, I wanted to study the NPs' fate and passage from the vessel lumen into retina tissue to identify and characterize the multifactorial influences which determine the distribution of NPs at biological barriers, as the interaction of NPs with peripheral compartments and molecules significantly

influences their distribution (146,147). This was achieved using ICON which can provide retina live imaging in living rats. Albeit ICON was successfully used to visualize the entry of polymeric NPs through the BRB, so far only qualitative data are available to demonstrate the BRB passage. Therefore, I implemented image analysis workflows based on the Arivis Vision4D software (167). This allowed me to quantitatively analyze the co-localization of the double-labelled Amph-PVP NPs and to follow the spatial separation of the markers *in-vivo* and *ex-vivo*.

There are many tools for image analysis available in open sources (e.g. https://imagej.net/Introduction) and commercial software packages. However, putting together a sequence of specific image analysis steps to form a complete workflow is a tricky task. The Arivis Vision4D visualization and analysis software package helps to select and assemble numerous steps of the whole analysis workflow in one flexible pipeline. The user can choose from many functional components ranging from pre-processing, filtering, background correction, several segmentation tools and further processing of the detected objects as well as export of the data into Excel or CSV files. No programming skills are required for setting up such a pipeline according to the required workflow and the user can easily focus on developing a creative analysis strategy for the specific task. This pipeline is applicable to many data sets reducing bias and ensuring comparability. In addition, analysis pipelines can be shared among different users. In short, I studied and characterized the behavior of PVP NPs when loaded with different cargo variations and demonstrated that they can penetrate the rat retina parenchyma when linked to CFSE. To the best of my knowledge, the present study is the first to evaluate the PVP NPs as a nano-carrier to target the central nervous system and the first to test the effect of shell-linked fluorescent marker to induce the passage through the CNS as well.

3.2. Materials and methods

The materials and the respective suppliers for the preparation of nanoparticles were as follows: N-vinyl-2-pyrrolidone (VP) and 2, 2’-azobisisobutyronitrile (AIBN), 1, 4-dioxane and 6-hexanediamine were obtained from Acros (Moscow, Russia). Acrylic acid (AA), 5(6)-carboxyfluorescein diacetate N-succinimidyl ester (CFSE), 1,1′-dioctadecyl-3,3,3′,3′-tetramethylindocarbocyanine perchlorate (Dil), succinimide, N,N′-dicyclohexylcarbodiimide (DCC, 1.0 M solution in methylene chloride), octadecyl mercaptan (ODM), 1,6-diphenyl-1,3,5-hexatriene (DPHT), Fluorescein 5-isothiocyanate (FITC), and 3-chloroperoxybenzoic acid were obtained from Sigma-Aldrich (Taufkirchen, Germany). All chemicals were used without further purification unless

otherwise specified. All solvents and components of buffer solutions were of analytical grade and were used as received. A Milli-Q Plus System (Millipore) was used to prepare ultrapure water.

The materials for the animal study were as follows: Ketavet (ketamine hydrochloride; Zoetis Deutschland GmbH, Berlin, Germany), Dormitor (medetomidine hydrochloride; Orion Corporation, Espoo, Finland), Neosynephrine-POS 2.5% (Arzneimittelherstellung Uniklinik Magdeburg, Germany), Vidisic optical gel (Bausch & Lomb, Berlin, Germany), Saline (0.9% Fresenius Kabi Deutschland GmbH, Bad Homburg, Germany), FluoSpheres (ThermoFischer, Karlsruhe, Germany) and FITC-Dextran 70.000 (Sigma, Taufkirchen, Germany).

I used three different types of fluorescent NPs along with FITC-Dextran as a control; two types of NPs were loaded with either the fluorescent tracer Dil (Ex540/Em560 nm) or FITC (Ex 495/Em 519 nm). The third type was loaded with Dil and the NPs surface was linked to CFSE, a hydrophobic fluorescent dye (Ex 494/Em521).

3.2.1. Synthesis of Poly (N-vinyl-2-pyrrolidone) polymers

Two kinds of PVP polymers were synthesized for this study, PVP-ODM (Polyvinyl-pyrrolidone-octadecyl mercaptan) and PVP-AA-ODM (Polyvinyl-pyrrolidone-Acrylic acid- octadecyl mercaptan). Both polymers have undergone a similar synthesis procedure. The PVP-ODM was used to produce the PVP-Dil and PVP-FITC NPs production whilst the PVP-AA-ODM polymer was for the PVP-Dil-CFSE NPs production.

More specifically, 10.0 ml of N-vinyl-2-pyrrolidone were dissolved in 20 ml of 1, 4-dioxane. 0.286 g octadecyl mercaptan and 0.107 g of 2, 2'-azobisisobutyronitrile (AIBN) were sequentially added and the reaction mixture was stirred at 70 °C for 3 hours (Fig. 13a). The synthesis of PVP-AA-ODM was as follows: 10.0 ml of N-vinyl-2-pyrrolidone and 0.338 g of acrylic acid were dissolved in 40 ml of 1, 4-dioxane. 0.282 g octadecyl mercaptan and 0.107 g of AIBN were sequentially added and the reaction mixture was stirred at 70 °C for 2.5 hours (Fig. 13b). Afterwards, 50 ml of distilled water was added and the resulting crude polymer mixture was purified by dialysis against water (Slide-A-Lyzer ™ Dialysis Flask, 2K MWCO, Thermo Scientific, USA) and was lyophilized (Alpha 1-4 LD plus, Martin Christ, Germany) before storing.

3.2.2. PVP-Dil and PVP-FITC NPs production

All the NPs were prepared by using an emulsion method. To this end, 0.9 g of polymer was dispersed in 20 ml of water and 0.01 g of Dil or FITC was dissolved in chloroform. Both these solutions were then mixed under ultrasonic treatment (under cooling, during 12 min). At

the end of the homogenization, the chloroform was distilled off on a rotary evaporator (Hei-Vap Value Digital, Heidolph instruments, Germany). To separate the non-included Dil or FITC, the suspension was centrifuged (Sigma 4-5L, Germany). Afterwards, the supernatant was lyophilized. The lyophilized powder consisted of NPs that could be dispersed in water or PBS (0.07 g/ml) to produce stable particle suspension while unincorporated Dil or FITC remains in the precipitation.

3.2.3. PVP-Dil-CFSE NPs production

After the production of PVP-AA-ODM, a linkage with CFSE was achieved by carbodiimide chemistry. For this, the polymer was dissolved in chloroform and the equivalent amount of succinimide and N, N′-dicyclohexylcarbodiimide solution was added under stirring at room temperature (the mole ratio between carboxides groups: N, N′-dicyclohexylcarbodiimide: succinimide was 1: 1, 2: 1, 2). The solution was mixed for one hour. Thereafter, the excess of 6-hexanediamine was added and mixed for additional 30 min. The resulting mixture contained a PVP-AA-ODM copolymer with active amine groups which was then purified by dialysis against water and lyophilized. The lyophilized PVP-AA-ODM copolymer with active amine groups was dissolved in dry chloroform and the equivalent amount of CFSE was added under stirring at room temperature (the solution was mixed for 0.5 hr.). The mixture was purified by dialysis against water and lyophilized. After lyophilization, PVP-Dil-CFSE NPs were produced similarly as described above for PVP-Dil and PVP-FITC NPs. (Fig. 13c)

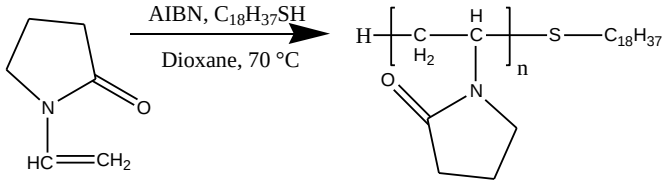

Fig. 13a: Polymerization scheme of PVP-ODM in the presence of a chain transfer agent

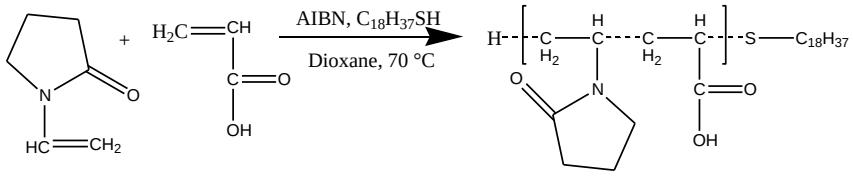

Fig. 13b: Polymerization scheme of PVP-AA-ODM in the presence of acrylic acid and a chain transfer agent

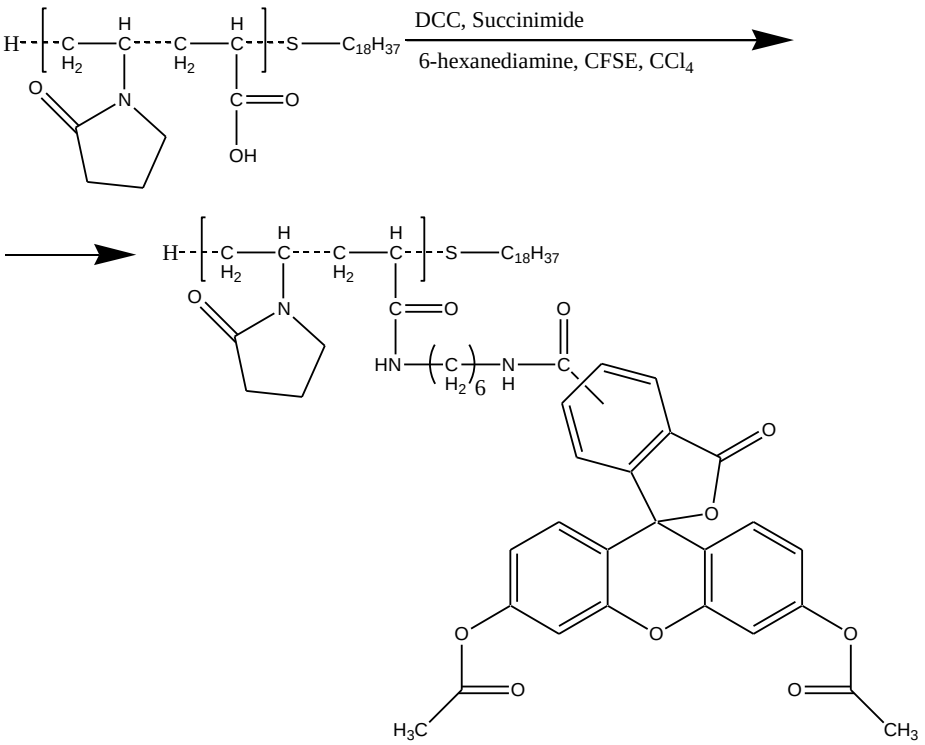

Fig. 13c: Linkage scheme of PVP-AA-ODM with CFSE by carbodiimide chemistry

3.2.4. Physicochemical NPs characterization

The average molecular weight of the PVP-ODM and PVP-AA-ODM polymers were determined by back titration of the sulfide group with 3-chloroperoxybenzoic acid (the reaction took place in a water-ethanol solution at +5°C for 16 hours). The excess of the acid was then determined by iodometry. The critical micelle concentration (CMC) was determined by fluorescence spectroscopy (Hitachi 650-10S, Japan) using 1,6-diphenyl-1,3,5-hexatriene (DPHT) as the fluorescent probe.

The particle size distribution, polydispersity index and ζ-potential were determined by the DLS (dynamic light scattering) method (Malvern Zetasizer Nano ZS, UK). PBS (pH 7.4) was used as the dispersion medium to then characterize the NPs. The intensity trace recorded during the experiment was used to calculate the size of the nano scaled aggregates.

The morphology of PVP-NPs was determined by TEM (transmission electron microscopy) using JEOL JEM-2100, USA at an acceleration voltage of 30 kV. The rest of parameters were as follows: Primary electron beam current = 18 pA, Type of detector used was WET-STEM, The size of two-dimensional images was 3072 × 2207 pix, Two-dimensional pixel size was 2.7 – 54 nm, Two-dimensional horizontal field of view was 2.07 – 41.4 mkm, microscope chamber pressure was 750 Pa, Humidity was 100%, Temperature 1.5°C and point accumulation time was 30 mcs. The concentration of Dil, FITC and linked

CFSE was determined by UV spectroscopy (Unico SQ-2802PCS UV-Vis spectrophotometer, Germany).

3.2.5. Animals

A total of 37 adult, male Lister hooded rats (Crl: LIS Stamm; Charles River, 280– 380 g) were kept on a 12-h light / 12-h dark cycle at an ambient temperature of 24–26 C and a humidity of 50–60%. For all procedures ethical approval was obtained according to the requirement of the German National Act on the use of experimental animals (Ethic committee Referat Verbraucherschutz, Veterinärangelegenheiten; Landesverwaltungsamt Sachsen-Anhalt, Halle). Following shipment, animals were kept at least 3 days for adaptation in group cages and handled for 3 days before starting the experiments.

3.2.6. Retrograde Labelling of Retinal Ganglion Cells (RGCs)

In order to perform a triple labelling technique, the RGCs were selectively labelled by retrograde axonal transport of fluorescent tracer which was injected into the brain. Before surgery, the rats were anaesthetized with an intraperitoneal injection of Ketavet (0.75 ml/kg) and Dormitor (0.5 ml/kg). Labelling was achieved by stereotactic injection of 4 µl of FluoSpheres (Ex 580/ Em 605) into both the right and left superior colliculus (Coordinates: 6.9 mm posterior to Bregma and -/+1.2 mm lateral from midline). The injections (0.5 µl each) were positioned at different depths below dura: 4.0 mm, 3.5 mm, 3.0 mm and 2.5 mm. Between each, 30 sec were allowed to elapse to ensure microspheres diffusion in the brain tissue. The intracerebral (I.C.) application was performed one week before NPs injection and preparation of wholemounts to ascertain complete labelling of the RGCs. (Fig. 14)

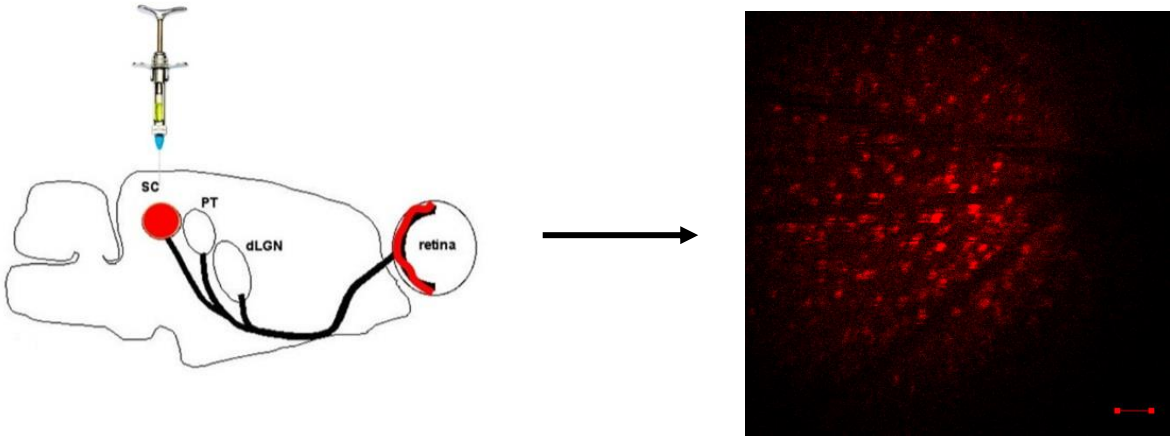

Fig. 14: Retrograde labeling of RGCs by injecting a fluorescent dye into the superior colliculus (left). SC: superior colliculus PT: Pretectal area and dlGN: dorsolateral geniculate nucleus. *In-vivo* neuroimaging of labelled RGCs (red) using Fluorospheres one week after injection, retinal blood vessels in black. Scale bar: 200 µm (right).

3.2.7. ICON-microscopy

ICON was carried out as described previously (143). Briefly, in rats anaesthetized by intraperitoneal injection of Ketavet (0.75 ml/kg) and Dormitor (0.5 ml/kg), the eye was treated with Neosynephrine-POS 2.5% to relax the iris. Vidisic optical gel was applied as an immersion medium for the contact lens and to prevent drying of the cornea. The rats were then positioned underneath a standard confocal laser scanning microscope (LSM 880, Carl Zeiss AG, Jena, Germany) with a large probe space and a long working distance objective lens. The rat was fixed on the microscope stage with the eye positioned directly underneath the objective lens (Plan Neofluar 5× /0.15) after a Hruby style -80 dioptre plan concave lens (KPC-013, Newport GmbH, Darmstadt, Germany) was placed directly onto the surface to adjust the path of the laser rays to the plain of the rat retina. (Fig. 15)

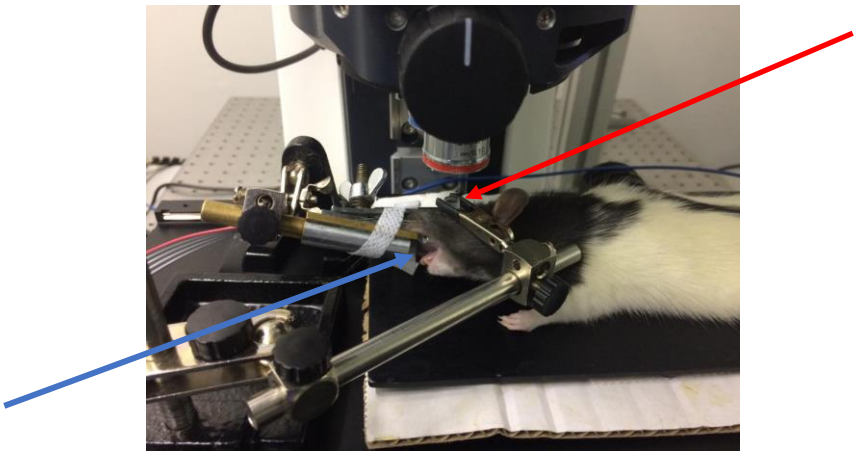

Fig. 15: *in-vivo* imaging of the retina setup using ICON. Image shows an anaesthetized rat placed under LSM. Yellow arrow indicates the mouth holder. Red arrow indicates the contact lens placed onto the rat eye to adapt the optics so the retina can be visualized.

3.2.8. Nanoparticle application

After the anaesthetized rat was positioned on the microscope stage, the NPs were injected intravenously (I.V.) via the tail vein with a single dose of (500 g NP-bound Dil or FITC per kilogram body weight) using a pre-implanted catheter (BD Adsyte Pro, 22 G, Heidelberg, Germany) (n=37). As a control (n=7), animals received only the fluorescent dye (FITC-Dextran) in saline (without NPs). Confocal images were taken before and up to 2 hours after injection at different time intervals.

3.2.9. *Ex-vivo* wholemount retina

Since the optical resolution in live imaging of the retina is limited, I also utilized an *ex-vivo* whole mount retina preparation. Moreover, to be able to visualize the localization of the fluorescent nanoparticles in the retina tissue, a double\triple fluorescent labelling technique was performed. With this technique I was able to stain the retinal cell nuclei with [Hoechst33342] (Ex350/Em 460 nm), retinal blood vessels with the fluorescent marker loaded in the NPs and the RGCs as stated before. In case of PVP-FITC NPs or the control FITC-Dextran, triple labelling was performed. In case of PVP-Dil or PVP-Dil-CFSE I used double labelling because labelling of RGCs with fluorospheres was not performed as Dil would overlap with the FluoSpheres' excitation (Ex540/Em560). One hour after fluorescent NPs injection, the rats were decapitated. Enucleated eyes were placed in Ca^{2}+-free solution containing 135 mM, NaCl, 5 mM NaOH, 2.5 mM KCl, 2 mM $CaCl_2$, 1 mM $MgCl_2$, 10 mM HEPES, 10 mM glucose. Cornea and lens were removed and the retina was separated from the pigment epithelium. Retinae were kept at room temperature under a constant supply of

oxygen. After incubation with Hoechst33342 for 20 min, the tissue was transferred into a petri dish and mounted at the microscope stage for imaging (LDC Epiplan-APOchromat 50×/0.5). The different steps of a triple labelling for FITC-Dextran are depicted in Fig. 16.

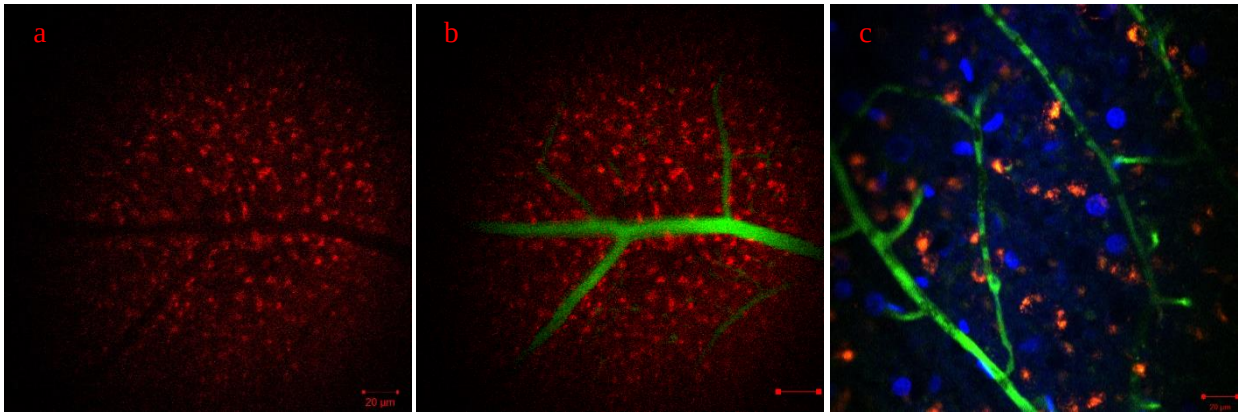

Fig. 16: Retina triple labeling technique **a:** RGCs in red, 4 µl of FluoSpheres (Ex 580/ Em 605), I.C. injection (5×), **b:** RGCs in red, FluoSpheres. Blood vessels in green, 23.34 mmol/l of FITC-Dextran (Ex 495/Em 519 nm), I.V. injection, micrograph taken 5 min after injection (5x). **c:** Cell nucleus in blue (Hoechst33342) (Ex350/Em 460 nm) by incubation. RGCs in red, Micro-vessels in green, micrograph taken 60 min after injection (50×). Scale bar **a** and **b** :200 µm. Scale bar **c**: 20 µm

3.2.10. Quantitative Comparisons of Different PVP-NPs

To achieve a quantitative examination of parameters and to be able to more automatically and thus more objectively decide whether NPs can pass the BRB or not, I implemented a new image analysis algorithm. In this work I quantitatively analyzed the NPs' fluorescent signal in the retina tissue and the relative concentration of NPs within the blood vessels as two promising parameters.

For extracting these parameters, I utilized Arivis Vision 4D (with the help of Steffen Hadlak), a modular image analysis and visualization software. It provides state of the art image correction and analysis algorithms as well as manual tools for proof reading, correction of analysis results with a large number of different statistics for evaluating the results (168).

BRB passages are based on the qualitative observation that when the NPs used in this study passed the BRB, they spread into the retina parenchyma, accumulated and represent regions with high intensities called blobs. Arivis Vision 4D provides a specialized algorithm, Blob Finder (169), for detecting this kind of structure. It is calculating the difference between two gaussians smoothing the image and partially removing differences in the intensity range at the same time. High values in this difference image then represent the regions I am looking for. However, blood vessels also sometimes fulfill this characteristic. We therefore used

additional filters based primarily on size and shape and also manual proof reading if required to minimize false positives. Regarding the concentration of NPs in blood vessels, we combined a mean filter for denoising and an objectness measure filter to extract and amplify vessel like structures. This is based on calculating a Hessian matrix for each pixel representing the main direction or vector along which high intensity values are located - if they so exist. By thresholding pixels based on the length of the vector we were able to separate vessels from the remaining retina tissue.

3.2.11. Statistical Analysis

Statistical analysis was carried out with Microsoft Office Excel 365. The outcome variables are presented as means and standard deviation. The group differences in the number of blobs and concentrations in blood vessels were evaluated by analyses of variance (One-way ANOVA) followed by post-hoc Tukey test for multiple comparisons. $*P < 0.05$ was considered to be statistically significant.

3.2.12. *Ex-Vivo* Co-localization of NPs in wholemount images

Regarding the PVP-Dil-CFSE NPs, I was also furthermore interested in whether both the (Dil and CFSE) penetrate the BRB together, or whether they split up. Therefore, I captured multi-labelled images with each label saving the intensities for a different part (Dil or CFSE) of the NPs and then employed co-localization features of Arivis Vision 4D to determine whether or not the different parts of the NPs stay together and where they were found. These features are based on first identifying pixels of higher intensities for both channels, thus identifying the distribution of both parts and then grouping them according to their co-localization in pixels showing only one part and pixels showing both parts.

3.2.13. *Ex-vivo* 3D videos of NPs in wholemount retina

Using Arivis vision 4D software, I was also able to perform a three-dimensional reconstruction of *ex-vivo* wholemount retina images as a supplementary confirmation of NPs´ passage. Therefore, Z stacks were obtained by capturing 30 confocal microscope images at different planes with a step size of 0.13 µm and a 50x magnification objective lens. Furthermore, PVP-Dil NPs were used as a control for comparison with PVP-Dil-CFSE NPs. Based on these Z stacks, I then rendered animations with Arivis Vision 4D to show the acquired image data from different perspectives.

3.3. Results

3.3.1. PVP Nanoparticles characterizations

The respective data relevant for my studies were as follows:

The characteristics of the three types of PVP NPs (sizes and zeta-potentials) used for the *in-vivo* imaging and kinetic studies are shown in table 1. The average molecular weight for PVP-AA-ODM and PVP-ODM was 5.8 kDa and 6.1 kDa, and the CMC value 0.073 and 0.054 mmol/l, respectively (Fig 17a). The presence of the highly hydrophobic octadecyl end-group in these polymers allowed the formation of micelles in an aqueous medium.

Particles size distribution by DLS and morphology obtained by TEM as shown in (Fig. 17b) confirmed the production of spherical Amph-PVP NPs with rather narrow size distribution (Fig 17c). Concentrations of fluorescent dyes used in NPs production were as follows: Dil (11.5 mg/g), FITC (35 mg/g) and CFSE (3.12 mg/g).

Table 1: PVP NPs Physicochemical Characteristics

(At least 3 measurements per sample) (n ≤ 3 batches, $\bar{x} \pm s$)

NPs type	Zeta potential (mv)	PDI	Size (nm)
PVP-Dil	+11.6±1.61 mv	0.235±0.013	218±2 nm
PVP-FITC	+8.08±1.29 mv	0.200±0.084	360±12 nm
PVP-Dil-CFSE	-15.2±1.14 mv	0.383±0.036	344±14 nm

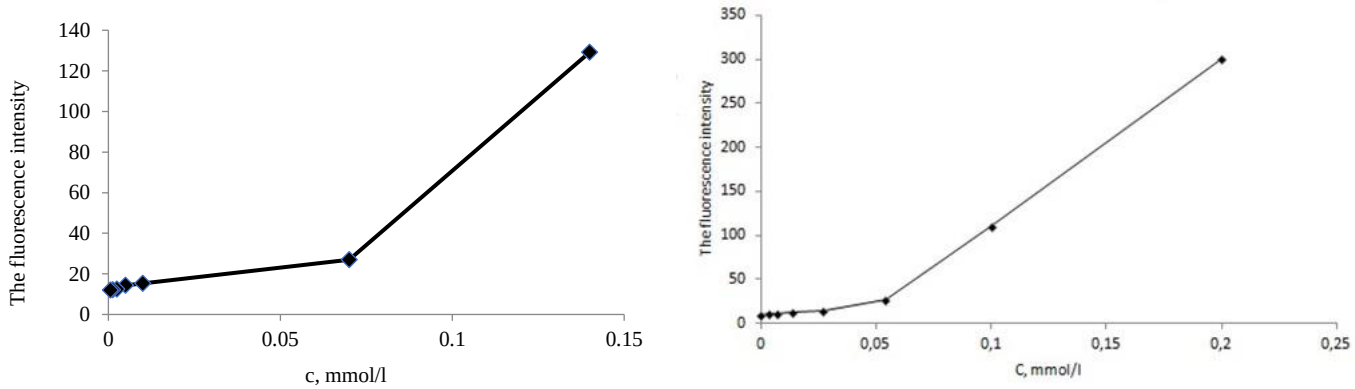

Fig. 17a: The plot of the fluorescence intensity of the solution of PVP-AA-ODM (left) and PVP-ODM (right) with DPHT at 25 °C.

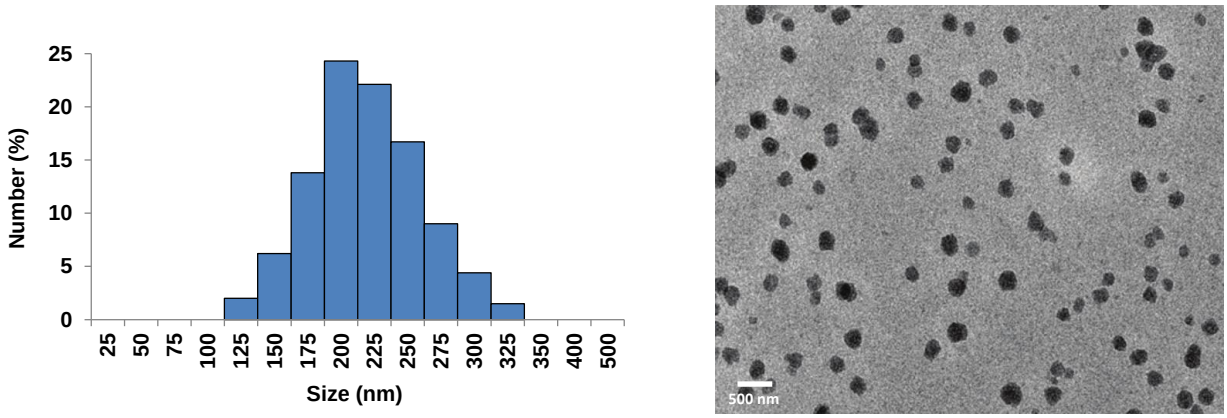

Fig. 17b: PVP-Dil nanoparticles size distribution (left) by DLS method and TEM Micrograph (right) showing the morphology of PVP-Dil nanoparticles. The image confirms the spherical shape of the NPs and their narrow monomodal size distribution. Scale bar: 500 nm.

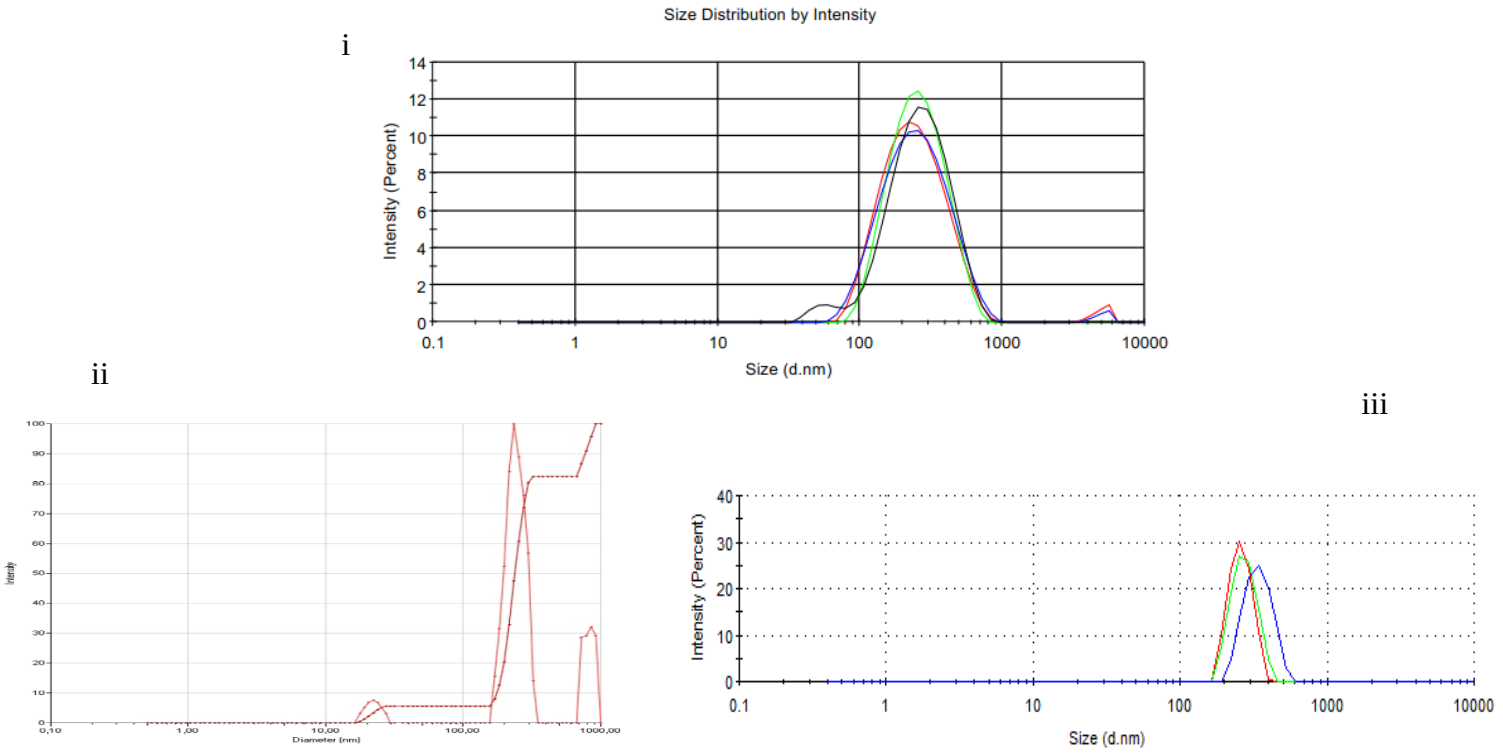

Fig. 17c: Distribution of particles by size for PVP-Dil NPs (i), PVP-FITC NPs (ii) and PVP-Dil-CFSE NPs (iii)

3.3.2. *In-vivo* neuroimaging for BRB passage kinetics

To study the kinetics of the BRB passage, three different types of PVP NPs (PVP-Dil, PVP-FITC and PVP-Dil-CFSE NPs) were injected. In addition, FITC-Dextran (without NPs) was injected and used as a control. Retina images were taken in a well-defined area of (2,6 mm)^2

with clearly visible blood vessels. The dyes were traced up to 2 hours after injection at different time intervals. The fluorescence signal after the intravenous injection of FITC-Dextran solution was clear and detected inside the blood vessels within seconds after injection and the dye did not diffuse across the vessel wall. This signal started to decrease after 30 min over the time but remained detectable in the main blood vessels for the imaging period time which was two hours (Fig. 18). As for the PVP-Dil, the fluorescence signal appeared also directly after injection and remained sustainable and detectable for the two hours strictly confined to the vessel. Concerning the PVP-FITC NPs, they also exhibited staining of blood vessels directly after injection, gradually decreasing from the veins after the first 30 min but were detectable in the blood vessels through the whole time of the experiment, again, without diffusion across the vessel wall (Fig.19 and 20). However, the intravenous injection of PVP-Dil-CFSE showed different behavior. The fluorescence signals of both the Dil and the CFSE diffused into the retina tissue after 5 min then increased gradually, reaching a maximum value within 10 min after injection in both tissues and vessels starting to decrease gradually for the following 60 min till not detectable in both the retinal blood vessels and tissues (Fig. 21).

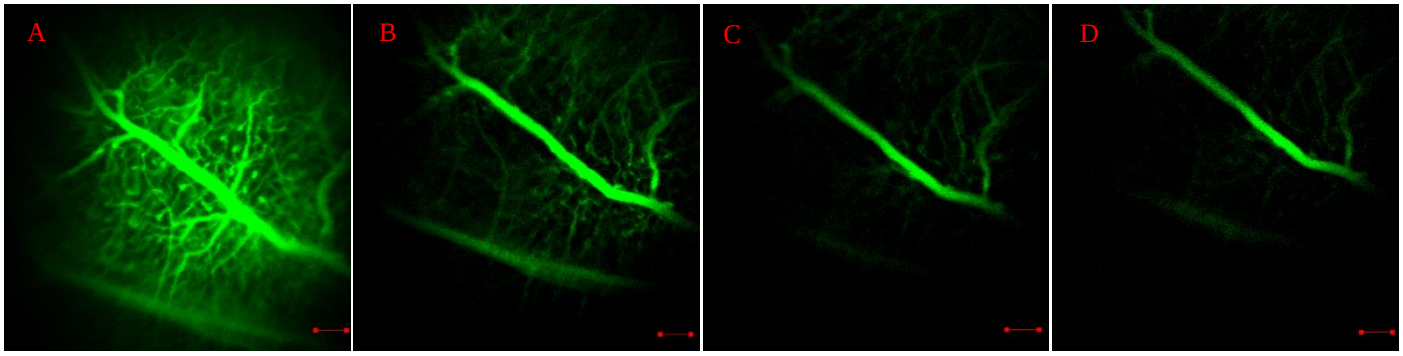

Fig. 18: *In-vivo* imaging, 5 X. FITC-Dextran, (Ex 495/Em 519 nm). **A**: 5 min**. B:** 30 min. **C**: 60 min. **D**: 120 min. FITC-Dextran fluorescence in vessels All animals were injected intravenously. Scale bar: 200µm.

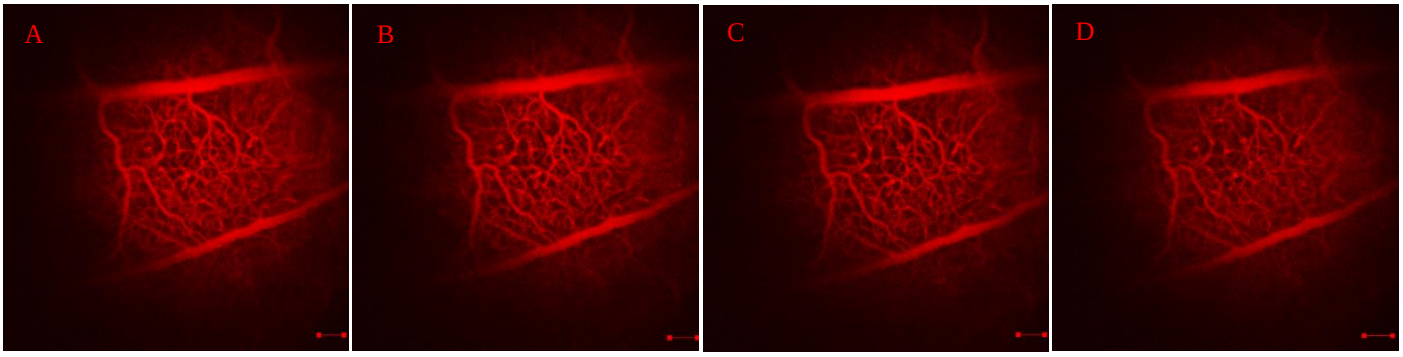

Fig.19: *In-vivo* imaging, 5 X. PVP-Dil NPs, Dil (11.5 mg/g), (Ex540/Em560 nm). **A:** 5 min. **B:** 30 min. **C:** 60 min. **D:** 120 min. Dil fluorescence in blood vessels. All animals were injected intravenously. Scale bar: 200µm.

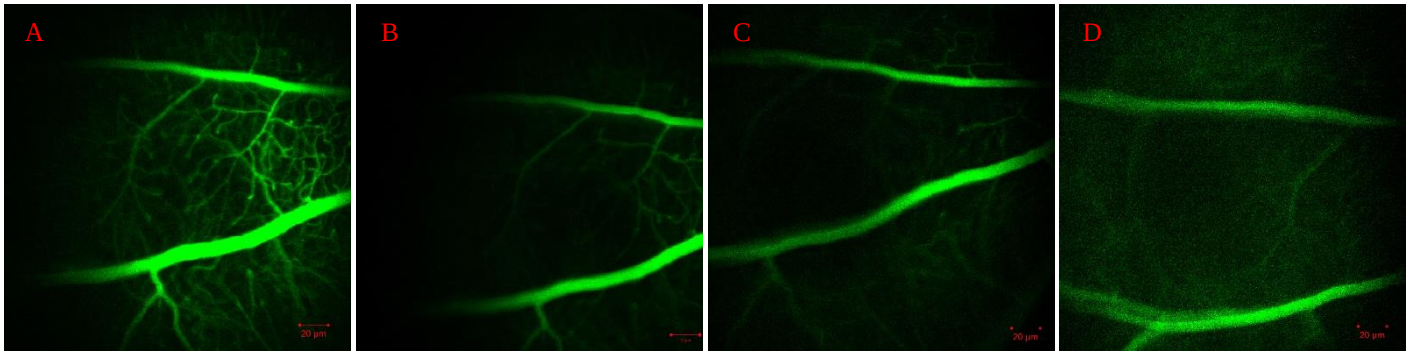

Fig. 20: *In-vivo* imaging, 5 X. PVP-FITC NPs, FITC (35 mg/g), (Ex 495/Em 519 nm). **A:** 5 min. **B:** 30 min. **C:** 60 min. D: 120 min. FITC fluorescence in blood vessels. All animals were injected intravenously. Scale bar: 200µm.

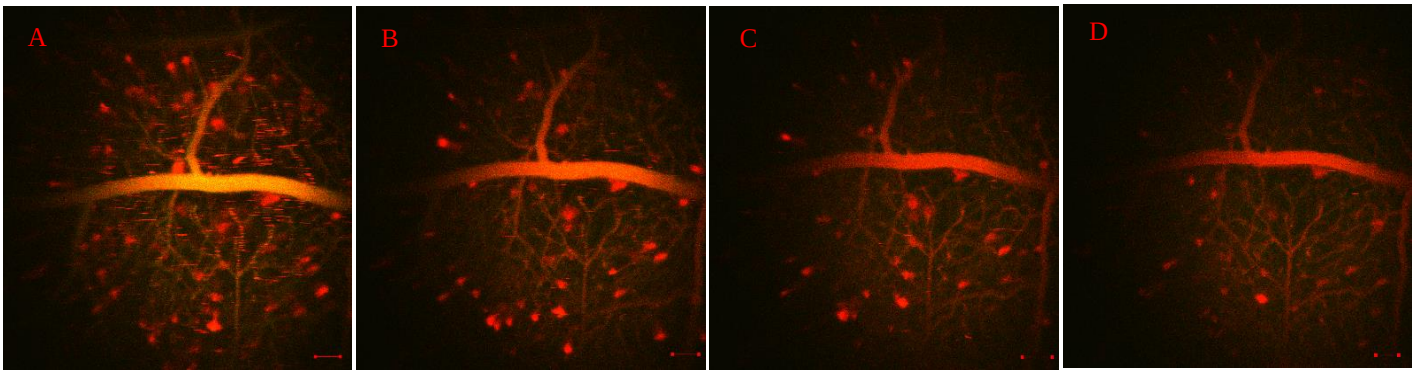

Fig. 21: *In-vivo* imaging, 5 X. PVP-Dil-CFSE NPs, CFSE (3.12 mg/g), (Ex540/Em560 nm) + (Ex 494/Em521). **A:** 5 min. **B:** 10 min. **C:** 30 min. **D:** 60 min. Dil fluorescence in vessels and diffused staining of Dil+CFSE in retinal tissue. All animals were injected intravenously. Scale bar: 200µm.

3.3.3. Nanoparticle fate as imaged in *ex-vivo* wholemount retinae

In order to verify the *in-vivo* results described above at higher resolution, I injected the same types of PVP NPs and FITC-Dextran and imaged their fluorescence signals *ex-vivo* in retina 60 min after injection to characterize the fate of the nanoparticle labelling. This was performed by removing the retinal tissue as a whole mount. RGCs were retrograde labeled *in-vivo* with carboxylate modified microspheres in red, Nuclei were stained *ex-vivo* with Hoechst33342 in blue. Images were 50x magnified in a well-defined are of $(0.24mm)^2$ selected for taking images. These retinal wholemount analyses confirmed that FITC-Dextran, PVP-Dil and PVP-FITC NPs were not able to pass the BRB. This could be seen by the absence of FITC or Dil signal outside the vessels which agree with the *in-vivo* finding where only the blood vessels were found to be regularly labeled by these signals, (Fig. 22, 23 and 24) with no distribution in the blood compartment. In contrast, the PVP-Dil-CFSE NPs

signals were found inside the blood cells (signals of both dyes) and outside the blood vessels (this will be demonstrated more specifically in the next sections) confirming the blood-retina-barrier passage (Fig. 25).

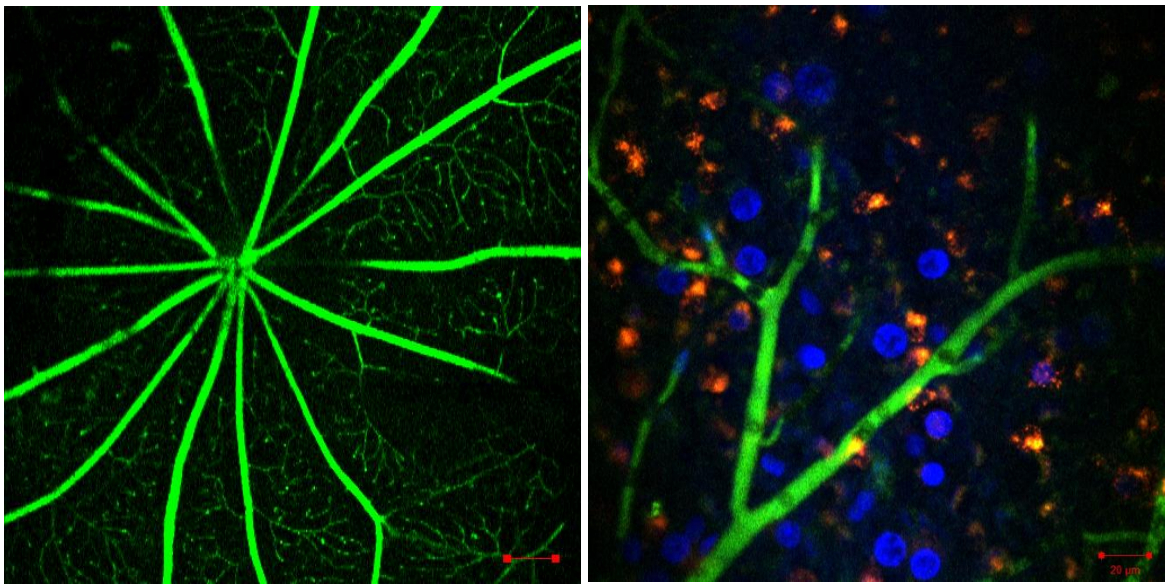

Fig. 22: *Ex-vivo* imaging, left :5X, right: 50X. Left: retina wholemount mono labelling, blood vessels in green by FITC-Dextran. Right: retina wholemount triple labelling, blood vessels in green by FITC-Dextran (Ex 495/Em 519 nm). RGCs in red (fluorospheres) (Ex540/Em560). Nuclei in blue (Hoechst33342) (Ex350/Em 460 nm). Virtually no blood cells staining. Micrographs taken 60 min after injection. Scale bar: left 200 µm, right: 20 µm.

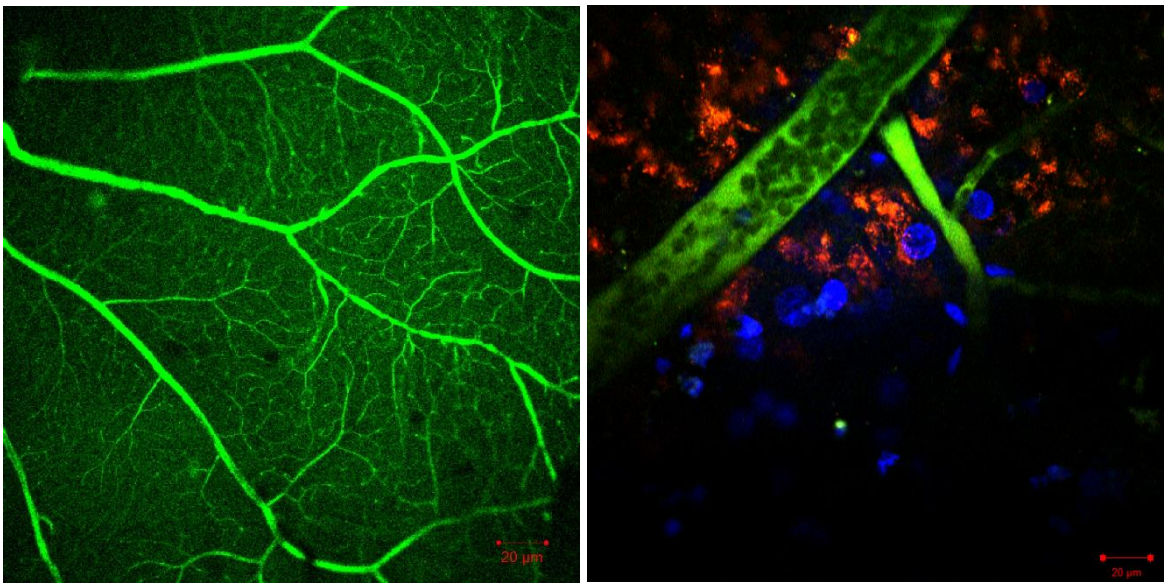

Fig. 23: *Ex-vivo* imaging, left :5X, right: 50X. Left: retina wholemount mono labelling, blood vessels in green by PVP-FITC NPs Right: retina wholemount triple labelling, Blood vessel in green by PVP-FITC NPs (Ex 495/Em 519 nm). RGCs in red (fluorospheres) (Ex540/Em560). Nuclei in blue (Hoechst33342) (Ex350/Em 460 nm). Virtually no blood cells staining. Micrographs taken 60 min after injection. Scale bar: left 200 µm, right: 20 µm.

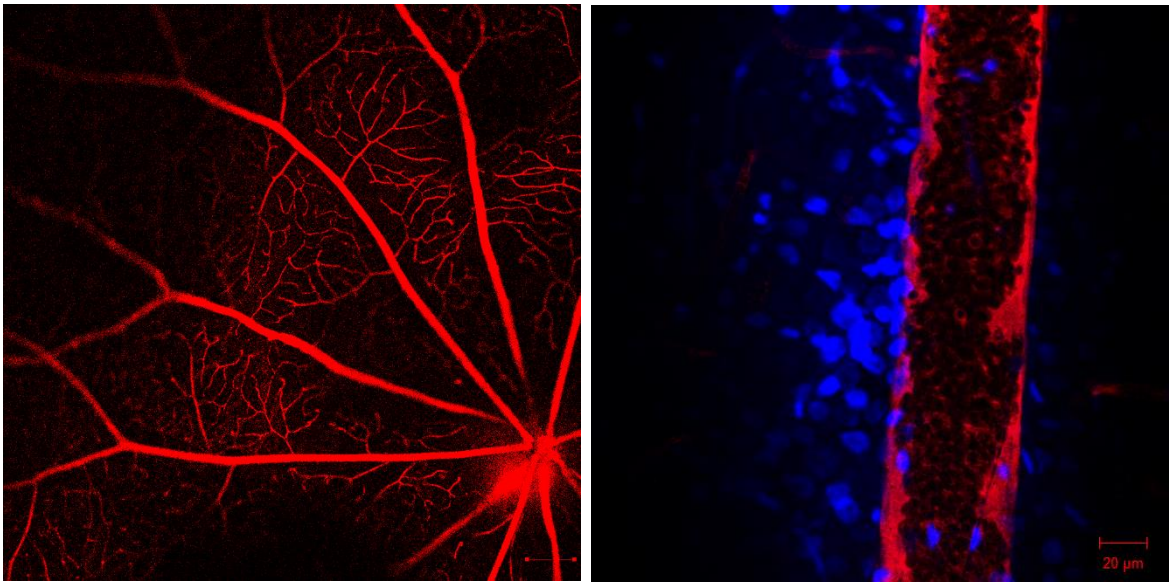

Fig. 24: *Ex-vivo* imaging, left :5X, right: 50X. Left: retina wholemount mono labelling, blood vessels in red by PVP-Dil NPs. Right: retina wholemount double labelling, blood vessels in red by PVP-Dil NPs (Ex540/Em560 nm), Nuclei in blue (Hoechst33342) (Ex350/Em 460 nm). Virtually no blood cells staining. Micrographs taken 60 min after injection. Scale bar: left 200 µm, right: 20 µm.

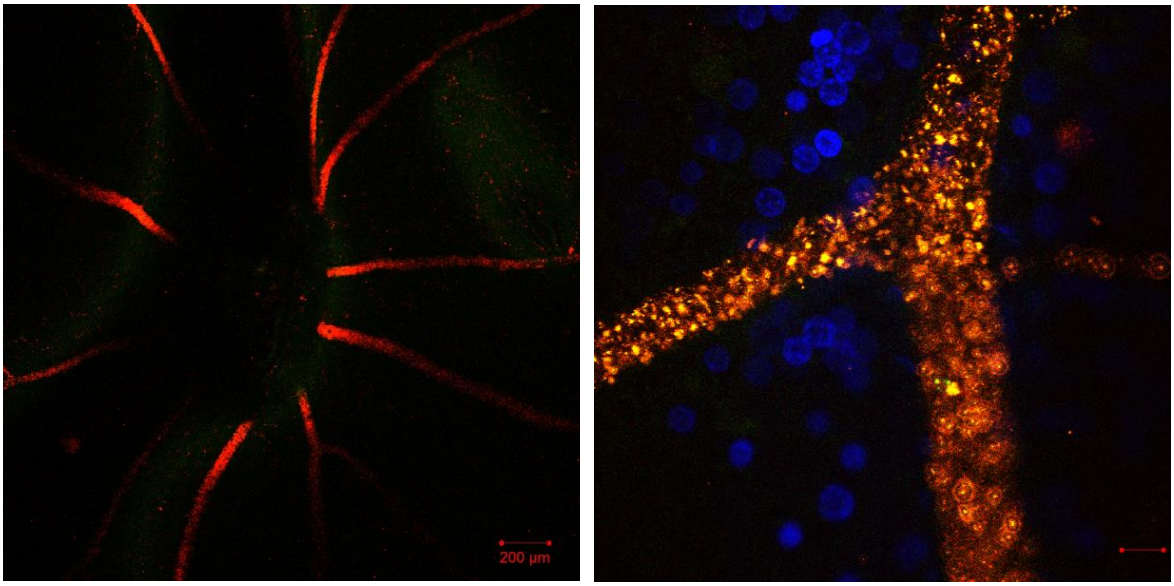

Fig. 25: *Ex-vivo* imaging, left :5X, right: 50X. Left: retina wholemount double labelling, blood vessels in green and red by PVP-Dil-CFSE NPs. Right: retina wholemount double labelling, Blood vessel in green + red (PVP-Dil-CFSE, merged signals of Dil and CFSE), (Ex540/Em560 nm), Nuclei in blue (Hoechst33342) (Ex350/Em 460 nm). Blood cells staining. Micrographs taken 60 min after injection. Scale bar: left 200 µm, right: 20 µm.

3.3.4. Quantitative comparisons of different NPs

As previously shown by others (144,148), it is possible to estimate qualitatively the passage of NPs through the BRB using ICON. As a next step I examined different quantitative parameters to be able to objectively decide whether NPs passed the BRB or not. To this end, I

compared the *in-vivo* imaging data from the three different NPs (PVP-Dil, PVP-FITC and PVP-Dil-CFSE) at different time points (1-10, 20, 30, 40, 50 and 60 min) and measured the intensities using Arivis Vision 4D software. Images of each individual rat before and at several time points after injection were aligned to focus the analysis on the same area of the retina throughout the experiment.

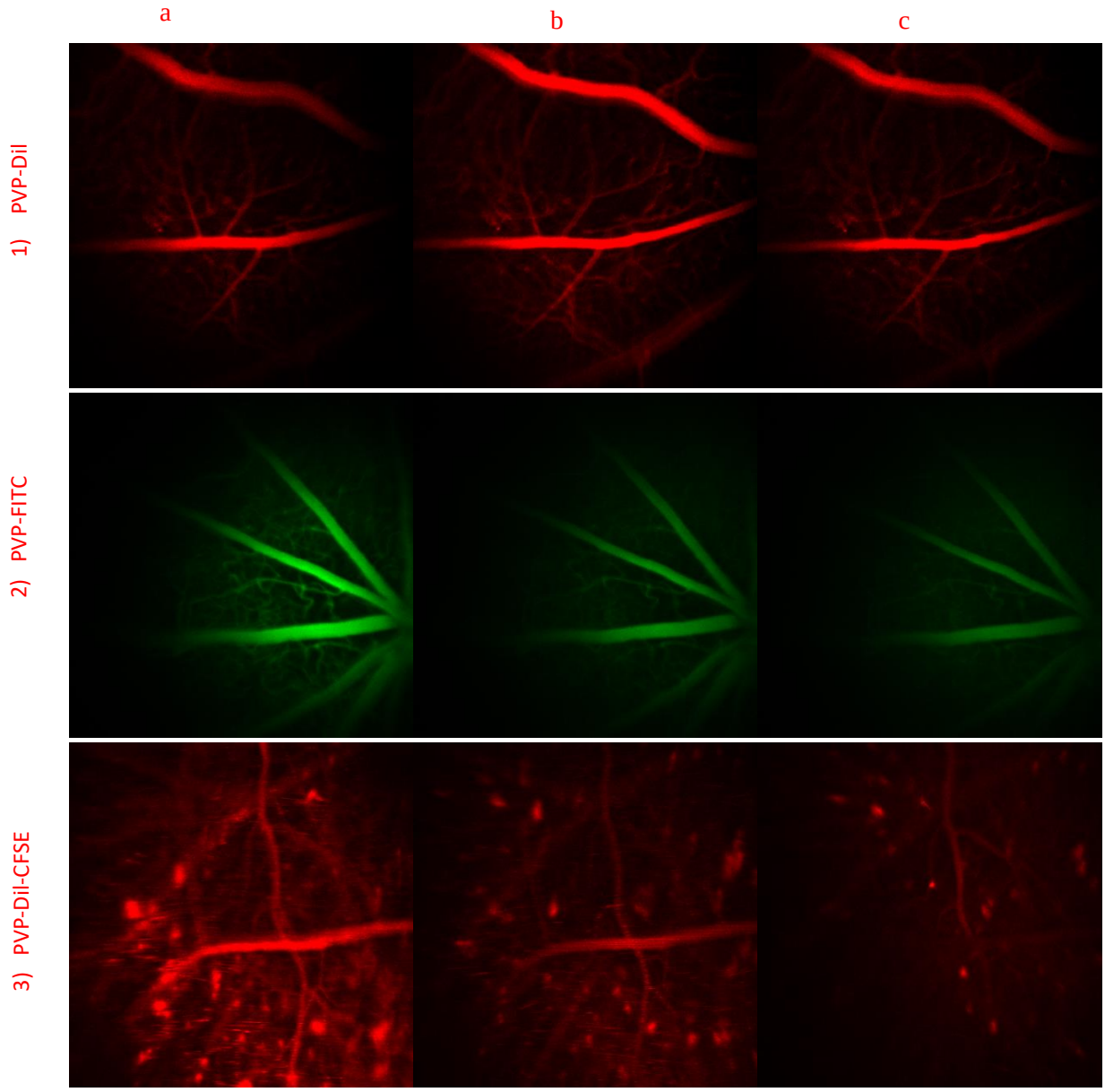

Fig. 26.1, **26.2**: PVP-Dil NPs and PVP-FITC NPs not passing the BRB and accumulating in the vessels. (Ex540/Em560 nm), (Ex 495/Em 519 nm) respectively. **Fig. 26.3**: PVP-Dil-CFSE passing the BRB and Dil signal accumulating in retina tissue, (Ex540/Em560 nm). (**A**: 1 min after injection, **B**: 10 minutes after, **C**: 60 minutes after). Scale bar: 200µm.

Figures 26.1, 26.2 and 26.3 show the three different NPs over multiple time points with very different results regarding BRB passage and overall image dynamics. Both PVP-Dil and

PVP-FITC show high intensity fluorescent signals which only appear in the blood vessels indicating no passage across the BRB. In contrast, the images of PVP-Dil-CFSE show multiple blobs like regions with high intensities outside the blood vessels (Dil signal). These blobs are clear signs for the passage of NPs through the BRB. Interestingly, the intensity values in the PVP-Dil and PVP-FITC images are not declining in the vessel compartment as in the case of PVP-Dil-CFSE NPs. In the case of quantifying the PVP-Dil-CFSE NPs, I used only one laser (540 nm) to excite the Dil without the (490 nm) which excites the CFSE to avoid any damage for the retina or laser bleaching which can alter the quantification process and also to use it as a comparison with the PVP-Dil NPs' kinetics.

3.3.5. Analysing PVP NPs' passage in retina tissue

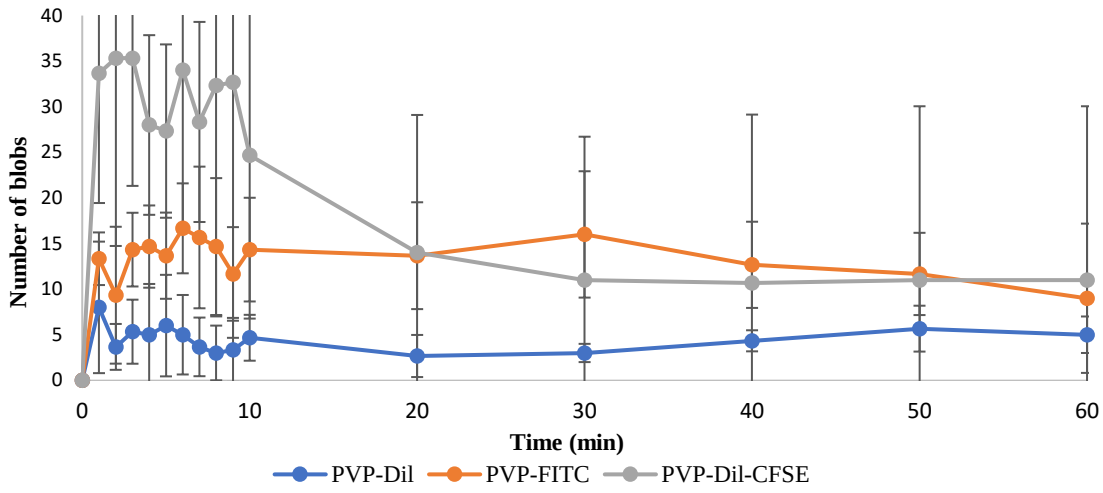

Time after injection (min)	PVP-Dil NPS	PVP-FITC NPs	PVP-Dil-CFSE NPs
1	*	*	*
5	*	*	*
10	*	*	*

Fig.27: Number of blobs of different Amph-PVP NPs in retina tissue over time (min). (n=3 per NP variant). Means±SD. Table 2 beneath the line graphs show the statistical results of fluorescence intensity at the first 10 minutes. *$P < 0.05$, compared between groups.

Figure 27 shows the quantitative analysis results of fluorescent signals of the incorporated marker for the three different NPs in retina tissue gathered with ICON over three different experiments as described in the previous section. It clearly shows two different behaviors. The blue and yellow curves (signals from PVP-Dil NPs and PVP-FITC NPs, respectively) show low values all over the chart (below 22), whereas 2 out 3 of the red curves (Dil signal in PVP-Dil-CFSE NPs) start with a high peak ranging from 30 up to 61 in the first 10 minutes and then dropping to smaller values. These numbers perfectly match the qualitative analysis showing penetrations only for PVP-Dil-CFSE NPs in these first 10 minutes. Thereafter, the markers seem to have been partially eliminated. Based on this observation I could now define a threshold to automatically judge when a NP passes the BRB such as at least 30 blobs per image which is basically the highest number of the control samples (around 20) plus a little margin of error (such as 50% more penetrations than the control) to remove false positives. Quantitative comparisons of different NPs fluorescence intensities in retina tissue (see Table 2) were found to be statistically significant during the first 10 minutes.

3.3.6. Analysing PVP NPs concentrations in blood vessels

Individual blobs could be found over all time points, i.e. their intensities are significantly higher than the background. Regarding all three NPs, such high intensities could be detected in blood vessels only directly after the injection of NPs (no blobs). After approximately 20 min the Dil signal of the PVP-Dil-CFSE NPs has been washed out of the blood vessels. It is therefore nearly impossible to identify vessel pixels in later time points. In case of PVP-Dil and PVP-FITC the signals inside the vessels could be observed longer. But for PVP-FITC the image with the highest intensities is also to be found in the first couple of minutes. Hence, I decided to augment the process of identifying the blood vessels as described in the section above by some additional steps. First, I identified the vessel pixels only in the first time point after the injection. Then, I mask out automatically all regions where I have found blobs in the previous steps. That means I only consider those pixels of the blood vessels where the BRB was not passed. In this way, I could make sure that the following analysis was not impaired by any interactions of the penetrating NPs and the surrounding retina tissue. Based on this result I then evaluated the mean intensity for all time points.

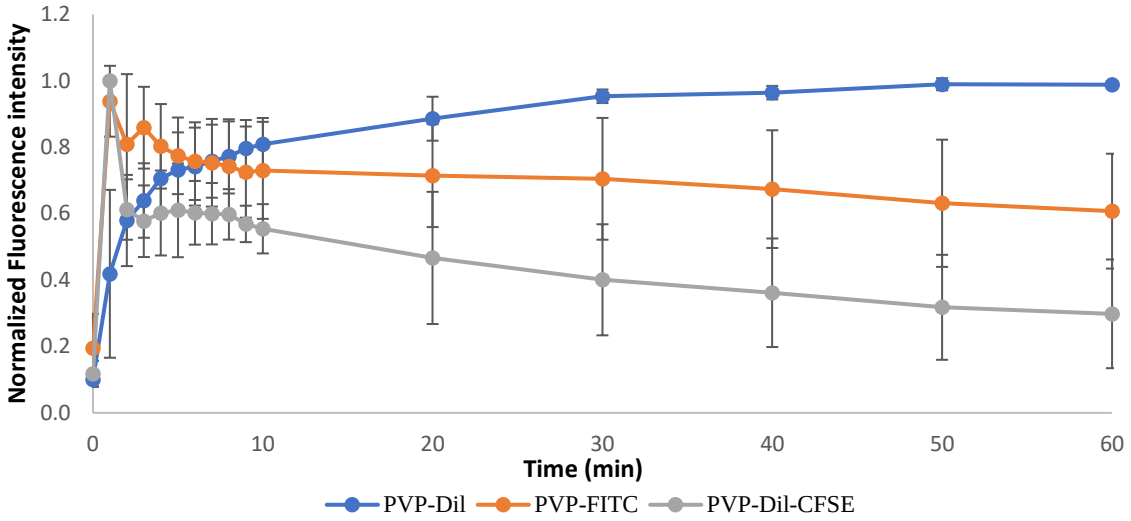

Time after injection (min)	PVP-Dil NPS	PVP-FITC NPs	PVP-Dil-CFSE NPs
1	*	*	*
5	*	*	*
10	*	*	*

Fig.28: Number of blobs of different Amph-PVP NPs in blood vessels over time (min). (n=3 per NP variant). Means±SD. Table 3 beneath the line graphs show the statistical results of fluorescence intensity at the first 10 minutes. *$P < 0.05$, compared between groups.

Figure 28 shows the result of the analysis of the *in-vivo* fluorescence intensities of the vessels from the same optical slices used for BRB penetration analysis in figure 27. As the intensity range differs between the different rats, I normalized the curves using only the maximum intensity value of each curve. Expectedly, in all cases the charts start with a high intensity increase immediately after the injection. But only for PVP-FITC and PVP-Dil-CFSE the curves then dropped down. In contrast, PVP-Dil curves' rises throughout the whole-time interval. From this plot one can easily discern different imaging dynamics regarding the entrapment of NPs in the veins or washing out of the system. Quantitative comparisons of

different NPs fluorescence intensities in blood vessels (see Table 3) were found to be statistically significant during the first 10 minutes.

3.3.7. *Ex-Vivo* Co-localization of NPs in wholemount images

Using *ex-vivo* co-localization tests it was possible to demonstrate the role of CFSE attached to the PVP surface for the distribution of the NPs between vessels and tissue by comparing the number of pixels induced by Dil (540 nm) and CFSE (490 nm) in the blood vessel compartment 60 min after injection. The results were still rather variable between individual rats, yet the mean difference is clear (n=3): 157,307.3 ± 65,260.8 pixels were counted on average for "Dil only" signals and 28,904 ± 14,245.4 for the "CFSE only" signals. Merged signals of Dil and CFSE resulted in 44,748.6 ± 24,105.4 pixels after thresholding above an intensity of 1,000. (Fig. 29)

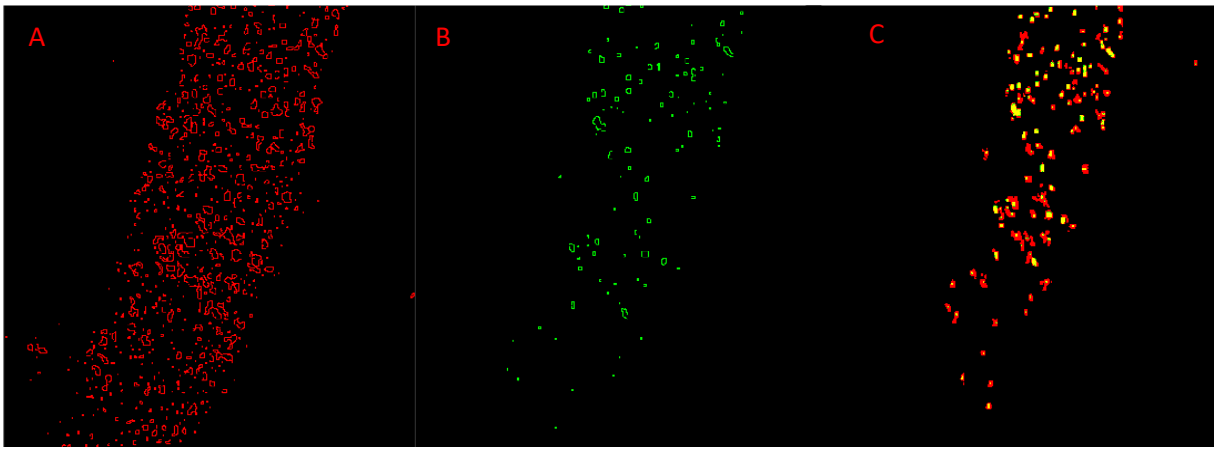

Fig. 29: *Ex-vivo* co-localization test in retinal blood vessel. A: Dil abundance in the blood vessel (Ex540/Em560 nm). B: Lower CFSE abundance (Ex 495/Em 519 nm). C: Both signals merged. (n=3).

3.3.8. *Ex-vivo* 3D videos of NPs in whole-mounted retina

Using the *ex-vivo* labelling method, it was possible in cooperation with Arivis AG to create 3D videos. They allowed us to evaluate the tissue depth of the imaging signals in a 3D construction to confirm that the PVP-Dil-CFSE NPs passage through the BRB. The confirmation came from detecting the Dil signal outside the blood vessel with the addition of the third dimension (https://www.youtube.com/watch?v=_-3GFI5rng8). (Fig. 30). The PVP-Dil-CFSE NPs distribution was different from the PVP-Dil NPs' because in the latter case the signal was detected only inside the blood vessels (https://www.youtube.com/watch?v=sDa-OW2H018) (Fig. 31).

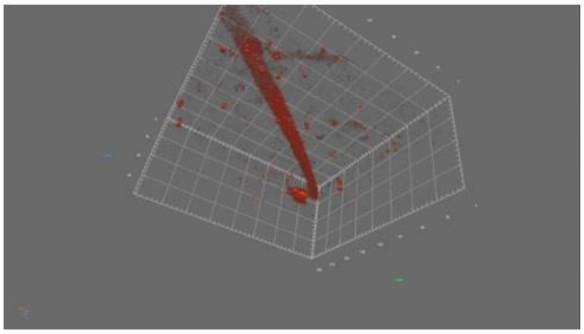

Fig. 30: *Ex-vivo* single labelling, 50X
Blood vessel in red (PVP-Dil-CFSE), 543 nm,
Detection of Dil signal in retinal tissue
(n=2).

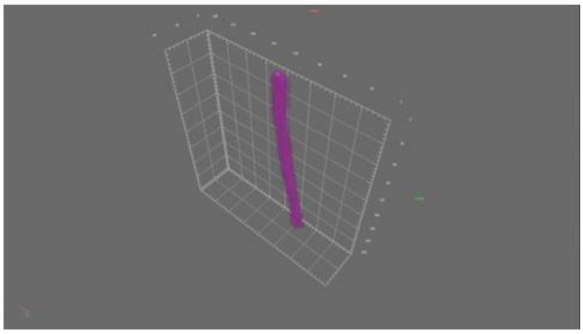

Fig. 31: *Ex-vivo* single labelling, 50X,
Blood vessel in violet (PVP-Dil), 543 nm,
No detection of Dil signal in retinal tissue
(n=2).

3.4. Discussion

A number of different retinal diseases are associated with pathological changes in the posterior segment of the eye. Although a remarkable achievement in drug delivery techniques has been attained, the finding of a safe and effective treatment for retinal diseases is still ongoing (170,171). In the same context, the present standard methods for analyzing pharmacokinetic parameters of the BRB passage such as the integration plot analysis, retinal uptake index or microdialysis are unfortunately complex and expensive. Besides, to study the pharmacokinetic profile of a drug single dose, around 120-150 experimental animals are sacrificed (172,173). In contrast, ICON can provide a live *in-vivo* imaging for the entry of NPs across the BRB without sacrificing the animal. Herein, the ICON method was used to visualize and analyze the BRB passage of nanoparticles. However, with ICON data it is difficult to quantify the NPs' entry. One reason is the movement of the rat's eye due to the heartbeat and respiration which results in drifts of the captured region. This makes the images inherently noisy when using the required (non-toxic) low laser intensity which prevents both damage to the rat's retina and reduces the probability of laser-induced bleaching. In addition, the intensity of the fluorescence range of NPs differs extensively depending on which dye is used. To solve these problems, I utilized the specialized Arivis Vision 4D software. Specifically, the eye movement problem was reduced by utilizing a semi-automatic drift correction approach. This analysis requires first a manual identification of at least one recurring position in the image such as a branching point of the blood vessels at each time point and then using their displacement for an automatic realignment of the images. Finally, the images are cropped to those regions which all time points have in common, so missing pixels will not falsify (or bias) the subsequent numerical

evaluation. To be able to remove any distortions by 2D or 3D rotations, two or three recurring positions have to be identified, respectively. Regarding the imaging noise and intensity range variations, I reduced these problems during the design phase of the methods by utilizing both denoising algorithms and partially intensity invariant analysis algorithm to distinguish retinal tissue from blood vessels. Hence, I did not need to identify individual analysis parameters for different NPs which enable us to automate the analysis. In this way I was able to test and characterize the different kinetics of the newly designed PVP-nanocarrier variations.

To date, intravitreal injection is the gold standard method widely to treat retinal disorders. However, its side effects are still critical such as cataract and increase in the intraocular pressure. In addition, intravitreal injection has a minimal target effect in the posterior section of the eye due to the thickness and function of the retina (174). In the same line of reasoning, systemic application, i.e. intravenous injection (i.v.), of bevacizumab for the treatment of wet AMD has achieved phase 2 of clinical trials (175). Hence, the problem of unspecific retina drug distribution, may be even solved with future innovative techniques such as photo-targeted nanoparticles which have been studied for the treatment of choroidal neovascularization after intravenous injection (176). This highlights that the potential of i.v. administration of NPs may be safer and more effective to target the retina. Still, the BRB is a challenge for most systemically applied pharmaceutics. Moreover, it has been shown that naked gold nanoparticles with particles size of 20 nm were found to cross the BRB after intravenous injection but not for particles with 100 nm of size showing that crossing the BRB is size dependent (177). But our lab previous findings showed that surface modification is the main key for passing the BRB (148).

Physicochemical characterizations showed that the values of CMC for both PVP polymers are in the micromolar range which means that these polymers will have a good ability to form stable aggregates in aqueous media and to incorporate hydrophobic drugs by forming NPs. At the same time, CMC values are not too low, therefore I expect the NPs to be rather stable. This contrast, for example, PVP-ODM polymers which have a molecular weight of 1kDa, a CMC of ~0,04 mmol/l and do not form stable NPs (178,179). As shown in table 1, PDI values of PVP-Dil, PVP-FITC and PVP-Dil-CFSE NPs were about 0.235, 0.200 and 0.383 respectively, which for micellar system means a rather narrow size distribution.

Concerning the zeta potential, the values of the nanoparticles are below the standard stability range (+/- 30 mV). However, fabricated NPs are stabilized not only by electrostatic forces but also by hydrophobic interactions. Further, Amph-PVP NPs can maintain their stability upon dilution by blood, which was confirmed by experiments that showed the NPs stability in blood with a wide range of concentrations (180,181). Moreover, the low molecular weight of the polymers may also

suggest their path of excretion (through kidneys and liver) which is expected to reduce additional cleavage within the organism (164). As also demonstrated by my experiments NPs can be taken up by blood cells, endothelial cells or remain in the plasma. I assume that the NPs studied in this project did not form significant agglomerations after injection as this would lead to obstruction of micro-vessels and capillaries, and, in worst case, to death. However, I neither detected obstructed vessels in the *ex-vivo* wholemount preparation nor did animals die after injection.

The first aim of my study was to investigate PVP NPs with two different incorporated hydrophobic compounds to observe how this might affect their fate or imaging dynamics as it was shown before by Zhang et al. that the cargo may affect the fate of the nano-system (182). I found that the type of cargo had no effect on passing the BRB. This suggests that they can be used for a "one fits all" carrier system for delivery of hydrophobic drugs. In fact, they exhibited almost the same residence time in blood vessels (2 hours) and Fig. 19 and 20 indicating that the cargo accumulates in the vessel walls. This rather long circulation can be attributed to their hydrophilic surface which slows down their recognition time by the reticuloendothelial system (183). However, further studies are needed to decide whether the NPs circulate in the blood vessels or if they are taken up the endothelial wall of the blood vessels.

The next step was to study the effect of surface modification of the NPs on the BRB passage after linkage with a hydrophobic fluorescent marker (CFSE) where the polymer (PVP-AA-ODM) was used resulting in the PVP-Dil-CFSE with a negative zeta potential. Results were promising as the accumulation of the NPs in the retina parenchyma was detected after 5 min of injection. The circulation time in the blood was around one hour. This shorter circulation –as compared to the PVP NPs without surface modification- is perhaps due to the hydrophobic surface induced by the CFSE, which, in turn, speeds up the opsonization process resulting into fast clearance (183). Still, this could be attributed to the fact that CFSE enhance the up-take into the retina tissue which consequently resulted in the disappearance of PVP-Dil-CFSE from blood vessels showing that the hydrophobic character of CFSE seems to be essential for crossing the BRB. This is in line with the results of the double-labelling analysis which revealed that only a minor part of the fluorescent signals was co-localized and the vast majority of DiI was detected as "DiI only" in the blood vessels (see Fig. 29). According to our lab previous data, "DiI only" will not pass the BRB (182). As neither application of DiI alone nor of PVP-Dil NPs leads to an accumulation of the fluorescent dye in the brain, I assume that the PVP NPs with the CSFE-modification crossed the BRB and delivered the cargo to the retina tissue. When investigating by *in-vivo* imaging of the same retina micrographs using two different lasers separately: one exciting the Dil (540 nm) and the other the CFSE (490 nm) 15 min after injection. Signals of Dil loaded in the NPs were found to be much more abundant than the

CFSE signal (Fig. 32) which was confirmed with the *ex-vivo* co-localization test. The images from the retina do not tell whether any of the fluorescent dyes is still associated with the nanoparticle-polymer. Therefore, pharmacokinetic release profiles *in-vitro* or *in-vivo* need to be performed in future studies. However, as outlined before, the BRB passage can most probably only be accomplished by the complete PVP-DiI-CFSE nano-carrier system. In this sense, the surface modification of PVP-NPs indicated again that the surface chemistry is a critical factor for passing the BRB which is in agreement with a previous study from our lab (148), Besides, finding a new NPs' composition rather than surfactants to facilitate the BBB passage might open new windows of opportunity for the development of nano-neuropharmacological treatments.

Imaging the wholemounted retinae allowed me to determine the NPs' distribution within the tissue, i.e. whether NPs remain within the lumen of vessels or cross the BRB. It was obvious that (PVP-Dil or PVP-FITC) remained in the blood vessels while circulating in the blood for 2 hours. In the case of PVP-Dil-CFSE, I was able to observe the NPs internalized by blood cells. This could be because CFSE is a substance that has been found to be particularly effective at monitoring blood cells proliferation (184,185). Therefore, the role of the CFSE in passing the NPs through the BRB as well as internalize them in the blood cells, could be understood. Thus, I assume that the uptake of the NPs into blood cells per se is not causal for the BRB passage of the cargo. Furthermore, imaging the same retinal location using the two lasers separately revealed as well the existence of CFSE and Dil in the blood cells (Fig. 33) which was not revealed by the *in-vivo* imaging (Fig. 32). In contrast, DIL can only penetrates the cell membrane when altered which probably was not the case under these conditions (186). Thus, being hidden in the blood cells, suggests strongly the usage of PVP-Dil-CFSE NPs as a nano-carrier which represent human-made delivery carrier that share characterizations fundamentally engineered by nature. Consequently, this could pave the road to use a biomimetic nanocarriers platform which links synthetic materials with natural compounds (82,187-190).

My results show promising first proof that it is possible to use ICON also for a quantitative analysis. In the future we might, in fact, be able to automatically evaluate different characteristics such as the passage of the BRB or agglomeration of NPs. Considering that the drift correction, the only required manual step, is only necessary for the projection of analysis results to other time points, the remaining steps are already processed automatically. For the task of counting blobs, human judgement might no longer be required but can run autonomously; especially when the filtering of false positives can be enhanced in the future. Besides the two proposed parameters additional morphological features can be evaluated such as the size of the blobs to filter out more false positives from the analysis or even test the efficacy of BRB penetration automatically.

Finally, because the retina can be used as a window to the brain and the BRB is an analogous for the BBB, I propose the PVP-Dil-CFSE NPs not only for ophthalmic purposes to treat posterior eye diseases, but I believe they are also valuable for drug delivery across the BBB into the brain. Nevertheless, knowing in which cells are the NPs taken up after they leave the retinal blood stream will help to narrow down the diseases they could target. The other two nano-carriers tested, i.e. PVP-Dil and PVP-FITC NPs, may be a promising tool for the diagnosis and treatment of retinal vascular diseases.

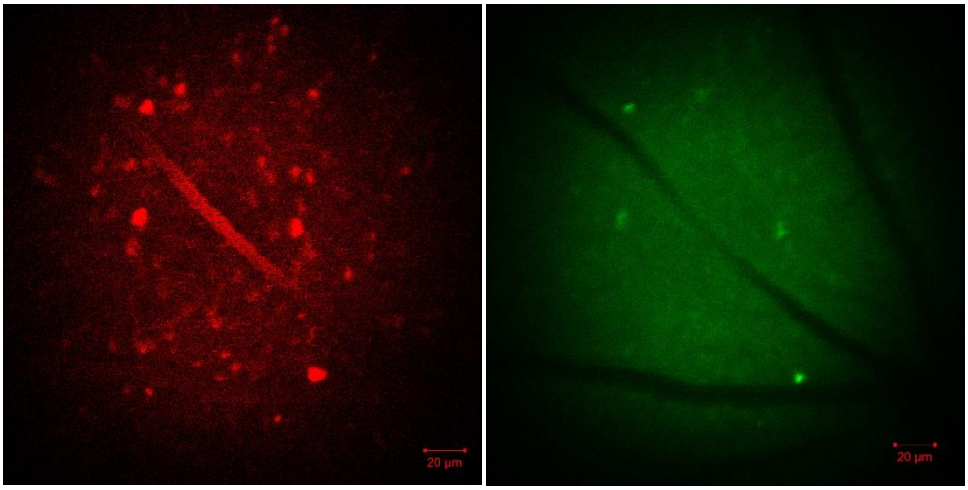

Fig. 32*:* Same *in-vivo* retinal location showing the effect of CFSE in crossing the BRB, (left) is showing the Dil (Ex540/Em560 nm), excitation with more blobs while (right) is showing the CFSE excitation with fewer blobs (Ex 495/Em 519 nm). Scale bar: 200µm

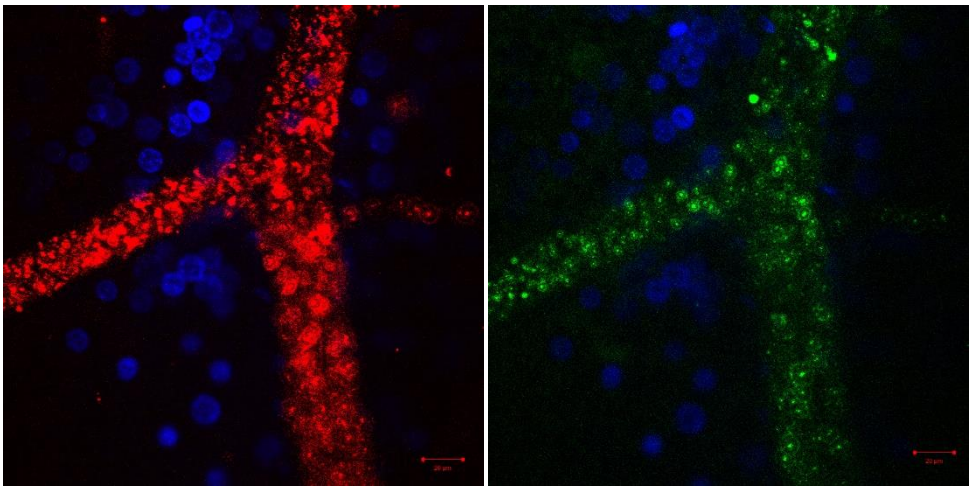

Fig. 33: Same *ex-vivo* retina location showing CFSE signals (Ex 495/Em 519 nm) in blood cells (left). Dil signals (Ex540/Em560 nm) in blood cells (right) Scale bar: 20µm.

4. Gene therapy with caspase-3 siRNA-nanoparticles is neuroprotective after optic nerve damage

4.1. Introduction

Apoptosis, a programmed cell death, plays a crucial role in development, degeneration, and regeneration in many body organs, also in the brain. Many factors such as aging and trauma can trigger apoptosis, but the cardinal trigger for apoptosis is caspase-3 (191,192). Because apoptosis in the central nervous system (CNS) can lead to irreversible neurological dysfunctions, finding means to reduce or stop caspace-3 synthesis could be a promising approach to slow down of halt neurodegenerative diseases (193). Thus, I selected the visual system as a model to evaluate the possibility of neuroprotection by blocking caspase-3 synthesis via nanoparticulate delivery of small interfering RNA (siRNA) to the retina (CaspNPs). Approximately, 95 % of RGCs population project to the superior colliculus and can be labelled via injection of a fluorescent marker into the rodent bilateral superior colliculus (194,195). ICON can visualize single RGCs non-invasively, repeatedly and in real time within their native environment and it has proven to be an effective tool to study the recovery mechanisms of RGCs after ONC *in-vivo*. (150,151).

As a CNS tissue, any findings in the retina might be applicable to other neuropsychiatric diseases. The loss of retinal ganglion cells (RGCs), a cardinal event in glaucoma, with associated optic nerve damage can happen suddenly or progress slowly towards irreversible neuronal death and vision loss. I used the well-studied preclinical glaucoma model of optic nerve crush (ONC) in adult rats, where 70% of the RGCs die by apoptosis within 28 days, through cleavage of caspases-3, -8 and -9. Especially elevated caspase-3 levels are problematic, reaching highest levels during a primary wave of RGCs loss, remaining high while RGCs degenerate (55,196,197).

Because caspase-3 is the key protein of apoptosis, its down-regulation may be achieved by blocking caspase-3 mRNA with its specific caspase-3 siRNA. On the one hand, pure siRNA injections and viral vectors possess certain limitations as well as inherent risks with unique safety challenges which require extensive engineering to satisfy governmental regulations and guidelines (198,199). On the other hand, pure siRNA cannot be utilized as a therapeutic agent because it has a short life span in serum, being rapidly degraded by ribonucleases, cleared by renal excretion, and non-specifically eliminated by the reticuloendothelial system. Even if siRNA is able to reach its target, it would be rapidly degraded by the highly acidic environment of the endosomes. In addition, pure siRNA could have adverse effects such as unwanted immune reactions or interferon responses

(200,201). Therefore, employing nanotechnology to protect siRNA from degradation and immune recognition would enhance bioavailability by reducing renal filtration and reticuloendothelial clearance (202). To overcome these pharmacokinetic limitations, I studied a siRNA delivery system using non-viral nanoparticle developed previously by Xiwei et al. While nanoparticles have been tested in clinical cancer trials before (203) and only one has received marketing approval for rare, inherited liver diseases using lipid NPs (204), none were successful for central nervous system delivery of siRNA where the blood brain barrier is an obstacle (205).

Biodegradable polymeric NP-systems are suitable delivery systems for the CNS, and they were already used in numerous preclinical studies for neurological and ophthalmic drug delivery (206,207). One kind of biodegradable nanoparticle widely studied for drug delivery across the blood brain barrier is fabricated with poly (butyl cyanoacrylate) nanoparticles (PBCA-NPs). Nucleic acids can be encapsulated in PBCA-NPs using mini-emulsion polymerization methods, but so far, their potential for gene therapy was only shown *in-vitro* by Zhang et al.

To this end, I have encapsulated caspase-3 siRNA in nanoparticles (CaspNPs) as a tool to down-regulate caspase-3 expression in neurons *in-vivo*. As I now show for the first time, following intraocular injections, CaspNPs can markedly downregulate caspase-3 and markedly reduce RGC death after optic nerve injury as visualized by repeated and non-invasive *in-vivo* confocal neuroimaging (ICON) for more than one month. CaspNPs are thus an effective siRNA-carrier-system for gene therapy to stop/prevent neuronal cell death for neural protection and rescue.

4.2. Materials and methods

4.2.1. Preparation of PBCA NPs

Briefly, 4.0 g Migyol 812N (a gift from Cremer Oleo GmbH) and the surfactant, which was composed of 0.08 g Tween 80 (Sigma-Aldrich) and 0.32 g Span 80 (Carl Roth), were mixed and marked as phase I. Then phase II, 1.2 g phosphate buffered saline (PBS, pH 7.4, 0.1 M) was added dropwise into phase I during stirring for a duration of 30 min. The emulsion was then homogenized by ultra-sonication with 50% amplitude for 60 sec. Thereafter, 100 µL butylcyanoacrylate (Henkel AG & Co. KGaA) monomer was added into the miniemulsion, drop by drop, whilst stirring. After 4 hrs, polymerization was completed, and the nanoparticles were collected by using centrifugation at 8,000 g for 5 min. The wet pellets were washed with ethanol 3 times and then redispersed in water. For siRNA loading, 5 nmol caspase-3 siRNA (Thermo Fisher) (Passenger: CCUUACUCGUGAAGAAAUUTT, Guide:

AAUUUCUUCACGAGUAAGGTC) in the 5′–3′ direction (Thermo Fisher) was diluted in phase II and then loaded into the PBCA NPs. The concentration of these siRNA in the PBCA NPs was 3.3 µM. All steps of the protocol were performed at room temperature (except the homogenization step which was performed on ice to prevent heating of the solution). The same procedure was used for producing blank NPs (PBS) for the in-vivo study, except that no siRNA was added (Performed by Ms. Lisa Grigatzik). (Fig. 34)

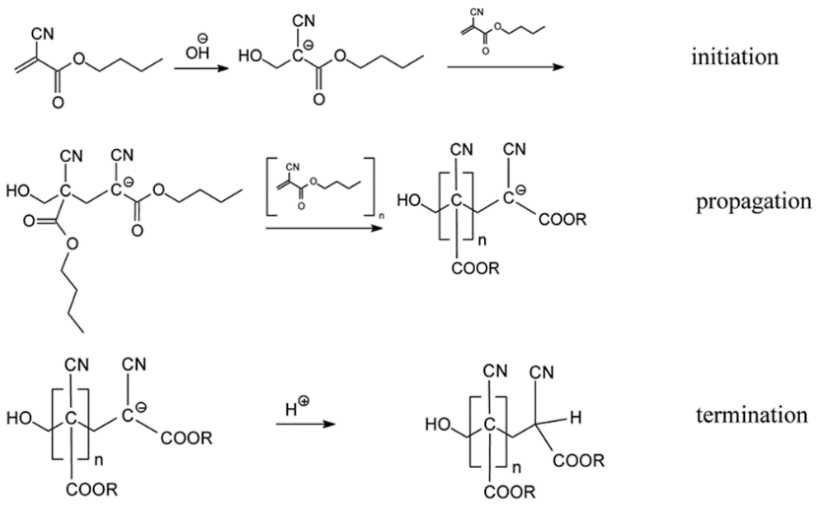

Fig. 34: Polymerization mechanisms of PBCA. (i) Initiation; (ii) Growth; (iii) Termination (102).

4.2.2. Intravitreal injection

Initially, the connective tissue was cut to detach the sclera, while pulling it with the colibri forceps. A sharp needle with a diameter of 0.8 mm then penetrated the sclera. The injection into the vitreous was performed by a Hamilton syringe with a blunt cannula (Performed by Ms. Lisa Grigartzik). (Fig. 35)

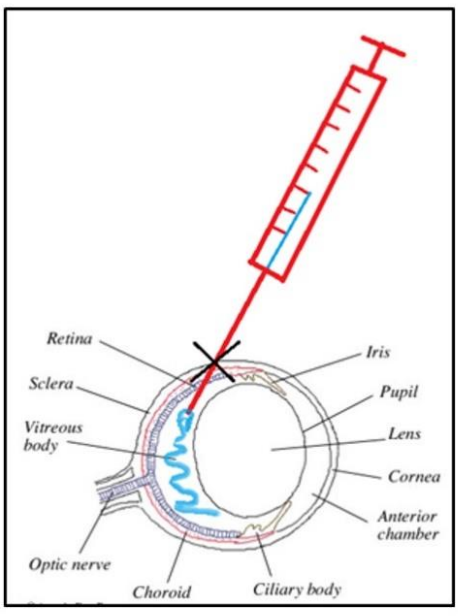

Fig. 35: The needle entered the vitreous body through the sclera. The black cross indicates where is the cut into the connective tissue and the insertion point for the needle and Hamilton syringe. Taken from reference (208).

4.2.3. Optic nerve crush and nanoparticles injection

Bilateral optic nerve crush surgery was performed, using a custom-made forceps as described in detail by Sautter et al. (209). Briefly, the rats were anesthetized, and the optic nerve crush was made with calibrated forceps (KLS Martin Group) applied for 30 s at 2-3 mm from the eye with the jaws of the forceps 0.2 mm apart, resulting in a moderate crush. Immediately after, the left eye was treated with 3 µL of casp3-NPs as the experimental condition, and the right eye was treated with blank PBCA-NPs as a control condition (Performed by Ms. Lisa Grigartzik). (Fig. 36)

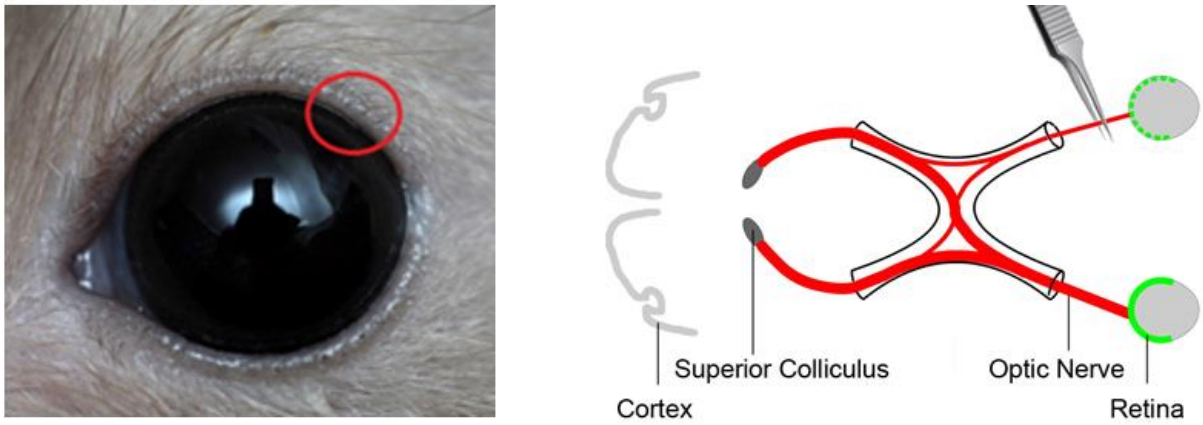

Fig. 36: Location of the intravitreal injection and optic nerve crush procedure. A rat eye, the red circle indicates the position of the cut site for the ONC (left). An illustrative diagram for the ONC procedure. Taken from reference (210,211).

4.2.4. Animals

A total of 18 adult, male Lister hooded rats (Crl:LIS Stamm; Charles River, 280– 380 g) were kept on a 12-h light / 12-h dark cycle (at 24–26°C and 50–60% humidity). For all procedures ethical approval was obtained as required by the German National Act on the use of experimental animals (Ethic committee Referat Verbraucherschutz, Veterinärangelegenheiten; Landesverwaltungsamt Sachsen-Anhalt, Halle), adhering to the ARVO Statement for the Use of Animals in Ophthalmic and Vision Research. Following shipment, animals were kept at least 3 days for adaptation in group cages and handled for 3 days before starting the experiments. The number of animals employed for ICON was as follows: a pilot study group; RGCs survival tracked 3 days post ONC (n=2); sub-group A: RGCs survival tracked for 21

days post ONC (n=10); sub-group B: RGCs survival tracked for 35 days post ONC (n=6). While CaspNPs were injected in the left eye (n=17), the right control eye (n=10) received Blank NPs. It turned out that imaging the same rats repeatedly with ICON on a weekly basis is a surgical (anesthesia and imaging) challenge. While all rats were treated and imaged on schedule (treatment: days 0 and 7; imaging: days 0, 7, 14, 21 and 35), I had several drop-outs when image quality was below standard because of spurious imaging artefacts and occasional problems with repetitive anesthesia. In order to reduce the artificial variability introduced by such dropouts, I pooled the cell counting results of the post-acute (days 7-14) and chronic phase (day 21-35). In addition, I calculated the average cell count across all time points (days 7-35) for each rat.

4.2.5. Surgery and RCG labelling

One week before retina baseline imaging, RGCs were selectively labelled by retrograde axonal transport of fluorescent tracer (n=18 rats). To this end, rats were anaesthetized by intraperitoneal injection of Ketavet/Dormitor (0.75/0.5 ml/kg). After drilling openings in the skull, carboxylate-modified microspheres were stereotactically injected (0.04 μm large FluoSpheres; Ex 580/ Em 605, Invitrogen GmbH, Karlsruhe, Germany) into the right and left superior colliculus (Coordinates: 6.9 mm posterior to Bregma and -/+1.2 mm lateral from midline). Slow injections of 0.5μl each were made at each of four different depths below dura (2.5, 3.5, 3.0, 4.0 mm), i.e. 2μl on each side with 30sec diffusion time per injection.

4.2.6. *In-vivo* microscopy with ICON

ICON was carried out 7 days after RGC labelling as previously described. Briefly, rats were anaesthetized by intraperitoneal injection of Ketavet (0.75 ml/kg) and Dormitor (0.5 ml/kg) and the eye' pupils was dilated with Neosynephrine-POS 2.5% (Arzneimittelherstellung Uniklinik Magdeburg, Germany). Vidisic optical gel was then applied as an immersion medium for the contact lens to prevent drying of the cornea (Bausch & Lomb, Berlin, Germany). Rats were then positioned under a standard confocal laser scanning microscope (LSM 880, Carl Zeiss AG, Jena, Germany) with a large probe space and a long working distance objective lens. The rat was fixed on the microscope stage with jaw holder to position the eye directly underneath the objective lens (Plan Neofluar 5x/0.15) after a Hruby style -80 dioptre plan concave lens (KPC-013, Newport GmbH, Darmstadt, Germany) was placed directly onto the cornea, and adjusted in such way that the path of the laser ray focused on the

retina plain. For each rat, I ascertained that images contained enough RGCs so that they could be located again for repeated imaging in the same rat at different time points (7, 14, 21 and 35 days) using blood vessels as landmarks (image size: 2.6 mm^2; image resolution: 800*800 pixels, 16-bit).

4.2.7. *Ex-vivo* retina wholemounts

Since the optics resolution of live retina imaging is limited, I also verified cell counts *ex-vivo* with wholemount retinae preparation. To this end, enucleated eyes (n=19) were placed *post-mortem* in Ca^{2+}-free solution (135 mM NaCl, 5 mM NaOH, 2.5 mM KCl, 2 mM $CaCl_2$, 1 mM $MgCl_2$, 10 mM HEPES, 10 mM glucose), the cornea and lens~~es~~ were removed, and the retina was separated from the pigment epithelium and kept on ice under constant oxygen supply. The tissue was then transferred into a petri dish and mounted on the microscope stage for LSM imaging (objective lens LDC Epiplan-APOchromat 50x/0.5; Image size: 0.24mm^2; image resolution: 800*800 pixels, 16-bit).

4.2.8. RGCs quantitative analysis *in-vivo* and *ex-vivo*

To avoid experimenter bias, RGCs images were coded and counted by me and another trained independent observer. We both were unaware of the animals group identity. At each imaging time point, we counted three separate images and both data sets were then averaged. To ascertain resolution-independent sampling, one observer counted the entire microscopic image (800*800 pixels) while the other counted smaller subsections (300*300 pixels). Thereafter, RGCs counts between time points were calculated as "percent change over baseline" (%COB) with the equation: ((post-value – pre-value) / pre-value) x 100 = %COB.

4.2.9. Statistical analysis

Cell counts were summarized as mean ± standard error mean (SEM) and statistically analyzed with SPSS Version Statistics 24.0 (IBM Corporation, Armonk, NY, USA). statistical differences between the two groups at each time point were analyzed using independent Student's t-test, where *P < 0.05 was considered significant. Statistical difference between the two groups with all the time points were analyzed by a two-way analysis of variance (ANOVA), where **P < 0.001 was considered significant. Post hoc least significant difference test (LSD) was performed to reveal statistical difference between groups. For a

better understanding of the ICON study sequence for sub-group A and B, timeline is presented in fig. 37:

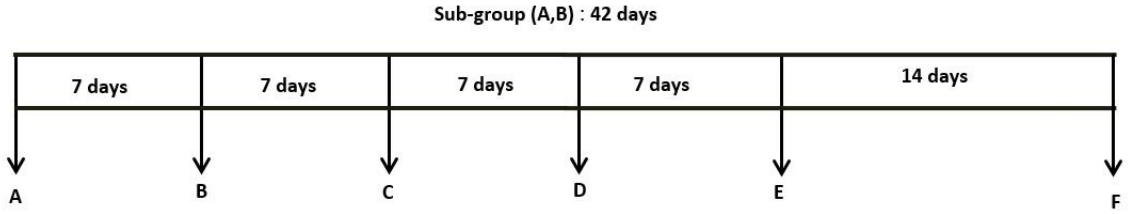

Fig. 37: (A): Day (-7) RGCs Labelling. (B): day (0), ICON baseline followed by ONC and 1st treatment. (C): day (7), ICON then 2nd treatment. (D): Day (14), ICON for sub-group A. (E): Day (21), Last ICON then wholemount retina for sub-group A. (F): Day (35), Last ICON then wholemount retina for sub-group B.

4.3. Results

4.3.1. PBCA Nanoparticles characterization

The particle size, the Zeta potential, and the polydispersity index (PDI) of PBCA NPs were measured using a Zetasizer. Results are shown are in Table 4

Table 4: PBCA-NPs physicochemical characterizations ($n \leq 5$ batches, $\bar{x} \pm s$)

	Z-Average (d.nm)	**PDI**	**Zeta Potential (mV)**
Empty PBCA NPs	124.08±16.24	0.26±0.02	-11.96±1.67
Casp-3-siRNA PBCA NPs	143.83±26.92	0.26±0.03	-9.87±2.74

4.3.2. RGCs *in-vivo* quantitative analysis

With ICON it is possible to repeatedly visualize retrogradely labelled RGCs *in-vivo* in anaesthetized rats (Fig. 38). Using image analysis, I compared the number of retrogradely labelled RGCs in ONC retinae treated either with CaspNPs or blank NPs (Fig. 39-42). The pilot study results were as follows: RGCs cell counts at baseline for group treated with CaspNPs and control group were (87.5 ±23.7, n=2) and (85 ±0.33, n=2) respectively. On day 3, counts became (84.5 ± 21.8, n=2) and (64.5±0.32, n=2) with a COB% of (-5.2% ± 0.78) and (-24% ±0.9), respectively. (Fig. 36) The main study results were as follows: At baseline, RGCs cell counts were similar in both groups (CaspNPs: 86.7±4.6, n=15; blank NP: 77.9 ±7.1, n=8), but during the acute post-acute phase following ONC

(days 7-14) more RGCs were found in CaspNPs (47.6 ± 5.7, n=15) compared to blank NPs treated rats (34.1±5.3, n=8) (n.s.). This difference was more apparent at later survival times in the chronic stage (days 21-35), where the CaspNPs group had significantly more RGCs (55.5±4.6, n=10) than the blank NPs group (30.2±6.5, n=5) (p=0.008). This was also true for the total count across all time points (CaspNPs: 50.9±5.4, n=15; blank NPs: 32.7±4.6, n=8; p=0.039). When expressed as percent change over baseline (%COB), in the post-acute phase, CaspNPs rats lost fewer RGCs (-45.3±4.8%, n=15) compared to blank NPs (-57.2±5.6%, n=8), but also here the differences were significant only in the chronic stage. Here, CaspNPs rats showed even a 25% recovery of RGC labelling (-36.1±4.2%, n=10) while the RGC number in rats treated with blank NP declined even further to -63.4±8% (n=5, p = 0.006). The %COB for the total time was -41.5±4.3% (n=15) in CaspNPs compared and -58.4 ±5.3% (n=8) in blank NP-treated rats (p=0.028).

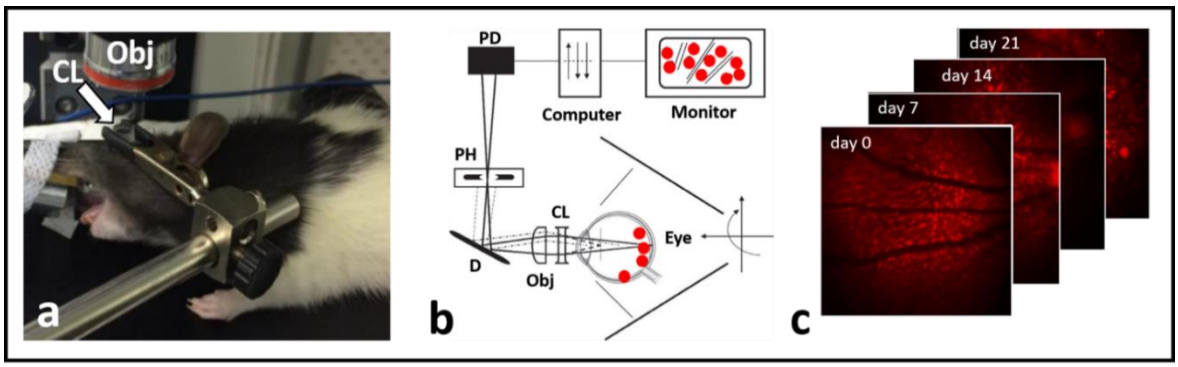

Fig. 38. *In-vivo* confocal neuroimaging (ICON) of RGCs. a: The head of an anaesthetized rat is positioned under the objective (Obj) of a scanning laser microscope (SLO) in a way that the laser beam can be focused on the retina of the eye. After passing through a contact lens (CL), the laser excites prelabelled RGCs. b: Cartoon of ICON set-up showing how a photodetector receives photons of fluorescent cell signals via deflector (D) and pinhole (PH). c: Red fluorescent cells in the retina then displayed for image analysis at different time points.

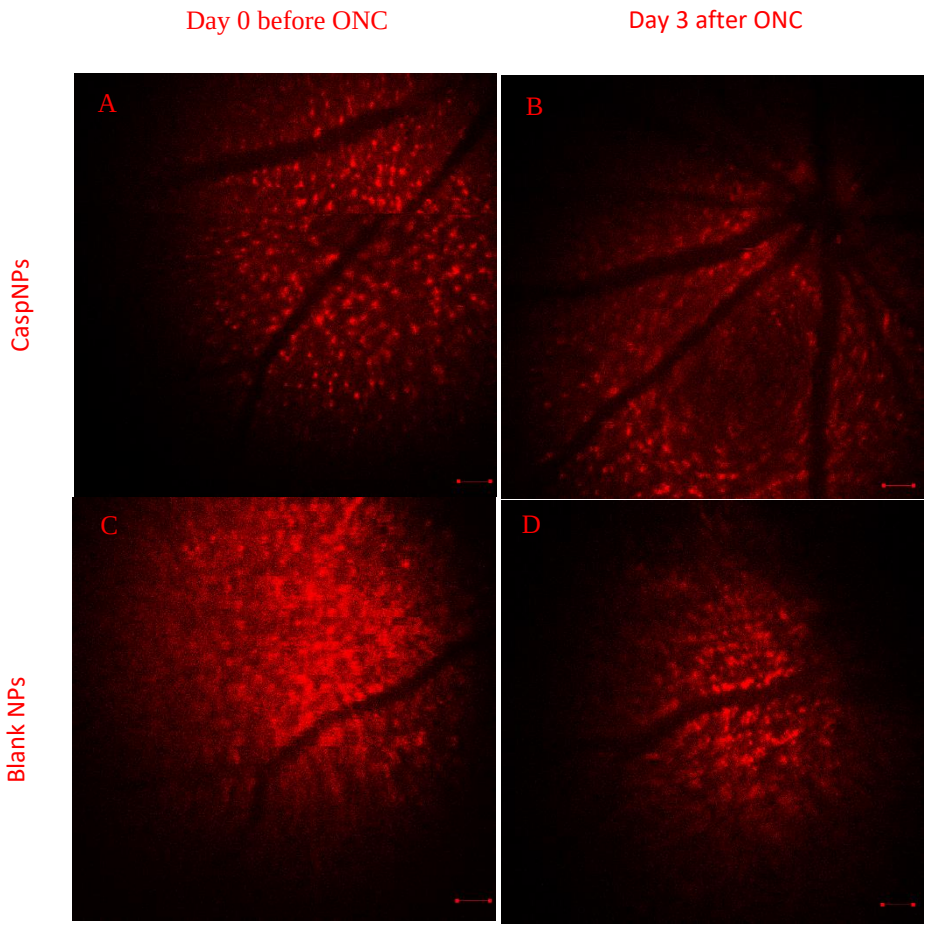

Fig. 39: Left, ICON baseline followed by ONC and 1st treatment. Right: day (3), ICON. Retinal blood vessels in black and RGCs in red. RGCs count in D less than B, (n=2). 2 µl microspheres (Ex 580/ Em 605). Scale bar 200 µm.

ICON micrographs showing RGCs before and after ONC for sub-group A. upper row retina treated with Casp3-NPs. Lower row retina treated with empty NPs. D0+T1; D7+T2; D14; D21

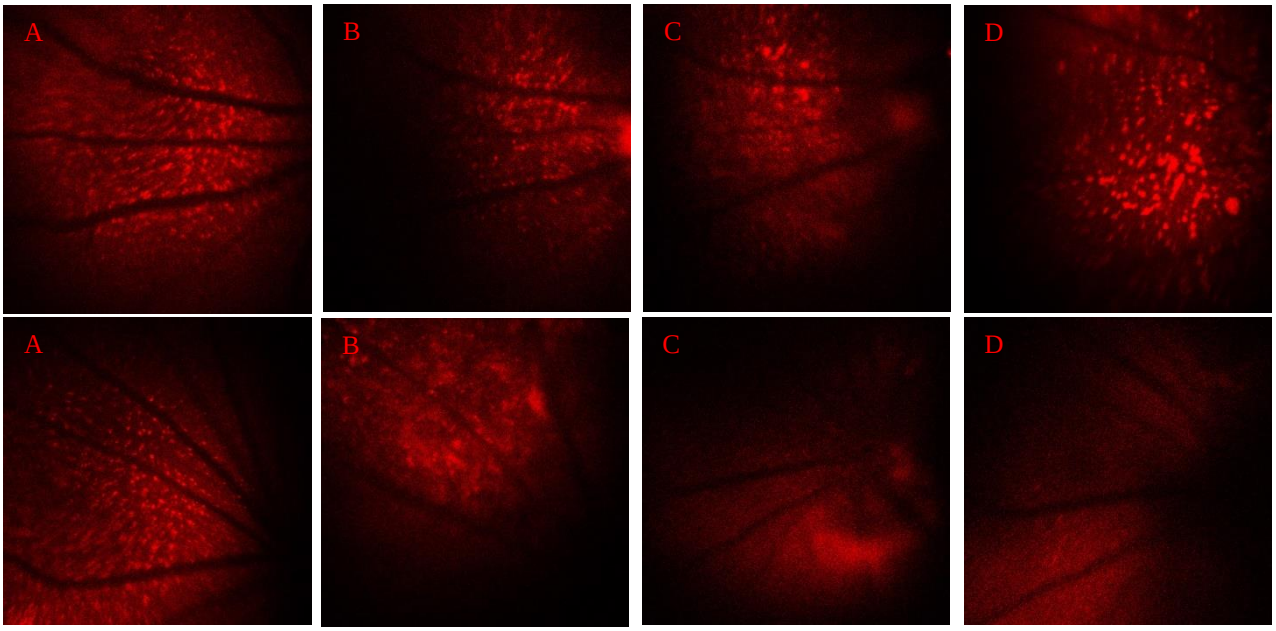

Fig. 40: Photomicrographs of ICON retinal images on (A) day 0 (baseline) followed by ONC plus 1st treatment; (B) Day 7, ICON plus 2nd treatment; (C, D) Day 14 and 21 ICON. Retinal blood vessels visible in black and RGCs retrogradely labelled with 2 µl microspheres (Ex 580/ Em 605) visible in red. The cell density decreased over time. Scale bar 200 µm.

ICON micrographs showing RGCs before and after ONC for sub-group B. upper row retina treated with CaspNPs. Lower row retina treated with empty NPs. D0+T1; D7+T2; D35

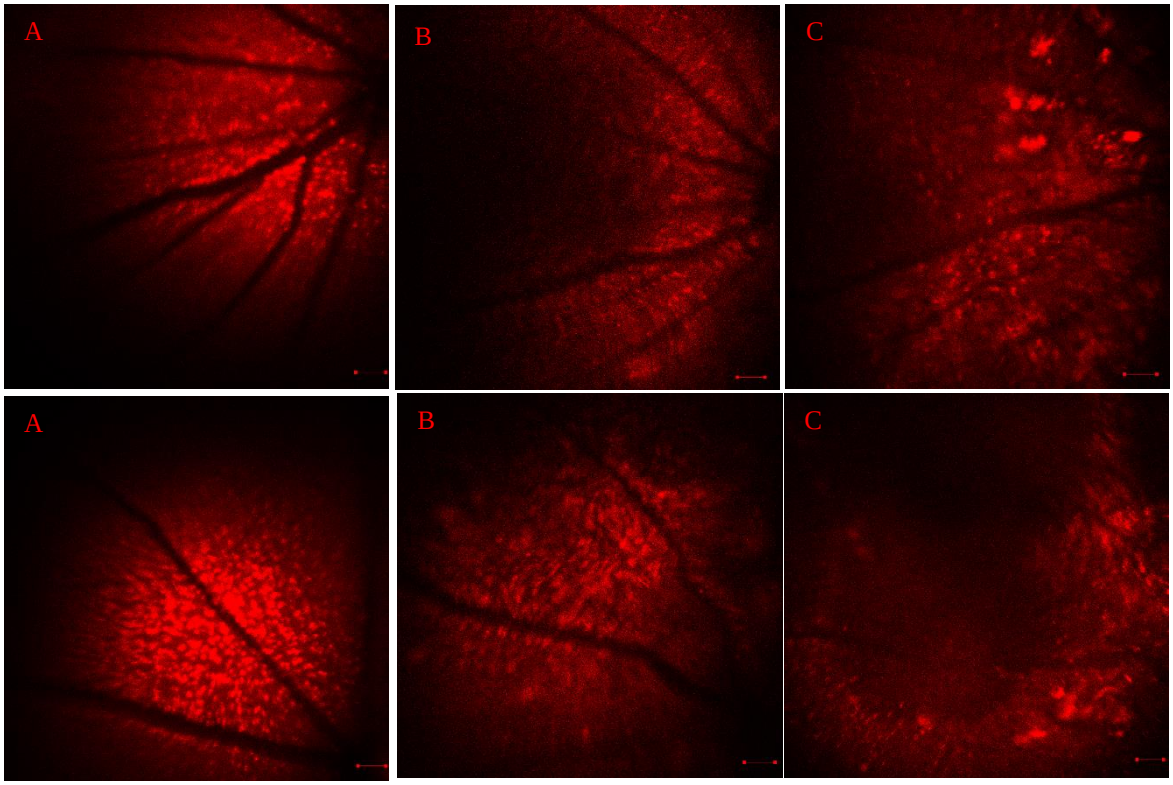

Fig. 41: (A) day (0), ICON baseline followed by ONC and 1st treatment. (B): day (7), ICON then 2nd treatment. (C): Day (35), Last ICON. Retinal blood vessels in black and RGCs in red. Cell numbers decrease during (B and C) in lower row, 2 µl microspheres (Ex 580/ Em 605). Scale bar 200 µm.

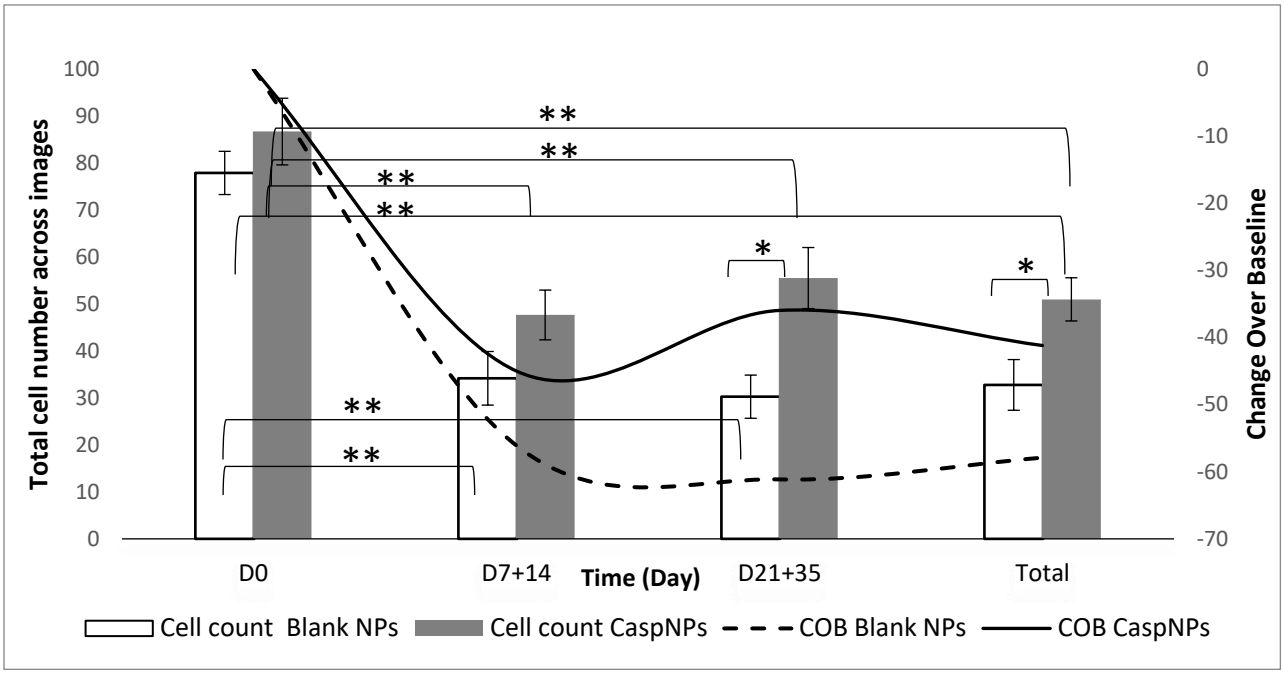

Fig. 42: Total RGCs number across all images (left Y axis) and change over baseline (right Y axis) as a fucntion of time. Sub-acute stage (D7+D14), chronic stage (D21+35) and across all time points (total) in experimental and control retinae. (D0) CaspNPs and blank NPs, n = 15 and 8 respectively. D7+14: n = 15 and 8 respectively. D21+35: n = 10 and 5 respectively. *P < 0.05 (Student's t-test); **P < 0.001 (two-way analysis of variance). Data are expressed as the mean ± SEM.

4.3.3. RGCs quantitative analysis using *ex-vivo* imaging

To independently verify the *in-vivo* imaging results, in a small sample of sacrificing rats, *ex-vivo* whole-mounted retinae were imaged at higher resolution (days 21/35). Here, at day 21, CaspNPs retinae still had more RGCs (49.7±3.6, n=6) than blank NPs retinae (34.8±3.3) (n=6). At day 35, the count was (23.95 ±2.7, n=4) and (15.87±2.0, n=3), respectively, confirming the ICON results (Fig. 43, 44). Unlike ICON results, ex-vivo RGCs counts were not statistically significant which can be explained by the lower signal strength due to laser bleaching after the continuous *in- vivo* imaging (day 0, day 7, day 14, day 21 and day 35) because of post-perfusions conditions such (HEPES buffer, air exposure) which might affect the retinal ganglion cells signal strength and counting results.

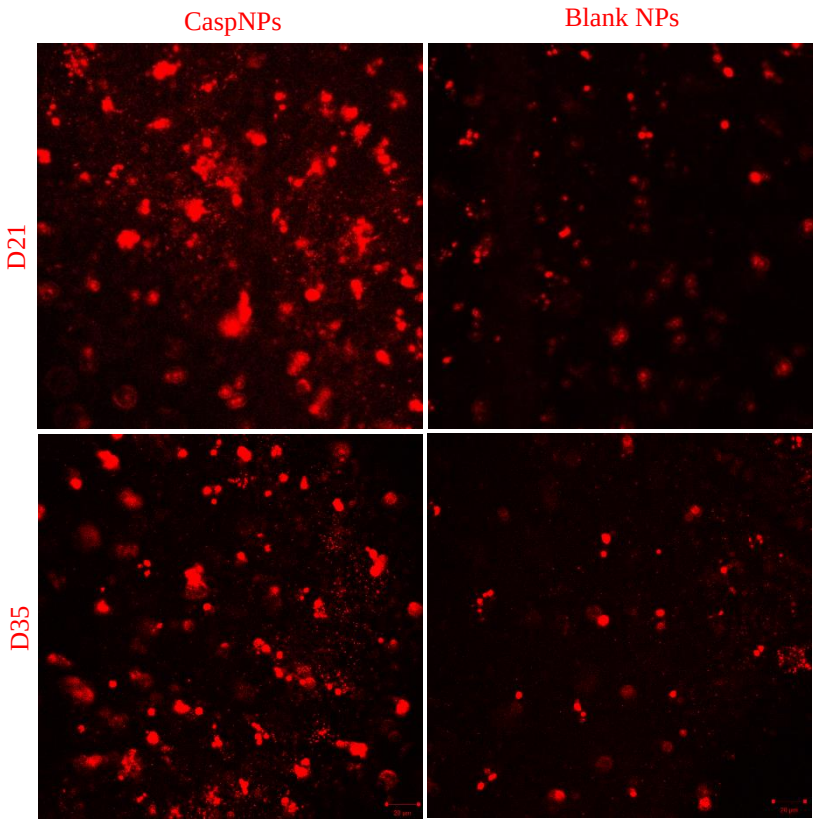

Fig. 43: Representative photomicrographs of retinal ganglions cells as labelled by 2 µl microspheres (Ex 580/ Em 605) in retinal wholemounts post-optic nerve damage. Day 21 shows more RGCs in rats treated with CaspNPs (left) than those treated with blank NPs (right). Scale bar 20 µm.

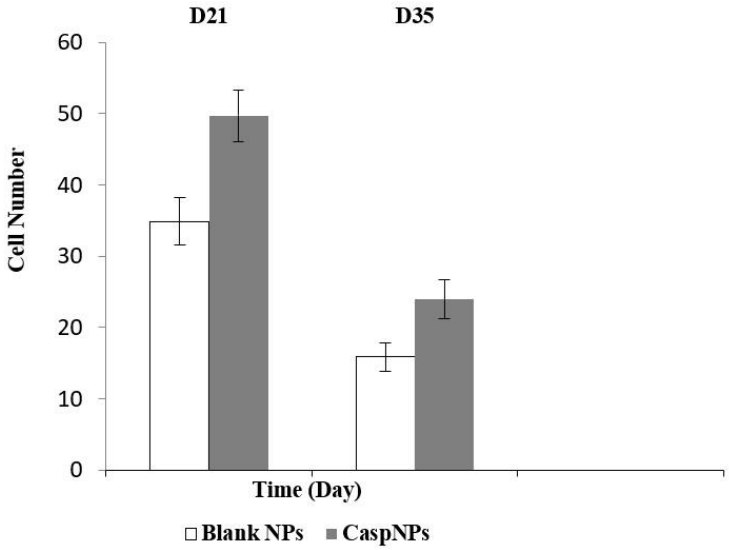

Fig. 44: Quantitative analysis of a small sample of RGCs cell counts at D21 and D35; however, group comparison was not significant, the average cell count was higher in the CaspNPs group; means±SEM.

4.4. Discussion

Here, I show for the first time that siRNA can be delivered, *in-vivo*, to the CNS with non-viral, polymeric nanoparticles, comprising a novel gene therapy approach to down-regulate caspase-3 expression and protect post-mitotic neurons from apoptosis. This was demonstrated by the novel and highly sensitive non-invasive *in-vivo* confocal neuroimaging (ICON) method which can repeatedly visualize the fate of individual neurons longitudinally for more than one month. My findings extend prior work of delivering DNA, RNA, or other oligonucleotides by viral vectors, liposomes, or nanoparticles, and even free siRNA has been tested clinically to treat cancer or infections (212-216). But non-viral delivery of siRNA to structures of the CNS has not been achieved: (i) liposomes are rather instable and evidence of reaching CNS neurons is still outstanding (217). (ii) Nanoparticles were so far only able to deliver DNA or siRNA to mitotic brain cancer cells where the blood-brain-barrier is damaged (140,215,218), and (iii) the delivery of free siRNA has limited bioavailability and biological effects (219). Unlike the present study, prior studies did not succeed to deliver highly specific siRNA to CNS tissues with non-viral delivery methods, and none has achieved neuroprotection.

My study therefore broadens the potential of NPs to deliver genes to CNS tissues. Delivery to the retina or brain is a fundamental challenge because the blood-retina barrier (which is similar to the blood-brain barrier) is a major hurdle for ophthalmological pharmacology. Today, the standard of clinical care to treat retinal and optic nerve diseases is the use of eye drops, or surgery. But intra-vitreous eye injections are now regularly used in clinical ophthalmology, suggesting that intraocular nanoparticle delivery of siRNA might be a realistic clinical option. According to Stokes' law, intravitreally injected NPs settle onto the inner limiting membranes of the retina within a few hours, allowing a controlled drug release for 21 hrs. to 7 weeks (62,220). But intravitreal injections of CaspNPs are more feasible than, for example, pure siRNA injections, because nanoparticles reduce or avoid poor cellular uptake and immunogenicity, and their biological half-life is much longer than the current siRNA approaches which last only several minutes to one hour (200,221). Therefore, nanoparticle formulations can overcome such pharmacokinetic problems and potentially achieve stable gene expression changes (140).

Because the retina is CNS tissue, the survival of post-mitotic neurons critically depends on a well-balanced homoeostasis. The challenge was to identify a nanoparticle design which is both effective and safe. I selected the PBCA-nano-technology proposed by Kreuter et al. and Fricker et al. who showed their feasibility to cross the blood brain barrier. Yet, the reported increased cytotoxicity when incubation time or concentration reaches a certain threshold beyond which reactive oxygen species could damage cells. To reduce this cytotoxicity risk, I used the water-in-oil mini-emulsions

containing only biologically benign Tween 80 and Span 80 as surfactants, which has established safe doses when used by Zhang et al. This suggested PBCA-NPs to be safe for intravitreal application.

Besides, in Zhang et al. study, *in-vitro* survival effects were seen with CaspNPs and with a mixture of blank NPs and free caspase-3 siRNA (casp3 & NPs). This suggests that siRNA can form a complex with nanoparticles due to their high surface activity which supports the argument that the NP-surface is a critical parameter for its interaction with biological systems and surface modification is the key determinant for drug delivery (here: for siRNA) (148). I concluded that the PBCA-NPs matrix is not rate limiting for release of incorporated siRNA.

I next checked the silencing effect of CaspNPs *ex-vivo* and *in-vivo* using a rat model of traumatic optic nerve axonal injury known the induce retrograde cell death of RGCs with delayed, apoptotic cell death (222), where caspase-3 is a key triggering signal. Neurotrauma following ONC significantly increases caspase-3 levels in the retina already 2 days post-lesion, but when receiving intravitreal injections of CaspNPs, caspase-3 associated immune-reactivity decreased to near normal levels.

However, in my results, both *in-vivo* and *ex-vivo* retina imaging showed a moderate soma swelling of the RGCs when treated with CaspNPs. This soma swelling may be a survival indicator and related to recovery of function (223). But this could also attribute to other facts. In unpublished data from our lab, it was found that labelled RGCs after ONC can still possess staining in the axons, not only the cell soma. In addition, it seems that the RGCs get leaky and lose the staining. This might provide the chance that leaky/invisible neurons will be still saved by the CaspNPs and regain staining by transport of the rest of the fluorescent marker from the axon to the cell soma, rendering the RGCs to re-appear.

The retina and brain have many cell types such as endothelial cells, neurons, rods, cones, glia, Muller cells etc. Because the *in-vivo* (tissue) environment is rather complex, it contains blood vessels and extracellular matrix, with membranes which (for good reasons) limit diffusion of foreign substances, such as siRNA, into nerve tissue. I suppose that especially the inner limiting membrane, separating the retina parenchyma from the vitreous humor, may be an unsurmountable obstacle for passage of free siRNA. Yet, CaspNPs were able to penetrate all retinal layers and knock-down caspase-3 synthesis. Thus, it was essential to follow up the work of Zhang et al. as *in-vitro* tests are of rather limited value to study NPs drug delivery systems and only *in-vivo* studies in a rodent model deliver the critical information for early-stage drug development. Furthermore, the negative zeta potential of CaspNPs enabled the particles to avoid the interaction with the negatively charged glycosaminoglycans of the vitreous, thus enhancing their diffusion and limit their aggregation (224).

In conclusion, I used a polymeric nanoparticle system, CaspNPs, for the delivery of nucleic acid sequences (here: siRNA) into central nervous system tissue (here: retina) which have led to a significant neuroprotective effect successfully. CaspNPs may thus comprise a potentially new gene therapy for glaucoma, a disease which is among the leading causes of blindness, expected to reach a prevalence of >100 million worldwide by 2040 (225).

Glaucoma is characterized by optic nerve damage with subsequent RGCs death due to abnormally high intraocular pressure (IOP) and/or vascular dysregulation (226), but lowering IOP with eye drops or surgery does not always stop progression of cell loss (82). Therefore, my new gene therapy approach using CaspNPs might be able to reduce or stop RGCs apoptosis more effectively than the current procedures. In fact, it is even conceivable that CaspNPs, like other PBCA-NPs, may also be safe and suitable for intravenous injections (149). But localized, intraocular injections may be preferable, allowing a lower dose of precious biologics and achieve improved targeting to the retina, thus reducing the probability of systemic adverse events. Nevertheless, the therapeutic potential of CaspNPs in rats does not translate directly to application in patients. Before assessing their clinical value in controlled clinical trials, we need to gain more understanding of the mechanisms of action, pharmacokinetic release profiles in-vitro or *in-vivo*, efficacy and safety studies. Furthermore, negative (non-coding) siRNA need to employed to determine the non-specific effects of siRNA delivery. Finally, optimal treatment regimen of treatment dose and duration following intravitreal injections have to be explored while compared with naked caspase-3 siRNA.

My findings have several general implications: firstly, I showed that nanoparticles can successfully deliver siRNA *in-vivo* to CNS neurons, blocking the cardinal trigger for apoptosis, caspase-3 gene expression, remaining biologically active for much longer than one day. Secondly, caspase-3 siRNA rescues neurons at risk, and thirdly, the *in-vivo* gene therapy of post-mitotic neurons is possible without the use of viral vectors. Therefore, gene therapy with siRNA-nanoparticles opens new perspectives for neuroprotection of cell loss in glaucoma and possibly other ophthalmological and neurodegenerative disorders, both of which are on the rise in our aging societies.

5. General Discussion

Since the approval of the first nanocarrier (pegylated liposomal doxorubicin) in 1995, much progress has been made towards the clinical development of nanocarriers. The same year has witnessed as well the first polymeric nanoparticles (PBCA NPs) to cross the BBB after coating with polysorbate 80 (123,227). However, brain-targeted nanocarriers are lagging behind mainly because of the added challenges associated with delivery to the brain and other inherent difficulties in CNS drug development. Therefore, several neurological disorders remain intractable to treatment by therapeutic agents because of the BBB, the brain's natural defense. By acting as a permeability barrier, the BBB impedes entry from blood to the brain of virtually all molecules greater than 400 Da molecular weight thus rendering many potent, neurologically active substances and drugs ineffective simply because they cannot be delivered to where they are needed. As a result, traversing the BBB remains the rate-limiting factor in brain drug delivery development (228). Consequently, only 379 CNS drugs have entered the clinical trials from 1990-2012, representing 8% of all novel drugs which achieved the clinical trials during this time period (229).

In my first study, in order to study PVP NPs' passage across the BRB in living animals -a suitable surrogate model of the BBB- I carried out real-time *in-vivo* imaging of blood vessels and retina tissue before and several time points after intravenous injection. Using Arivis 4D, I now have advanced the analysis to obtain qualitative and quantitative data on the kinetic profiles of fluorescence-labeled NPs and compared the NPs' BRB passage by determining the fluorescence signals in blood vessels and retina tissue. I revealed a new polymeric nanoparticle system produced from PVP which can pass the BRB after linkage with a fluorescent marker (CFSE), providing a new nano-carrier platform for developing a safe and efficient nano-neuropharmacological treatment. Furthermore, being internalized by blood cells ascertains the drug delivery potential of PVP-Dil-CFSE NPs. Blood cells have been extensively studied and suggested as possible drug carriers because they can avoid the immune system which will provide a long residence time for the NPs in the body (230,231). The previous experience of loading PVP NPs with DNA and their ability to achieve an intranuclear drug delivery propose as well their ability to deliver nucleic acids to the brain which requires further studies (164,232). Finally, crosslinked PVP will exhibit a longer blood circulation time and a better drug release stability (166).

In the same line of reasoning, after its discovery, siRNA became a popular tool in medical research as it allows specific inhibition of genes using a base sequence alone, suppressing genes which encode proteins which cannot be targeted pharmacologically. Furthermore, siRNA is diluted with every cell division, hence, the same siRNA can achieve multiple transcripts and knock down gene expression in non-dividing cells such as the neurons, for weeks (219). Anyway, it took 20 years

till the first siRNA therapy achieve the market (Patisiran), for the treatment of hereditary transthyretin amyloidosis in the liver, using lipid nano-carrier. This, in fact, highlights the necessity of using nano-carriers for the delivery of nucleic acids. However, Patisiran still suffers from some side effects such as peripheral edema and infusion related reactions. Therefore, patients receive antihistamines, nonsteroidal antihistamines and glucocorticoid prior to infusion (233). Anyway, the success of this candidate, or other siRNA candidates, such as GalNac-siRNA in clinical trials mainly happened because they accumulate more in the liver than other organs. This directed the drug developers to target liver diseases mainly rather than other diseases (201,234). It shows that the therapy design process does not necessarily follow the top-down approach which targets a particular disease first and thereafter designs the nanomedicine platform not vice versa (235).

Therefore, there is still no sight of siRNA-based therapy for neuroprotection. Although intraocularly injected pure caspase-2-siRNA has achieved human clinical trials for RGCs neuroprotection (QPI-1007), there are serious caveats concerning its scientific output including: (i) The short bioavailability of pure siRNA. (ii) The low number of patients at phase I study. (iii) The mentioned data remains unpublished. (iv) The number of scattered study centers worldwide for phase III rises the potential of data variation (236). In my second study, following up a previous *in-vitro* and *ex-vivo* work from our lab, I showed for the first time the *in-vivo* neuroprotection induced by caspase-3-siRNA when encapsulated in PBCA NPs for 35 days after optic nerve damage. My results show that CaspNPs treatment can lead to a significant neuroprotection, cutting cell death in half. This finding opens a new horizon for the use of siRNA as a molecular-specific approach to counteract progressing neurodegeneration in the retina and the brain, including glaucoma. Nevertheless, it would be important to also determine the levels of activated caspase-2 to gain a better understanding of the activated caspase-3. While I report neuroprotection of retinal ganglion cells using the downregulation of caspase-3, there are also other options of neuroprotection such as caspase-2 and caspase-7 (237,238) which, in my case, can still induce the cell death pathway even with blocking caspase-3. Hence, before recommending clinical application of the present approach, behavioral studies are needed to document the functional significance of it.

6. Conclusion

Potential neurodegenerative treatments are in large measure hindered by the blood-neural barriers. These barriers severely restrict molecules' entry from the blood into the retina and brain tissue. Recent research has shown that biocompatible and biodegradable nanoparticles with functionalized surface properties can deliver drugs across these barriers. Therefore, brain drug delivery using nanoparticles is currently a hot topic with a potential to be translated into clinical use.

My findings in the PVP study show that PVP-NPs can successfully deliver hydrophobic active compounds *in-vivo* to brain tissue. Second, CFSE can induce the passage through a blood-neural barrier as well as internalize the NPs inside blood cells. This I showed, for the first time, in real-time *in-vivo* imaging and confirmed this by high resolution *ex-vivo* imaging of wholemounted retinae. Third, it is possible to use *in-vivo*, repeated imaging with ICON to obtain a quantitative analysis.

As for the PBCA study, I showed that nanoparticles can successfully deliver siRNA *in-vivo* to CNS neurons, blocking the cardinal trigger for apoptosis, caspase-3 gene expression. Based on this study, PBCA NPs delivery system using caspase-3 siRNA can be delivered not only into the retina for the treatment of retinal disease (e.g. glaucoma and macular degeneration) but they might also be useful to delivery to other brain structures which are relevant for other CNS diseases, for example Alzheimer’s disease.

Briefly, PVP-Dil-CFSE NPs may open new perspectives for the treatment of neurological disorders. Future studies should include the optimization of the circulation time of NPs to increase their efficacy to deliver diagnostic or therapeutic agents to the retina. Moreover, CaspNPs should be tested further. For example, the survival of the RGCs after systemic administration of CaspNPs that suffer from the ONC is worth to be investigated. Besides this, CaspNPs modified with PEG can control the speed of their biodegradation to meet different requirements for the complex environment in animals or humans (183).

7. References

1. Yuan J., & Yankner B. A. (2000). Apoptosis in the nervous system. *Nature*, **407,** 802-809.

2. Gokoffski K. K., Peng M., Alas B., & Lam P. (2020). Neuro-protection and neuro-regeneration of the optic nerve: recent advances and future directions. *Current opinion in neurology*, **33,** 93-105.

3. Kumar P. et al. (2007). Transvascular delivery of small interfering RNA to the central nervous system. *Nature*, **448,** 39-43.

4. Fire A. et al. (1998). Potent and specific genetic interference by double-stranded RNA in Caenorhabditis elegans. *Nature*, **391,** 806-811.

5. Luo D., & Saltzman W. M. (2000). Synthetic DNA delivery systems. *Nature biotechnology*, **18,** 33-37.

6. Hasan W. et al. (2012). Delivery of multiple siRNAs using lipid-coated PLGA nanoparticles for treatment of prostate cancer. *Nano letters*, **12,** 287-292.

7. Guo J. et al. (2011). Aptamer-functionalized PEG–PLGA nanoparticles for enhanced anti-glioma drug delivery. *Biomaterials*, **32,** 8010-8020.

8. Sweeney M. D., Zhao Z., Montagne A., Nelson A. R., & Zlokovic B. V. (2019). Blood-brain barrier: from physiology to disease and back. *Physiological reviews*, **99,** 21-78.

9. Tian X. H. et al. (2011). Enhanced brain targeting of temozolomide in polysorbate-80 coated polybutylcyanoacrylate nanoparticles. *International journal of nanomedicine*, **6,** 445.

10. Occhiutto M. L., Freitas F. R., Maranhao R. C., & Costa V. P. (2012). Breakdown of the blood-ocular barrier as a strategy for the systemic use of nanosystems. *Pharmaceutics*, **4,** 252-275.

11. Tsou Y. H., Zhang X. Q., Zhu H., Syed S., & Xu X. (2017). Drug delivery to the brain across the blood–brain barrier using nanomaterials. *Small*, **13,** 1701921.

12. Saraiva C., Praça C., Ferreira R., Santos T., Ferreira L., & Bernardino L. (2016). Nanoparticle-mediated brain drug delivery: overcoming blood–brain barrier to treat neurodegenerative diseases. *Journal of Controlled Release*, **235,** 34-47.

13. Naldini L. (2015). Gene therapy returns to centre stage. *Nature*, **526,** 351-360.

14. Mulligan R. C. (1993). The basic science of gene therapy. *Science*, **260,** 926-932.

15. Yin H. et al. (2016). Therapeutic genome editing by combined viral and non-viral delivery of CRISPR system components in vivo. *Nature biotechnology*, **34,** 328-333.

16. Goodwin S., McPherson J. D., & McCombie W. R. (2016). Coming of age: ten years of next-generation sequencing technologies. *Nature reviews genetics*, **17,** 333.

17. Stratton M. R. (2011). Exploring the genomes of cancer cells: progress and promise. *Science*, **331,** 1553-1558.

18. Lin M. K., & Farrer M. J. (2014). Genetics and genomics of Parkinson's disease. *Genome medicine*, **6,** 48.

19. Bertram L., & Tanzi R. E. (2008). Thirty years of Alzheimer's disease genetics: the implications of systematic meta-analyses. *Nature reviews neuroscience*, **9,** 768-778.

20. Verdine G. L., & Walensky L. D. (2007). The challenge of drugging undruggable targets in cancer: lessons learned from targeting BCL-2 family members. *Clinical cancer research*, **13,** 7264-7270.

21. Watson J. D., & Crick F. H. (1953). Molecular structure of nucleic acids. *Nature*, **171,** 737-738.

22. Ginn S. L., Alexander I. E., Edelstein M. L., Abedi M. R., & Wixon J. (2013). Gene therapy clinical trials worldwide to 2012–an update. *The journal of gene medicine*, **15,** 65-77.

23. Lächelt U., & Wagner E. (2015). Nucleic acid therapeutics using polyplexes: a journey of 50 years (and beyond). *Chemical reviews*, **115,** 11043-11078.

24. Hendrickx R. et al. (2014). Innate immunity to adenovirus. *Human gene therapy*, **25,** 265-284.

25. Thomas C. E., Ehrhardt A., & Kay M. A. (2003). Progress and problems with the use of viral vectors for gene therapy. *Nature review genetics*, **4,** 346-358.

26. Pack D. W., Hoffman A. S., Pun S., & Stayton P. S. (2005). Design and development of polymers for gene delivery. *Nature reviews drug discovery*, **4,** 581-593.

27. Anderson D. G., Lynn D. M., & Langer R. (2003). Semi-automated synthesis and screening of a large library of degradable cationic polymers for gene delivery. *Angewandte chemie international edition*, **42,** 3153-3158.

28. Mintzer M. A., & Simanek E. E. (2009). Nonviral vectors for gene delivery. *Chemical reviews*, **109,** 259-302.

29. https://microbenotes.com/rna-properties-structure-types-and-functions/

30. Bennett C. F., & Swayze E. E. (2010). RNA targeting therapeutics: molecular mechanisms of antisense oligonucleotides as a therapeutic platform. *Annual review of pharmacology and toxicology*, **50,** 259-293.

31. Evers M. M., Toonen L. J., & van Roon-Mom W. M. (2015). Antisense oligonucleotides in therapy for neurodegenerative disorders. *Advanced drug delivery reviews*, **87,** 90-103.

32. Deng Y. et al. (2014). Therapeutic potentials of gene silencing by RNA interference: principles, challenges, and new strategies. *Gene*, **538,** 217-227.

33. Elbashir S. M., Harborth J., Lendeckel W., Yalcin A., Weber K., & Tuschl T. (2001). Duplexes of 21-nucleotide RNAs mediate RNA interference in cultured mammalian cells. *Nature*, **411,** 494-498.

34. Pecot C. V., Calin G. A., Coleman R. L., Lopez-Berestein G., & Sood A. K. (2011). RNA interference in the clinic: challenges and future directions. *Nature reviews cancer*, **11,** 59-67.

35. Mello C., & Conte, D. (2004). Revealing the world of RNA interference. *Nature,* **431,** 338–342

36. Agrawal N., Dasaradhi P. V. N., Mohmmed A., Malhotra P., Bhatnagar R. K., & Mukherjee S. K. (2003). RNA interference: biology, mechanism, and applications. *Microbiology and molecular biology reviews,* **67,** 657-685.

37. Wasi S. (2003). RNA interference: the next genetics revolution. In *Horizon Symposia; Understanding the RNAissance* (pp. 1-4).

38. Kerr J. F., Wyllie A. H., & Currie A. R. (1972). Apoptosis: a basic biological phenomenon with wideranging implications in tissue kinetics. *British journal of cancer,* **26,** 239-257.

39. Wyllie A. H. (1997). Apoptosis and carcinogenesis. *European journal of cell biology*, **73,** 189-197.

40. Mattson M. P. (2000). Apoptosis in neurodegenerative disorders. *Nature reviews molecular cell biology*, **1,** 120-130.

41. Vaux D. L., & Flavell R. A. (2000). Apoptosis genes and autoimmunity. *Current opinion in immunology*, **12,** 719-724.

42. Green D. R., & Evan G. I. (2002). A matter of life and death. *Cancer cell*, **1,** 19-30.

43. Thompson C. B. (1995). Apoptosis in the pathogenesis and treatment of disease. *Science,* **267,** 1456-1462.

44. Danial N. N., & Korsmeyer S. J. (2004). Cell death: critical control points. *Cell*, **116,** 205-219.

45. Bredesen D. E., Rao R. V., & Mehlen P. (2006). Cell death in the nervous system. *Nature,* **443,** 796-802.

46. Haase G., Pettmann B., Raoul C., & Henderson C. E. (2008). Signaling by death receptors in the nervous system. *Current opinion in neurobiology,* **18,** 284-291.

47. Micheau O., & Tschopp J. (2003). Induction of TNF receptor I-mediated apoptosis via two sequential signaling complexes. *Cell*, **114,** 181-190.

48. Fricker M., Tolkovsky A. M., Borutaite V., Coleman M., & Brown G. C. (2018). Neuronal cell death. *Physiological reviews*, **98,** 813-880.

49. Caroline H. Y., & Yuan J. (2009). The Jekyll and Hyde functions of caspases. *Developmental cell*, **16,** 21-34.

50. Hyman B. T., & Yuan, J. (2012). Apoptotic and non-apoptotic roles of caspases in neuronal physiology and pathophysiology. *Nature reviews neuroscience*, **13,** 395-406.

51. Gill R. et al. (2002). Role of caspase-3 activation in cerebral ischemia-induced neurodegeneration in adult and neonatal brain. *Journal of cerebral blood flow & metabolism*, **22,** 420-430.

52. Rami A., Sims J., Botez G., & Winckler J. (2003). Spatial resolution of phospholipid scramblase 1 (PLSCR1), caspase-3 activation and DNA-fragmentation in the human hippocampus after cerebral ischemia. *Neurochemistry international*, ***43,*** 79-87.

53. d'Amelio M. et al. (2011). Caspase-3 triggers early synaptic dysfunction in a mouse model of Alzheimer's disease. *Nature neuroscience*, **14,** 69.

54. Grosskreutz C. L., Hänninen V. A., Pantcheva M. B., Huang W., Poulin N. R., & Dobberfuhl A. P. (2005). FK506 blocks activation of the intrinsic caspase cascade after optic nerve crush. *Experimental eye research*, **80,** 681-686.

55. Sánchez-Migallón M. C., Valiente-Soriano F. J., Nadal-Nicolás F. M., Vidal-Sanz M., & Agudo-Barriuso M. (2016). Apoptotic retinal ganglion cell death after optic nerve transection or crush in mice: delayed RGC loss with BDNF or a caspase 3 inhibitor. *Investigative ophthalmology & visual science*, **57,** 81-93.

56. Clarke P., & Tyler K. L. (2009). Apoptosis in animal models of virus-induced disease. *Nature reviews microbiology*, **7,** 144-155.

57. Abbott N. J. (2014). Anatomy and physiology of the blood–brain barriers. In *Drug Delivery to the Brain* (pp. 3-21). Springer, New York, NY.

58. Engelhardt B., & Coisne C. (2011). Fluids and barriers of the CNS establish immune privilege by confining immune surveillance to a two-walled castle moat surrounding the CNS castle. *Fluids and barriers of the CNS*, **8,** 4.

59. Reese T. S., & Karnovsky M. J. (1967). Fine structural localization of a blood-brain barrier to exogenous peroxidase. *The Journal of cell biology*, **34,** 207-217.

60. Nabeshima S., Reese T. S., Landis D. M., & Brightman M. W. (1975). Junctions in the meninges and marginal glia. *Journal of comparative neurology*, **164,** 127-169.

61. Barichello T., Collodel A., Hasbun R., & Morales R. (2019). An Overview of the Blood-Brain Barrier. In *Blood-Brain Barrier* (pp. 1-8). Humana Press, New York, NY.

62. Edelhauser H. F. et al. (2010). Ophthalmic drug delivery systems for the treatment of retinal diseases: basic research to clinical applications. *Investigative ophthalmology & visual science*, **51,** 5403-5420.

63. Choi Y. K., & Kim, K. W. (2008). Blood-neural barrier: its diversity and coordinated cell-to-cell communication. *BMB reports*, **41,** 345-352.

64. Lahkar S., & Das M. K. (2019). Brain-Targeted Drug Delivery with Surface-Modified Nanoparticles. In *Surface Modification of Nanoparticles for Targeted Drug Delivery* (pp. 277-310). Springer, Cham.

65. Patel M. M., Goyal B. R., Bhadada S. V., Bhatt J. S., & Amin A. F. (2009). Getting into the brain. *CNS drugs*, **23,** 35-58.

66. Brightman M. W. (1977). Morphology of blood-brain interfaces. *Experimental eye research*, **25,** 1-25.

67. Ricci M., Blasi P., Giovagnoli S., & Rossi C. (2006). Delivering drugs to the central nervous system: a medicinal chemistry or a pharmaceutical technology issue?. *Current medicinal chemistry*, **13,** 1757-1775.

68. Abbott N. J., Patabendige A. A., Dolman D. E., Yusof S. R., & Begley D. J. (2010). Structure and function of the blood–brain barrier. *Neurobiology of disease*, **37,** 13-25.

69. Neerati P., Mohammad R., Bangaru R., Devde R., & Kanwar J. R. (2012). The effects of verapamil, curcumin, and capsaicin pretreatments on the BBB uptake clearance of digoxin in rats. *Journal of pharmacy research*, **5,** 2126-2133.

70. Sanchez-Covarrubias L., Slosky L. M., Thompson B. J., Davis T. P., & Ronaldson P. T. (2014). Transporters at CNS barrier sites: obstacles or opportunities for drug delivery?. *Current pharmaceutical design*, **20,** 1422-1449.

71. Chen Y., & Liu L. (2012). Modern methods for delivery of drugs across the blood–brain barrier. *Advanced drug delivery reviews*, **64,** 640-665.

72. Pardridge W. M. (2012). Drug transport across the blood–brain barrier. *Journal of cerebral blood flow & metabolism*, **32,** 1959-1972.

73. Banks W. A. (2016). From blood–brain barrier to blood–brain interface: new opportunities for CNS drug delivery. *Nature reviews drug discovery*, **15,** 275.

74. Ballabh P., Braun A., & Nedergaard M. (2004). The blood–brain barrier: an overview: structure, regulation, and clinical implications. *Neurobiology of disease*, **16,** 1-13.

75. Abbott N. J., Rönnbäck L., & Hansson E. (2006). Astrocyte–endothelial interactions at the blood–brain barrier. *Nature reviews neuroscience*, **7,** 41.

76. Hersh D. S. et al. (2016). Evolving drug delivery strategies to overcome the blood brain barrier. *Current pharmaceutical design*, **22,** 1177-1193.

77. Chen P. Y. et al. (2017). Drug-carrying microbubbles as a theranostic tool in convection-enhanced delivery for brain tumor therapy. *Oncotarget*, **8,** 42359.

78. Jornada D. H., dos Santos Fernandes G. F., Chiba D. E., De Melo T. R. F., Dos Santos J. L., & Chung M. C. (2016). The prodrug approach: A successful tool for improving drug solubility. *Molecules*, **21,** 42.

79. Minn A. et al. (2002). Drug transport into the mammalian brain: the nasal pathway and its specific metabolic barrier. *Journal of drug targeting*, **10,** 285-296.

80. Fine B. S., & Yanoff M. (1979). Ocular histology. A Text and Atlas. Harper & Row, Hagerstown, Maryland.

81. Masland R. H. (2001). The fundamental plan of the retina. *Nature neuroscience*, **4,** 877-886.

82. Zhang K., Zhang L., & Weinreb R. N. (2012). Ophthalmic drug discovery: novel targets and mechanisms for retinal diseases and glaucoma. *Nature reviews drug discovery*, **11,** 541-559.

83. Kita Y. et al. (2017). Changes in the size of the foveal avascular zone after vitrectomy with internal limiting membrane peeling for a macular hole. *Japanese journal of ophthalmology*, **61,** 465-471.

84. Holmes D. (2018). Reconstructing the retina. *Nature*, **561,** S2-S2.

85. Sernagor E., & Hennig M. H. (2013). Retinal waves: underlying cellular mechanisms and theoretical considerations. In *Cellular migration and formation of neuronal connections* (pp. 909-920). Academic Press, Cambridge, Massachusetts.

86. Hämäläinen K. M., Kananen K., Auriola S., Kontturi K., & Urtti A. (1997). Characterization of paracellular and aqueous penetration routes in cornea, conjunctiva, and sclera. *Investigative ophthalmology & visual science*, **38,** 627-634.

87. Smith R. S., & Rudt L. A. (1975). Ocular vascular and epithelial barriers to microperoxidase. *Investigative Ophthalmology & Visual Science*, **14,** 556-560.

88. Törnquist P., Alm A., & Bill A. (1990). Permeability of ocular vessels and transport across the blood-retinal-barrier. *Eye*, **4,** 303-309.

89. Tachikawa M., Takeda Y., Tomi M., & Hosoya K. I. (2010). Involvement of OCTN2 in the transport of acetyl-L-carnitine across the inner blood–retinal barrier. *Investigative ophthalmology & visual science*, **51,** 430-436.

90. Thornit D. N., Vinten C. M., Sander B., Lund-Andersen H., & la Cour M. (2010). Blood–retinal barrier glycerol permeability in diabetic macular edema and healthy eyes: Estimations from Macular Volume Changes after Peroral Glycerol. *Investigative ophthalmology & visual science*, **51,** 2827-2834.

91. Duvvuri S., Majumdar S., & Mitra A. K. (2003). Drug delivery to the retina: challenges and opportunities. *Expert opinion on biological therapy*, **3,** 45-56.

92. Macwan J. S., Hirani A., & Pathak Y. (2016). Challenges in ocular pharmacokinetics and drug delivery. In *Nano-biomaterials for ophthalmic drug delivery* (pp. 593-611). Springer, Cham.

93. Del Amo E. M. et al. (2017). Pharmacokinetic aspects of retinal drug delivery. *Progress in retinal and eye research*, **57,** 134-185.

94. Janagam D. R., Wu, L., & Lowe, T. L. (2017). Nanoparticles for drug delivery to the anterior segment of the eye. *Advanced drug delivery reviews*, **122,** 31-64.

95. Del Amo E. M., & Urtti A. (2008). Current and future ophthalmic drug delivery systems: a shift to the posterior segment. *Drug discovery today*, **13,** 135-143.

96. Yasukawa T., Ogura Y., Tabata Y., Kimura H., Wiedemann P., & Honda Y. (2004). Drug delivery systems for vitreoretinal diseases. *Progress in retinal and eye research*, **23,** 253-281.

97. Gaudana R., Jwala J., Boddu S. H., & Mitra A. K. (2009). Recent perspectives in ocular drug delivery. *Pharmaceutical research*, **26,** 1197.

98. Wadhwa S., Paliwal R., Paliwal S. R., & Vyas S. P. (2009). Nanocarriers in ocular drug delivery: an update review. *Current pharmaceutical design*, **15,** 2724-2750.

99. London A., Benhar I., & Schwartz M. (2013). The retina as a window to the brain—from eye research to CNS disorders. *Nature reviews neurology*, **9,** 44.

100. Steuer H. et al. (2005). Functional characterization and comparison of the outer blood–retina barrier and the blood–brain barrier. *Investigative ophthalmology & visual science*, **46,** 1047-1053.

101. Steuer H., Jaworski A., Stoll D., & Schlosshauer B. (2004). In vitro model of the outer blood–retina barrier. *Brain research protocols*, **13,** 26-36.

102. You Q. (2020). *The role of physicochemical parameters on polybutylcyanoacrylate nanoparticles' delivery to the central nervous system.* (unpublished doctoral thesis). University of Otto-von-Guericke university, Magdeburg, Germany. Retrieved from: https://opendata.uni-halle.de/handle/1981185920/32891.

103. Reichel A. (2006). The role of blood-brain barrier studies in the pharmaceutical industry. *Current drug metabolism*, **7,** 183-203.

104. Bickel U., Yoshikawa T., & Pardridge W. M. (2001). Delivery of peptides and proteins through the blood–brain barrier. *Advanced drug delivery reviews*, **46,** 247-279.

105. Pardridge W. M. (1995). Transport of small molecules through the blood-brain barrier: biology and methodology. *Advanced drug delivery reviews*, **15,** 5-36.

106. Kreuter J. (1978). Nanoparticles and nanocapsules--new dosage forms in the nanometer size range. *Pharmaceutica acta helvetiae*, **53,** 33-39.

107. Vieira D. B., & Gamarra L. F. (2018). Multifunctional nanoparticles for successful targeted drug delivery across the blood-brain barrier. In *Molecular insight of drug design*. IntechOpen.

108. Anselmo A. C., & Mitragotri S. (2016). Nanoparticles in the clinic. *Bioengineering & translational medicine*, **1,** 10-29.

109. Olivier J. C. (2005). Drug transport to brain with targeted nanoparticles. *NeuroRx*, **2,** 108-119.

110. Furtado D., Björnmalm M., Ayton S., Bush A. I., Kempe K., & Caruso F. (2018). Overcoming the blood–brain barrier: the role of nanomaterials in treating neurological diseases. *Advanced materials*, **30**, 1801362.

111. Bhaskar S. et al. (2010). Multifunctional Nanocarriers for diagnostics, drug delivery and targeted treatment across blood-brain barrier: perspectives on tracking and neuroimaging. *Particle and fibre toxicology*, **7,** 3.

112. Osuka S., & Van Meir E. G. (2017). Cancer therapy: Neutrophils traffic in cancer nanodrugs. *Nature nanotechnology*, **12,** 616.

113. Sercombe L., Veerati T., Moheimani F., Wu S. Y., Sood A. K., & Hua S. (2015). Advances and challenges of liposome assisted drug delivery. *Frontiers in pharmacology*, **6,** 286.

114. Torchilin V. P. (2005). Recent advances with liposomes as pharmaceutical carriers. *Nature reviews drug discovery*, **4,** 145-160

115. Grimaldi N. et al. (2016). Lipid-based nanovesicles for nanomedicine. *Chemical society reviews*, **45,** 6520-6545.

116. Blasi P., Giovagnoli S., Schoubben A., Ricci M., & Rossi C. (2007). Solid lipid nanoparticles for targeted brain drug delivery. *Advanced drug delivery reviews*, **59,** 454-477.

117. Kreuter J. (1994). Nanoparticles. In *Colloidal drugs delivery systems* (pp. 219–342). Marcel Dekker, New York.

118. Jose S., Anju S. S., Cinu T. A., Aleykutty N. A., Thomas S., & Souto E. B. (2014). In vivo pharmacokinetics and biodistribution of resveratrol-loaded solid lipid nanoparticles for brain delivery. *International journal of pharmaceutics*, **474,** 6-13.

119. Ramteke K. H., Joshi S. A., & Dhole S. N. (2012). Solid lipid nanoparticle: a review. *IOSR Journal of pharmacy*, **2,** 34-44.

120. Yang Z. et al. (2010). A review of nanoparticle functionality and toxicity on the central nervous system. *Journal of the royal society interface*, **7,** S411-S422.

121. Feng X., Chen A., Zhang Y., Wang J., Shao L., & Wei L. (2015). Central nervous system toxicity of metallic nanoparticles. *International journal of nanomedicine*, **10,** 4321.

122. Leite P. E. C., Pereira M. R., & Granjeiro J. M. (2015). Hazard effects of nanoparticles in central nervous system: searching for biocompatible nanomaterials for drug delivery. *Toxicology in vitro*, **29,** 1653-1660.

123. Kreuter J., Alyautdin R. N., Kharkevich D. A., & Ivanov A. A. (1995). Passage of peptides through the blood-brain barrier with colloidal polymer particles (nanoparticles). *Brain research*, **674,** 171-174.

124. Zhao Y., Zheng C., & Liu Y. (2019). Polymeric Nanomedicine. In *Nanomedicine in Brain Diseases* (pp. 233-267). Springer, Singapore.

125. Ozkizilcik A., Davidson P., Turgut H., Sharma H. S., Sharma A., & Tian Z. R. (2017). Nanocarriers as CNS drug delivery systems for enhanced neuroprotection. In *Drug and Gene Delivery to the Central Nervous System for Neuroprotection* (pp. 33-55). Springer, Cham.

126. Gaillard P. J., Visser C. C., de Boer M., Appeldoorn C. C., & Rip, J. (2014). Blood-to-brain drug delivery using nanocarriers. In *Drug delivery to the brain* (pp. 433-454). Springer, New York.

127. Koczkur K. M., Mourdikoudis S., Polavarapu L., & Skrabalak S. E. (2015). Polyvinylpyrrolidone (PVP) in nanoparticle synthesis. *Dalton transactions*, **44,** 17883-17905.

128. Jatzkewitz H. (1955). An ein kolloidales Blutplasma-Ersatzmittel (Polyvinylpyrrolidon) gebundenes Peptamin (Glycyl-L-leucyl-mezcalin) als neuartige Depotform für biologisch aktive primäre Amine (Mezcalin). *Zeitschrift für naturforschung B,* **10,** 27-31.

129. Mitra S., Bharali D. J., & Maitra A. (2004). Hydrogel nanoparticles made of cross-linked polyvinylpyrrolidone. *Encyclopedia of nanoscience and nanotechnology. Marcel Dekker, New York,* 1403-1414.

130. Kamada H. et al. (2000). Antitumor activity of tumor necrosis factor-α conjugated with polyvinylpyrrolidone on solid tumors in mice. *Cancer research,* **60,** 6416-6420.

131. Kaneda Y. et al. (2004). The use of PVP as a polymeric carrier to improve the plasma half-life of drugs. *Biomaterials,* **25,** 3259-3266.

132. Kuskov A. N. et al. (2017). Amphiphilic poly-N-vinylpyrrolidone nanoparticles as carriers for non-steroidal, anti-inflammatory drugs: in vitro cytotoxicity and in vivo acute toxicity study. *Nanomedicine: Nanotechnology, biology and medicine,* **13,** 1021-1030.

133. Kuskov A. N. et al. (2016). Amphiphilic poly-N-vynilpyrrolidone nanoparticles: Cytotoxicity and acute toxicity study. *Food and chemical toxicology,* **96,** 273-279.

134. Alyautdin R. N., Tezikov E. B., Ramge P., Kharkevich D. A., Begley D. J., & Kreuter J. (1998). Significant entry of tubocurarine into the brain of rats by adsorption to polysorbate 80–coated polybutylcyanoacrylate nanoparticles: an in-situ brain perfusion study. *Journal of microencapsulation,* **15,** 67-74.

135. Gelperina S. E. et al. (2002). Toxicological studies of doxorubicin bound to polysorbate 80-coated poly (butyl cyanoacrylate) nanoparticles in healthy rats and rats with intracranial glioblastoma. *Toxicology letters,* **126,** 131-141.

136. Pereverzeva E. et al. (2007). Influence of the formulation on the tolerance profile of nanoparticle-bound doxorubicin in healthy rats: focus on cardio-and testicular toxicity. *International journal of pharmaceutics,* **337,** 346-356.

137. Pereverzeva E., Treschalin I., Bodyagin D., Maksimenko O., Kreuter J. A., & Gelperina S. (2008). Intravenous tolerance of a nanoparticle-based formulation of doxorubicin in healthy rats. *Toxicology letters*, **178,** 9-19.

138. Kolter M., Ott M., Hauer C., Reimold I., & Fricker G. (2015). Nanotoxicity of poly (n-butylcyano-acrylate) nanoparticles at the blood–brain barrier, in human whole blood and in vivo. *Journal of controlled release,* **197,** 165-179.

139. Zhou Q., Sun X., Zeng L., Liu J., & Zhang Z. (2009). A randomized multicenter phase II clinical trial of mitoxantrone-loaded nanoparticles in the treatment of 108 patients with unresected hepatocellular carcinoma. *Nanomedicine: Nanotechnology, biology and medicine*, **5,** 419-423.

140. Musyanovych A., & Landfester K. (2008). Synthesis of poly (butylcyanoacrylate) nanocapsules by interfacial polymerization in miniemulsions for the delivery of DNA molecules. In *Surface and Interfacial Forces–From Fundamentals to Applications* (pp. 120-127). Springer, Berlin, Heidelberg.

141. Tomcin S., Baier G., Landfester K., & Mailänder V. (2014). Pharmacokinetics on a microscale: visualizing Cy5-labeled oligonucleotide release from poly (n-butylcyanoacrylate) nanocapsules in cells. *International journal of nanomedicine*, **9,** 5471.

142. Zhang X., Zhang E., Grigartzik L., Henrich-Noack P., Hintz W., & Sabel B. A. (2018). Anti-apoptosis Function of PBCA nanoparticles containing caspase-3 siRNA for neuronal protection. *Chemie Ingenieur Technik*, **90,** 451-455.

143. Sabel B. A., Engelmann R., & Humphrey M. F. (1997). In vivo confocal neuroimaging (ICON) of CNS neurons. *Nature medicine*, **3,** 244-247.

144. Henrich-Noack P. et al. (2012). In vivo visualisation of nanoparticle entry into central nervous system tissue. *Archives of toxicology*, **86,** 1099-1105.

145. Prilloff S., Fan, J., Henrich-Noack P., & Sabel B. A. (2010). In vivo confocal neuroimaging (ICON): non-invasive, functional imaging of the mammalian CNS with cellular resolution. *European journal of neuroscience*, **31,** 521-528.

146. You Q. et al. (2019). Major effects on blood-retina barrier passage by minor alterations in design of polybutylcyanoacrylate nanoparticles. *Journal of drug targeting*, **27,** 338-346.

147. You Q. et al. (2019). How nanoparticle physicochemical parameters affect drug delivery to cells in the retina via systemic interactions. *Molecular pharmaceutics*, **16,** 5068-5075.

148. Voigt N., Henrich-Noack P., Kockentiedt S., Hintz W., Tomas J., & Sabel B. A. (2014). Surfactants, not size or zeta-potential influence blood–brain barrier passage of polymeric nanoparticles. *European journal of pharmaceutics and biopharmaceutics*, **87,** 19-29.

149. Voigt N., Henrich-Noack P., Kockentiedt S., Hintz W., Tomas J., & Sabel B. A. (2014). Toxicity of polymeric nanoparticles in vivo and in vitro. *Journal of nanoparticle research*, **16,** 2379.

150. Prilloff S., Henrich-Noack P., & Sabel B. A. (2012). Recovery of axonal transport after partial optic nerve damage is associated with secondary retinal ganglion cell death in vivo. *Investigative ophthalmology & visual science*, **53,** 1460-1466.

151. Prilloff S., Noblejas M. I., Chedhomme V., & Sabel B. A. (2007). Two faces of calcium activation after optic nerve trauma: life or death of retinal ganglion cells in vivo depends on calcium dynamics. *European journal of neuroscience*, **25,** 3339-3346.

152. Zhang E. et al. (2020). Release kinetics of fluorescent dyes from PLGA nanoparticles in retinal blood vessels: in vivo monitoring and ex vivo localization. *European Journal of Pharmaceutics and Biopharmaceutics*.

153. Guthoff R. F., Zhivov A., & Stachs O. (2009). In vivo confocal microscopy, an inner vision of the cornea–a major review. *Clinical & experimental ophthalmology*, **37,** 100-117.

154. Feigin V. L. et al. (2017). Global, regional, and national burden of neurological disorders during 1990–2015: a systematic analysis for the Global Burden of Disease Study 2015. *The Lancet neurology*, **16,** 877-897.

155. Feigin V. L. Et al. (2019). Global, regional, and national burden of neurological disorders, 1990–2016: a systematic analysis for the Global Burden of Disease Study 2016. *The Lancet neurology*, **18,** 459-480.

156. Zimmer A., & Kreuter J. (1995). Microspheres and nanoparticles used in ocular delivery systems. *Advanced drug delivery reviews,* **16,** 61-73.

157. Myles M. E., Neumann D. M., & Hill J. M. (2005). Recent progress in ocular drug delivery for posterior segment disease: emphasis on transscleral iontophoresis. *Advanced drug delivery reviews,* **57,** 2063-2079.

158. Luo L. et al. Targeted intraceptor nanoparticle therapy reduces angiogenesis and fibrosis in primate and murine macular degeneration. *ACS nano,* **7,** 3264-3275.

159. Kompella U. B., Amrite A. C., Ravi R. P., & Durazo S. A. (2013). Nanomedicines for back of the eye drug delivery, gene delivery, and imaging. *Progress in retinal and eye research,* **36,** 172-198.

160. Joseph R. R., & Venkatraman S. S. (2017). Drug delivery to the eye: what benefits do nanocarriers offer?. *Nanomedicine,* **12,** 683-702.

161. Bisht R., Mandal A., Jaiswal J. K., & Rupenthal I. D. (2018). Nanocarrier mediated retinal drug delivery: overcoming ocular barriers to treat posterior eye diseases. *Wiley Interdisciplinary Reviews: Nanomedicine and nanobiotechnology,* **10,** e1473.

162. Patel T., Zhou J., Piepmeier J. M., & Saltzman W. M. (2012). Polymeric nanoparticles for drug delivery to the central nervous system. *Advanced drug delivery reviews*, **64,** 701-705.

163. Grabowski N. et al. (2015). Surface coating mediates the toxicity of polymeric nanoparticles towards human-like macrophages. *International journal of pharmaceutics*, **482,** 75-83.

164. Luss A. L. et al. (2018). Nanosized carriers based on amphiphilic poly-N-vinyl-2-pyrrolidone for intranuclear drug delivery. *Nanomedicine,* **13,** 703-715.

165. Teodorescu M., Bercea M., & Morariu S. (2019). Biomaterials of PVA and PVP in medical and pharmaceutical applications: Perspectives and challenges. *Biotechnology advances*, **37,** 109-131.

166. Gupta S. V. (2016). Physicochemical requirements for polymers and polymer-based nanomaterial for ophthalmic drug delivery. In *Nano-biomaterials for ophthalmic drug delivery* (pp. 131-146). Springer, Cham.

167. https://www.arivis.com/en/imaging-science/arivis-vision4d

168. Najman L., & Couprie M. (2003). Watershed algorithms and contrast preservation. In *International conference on discrete geometry for computer imagery* (pp. 62-71). Springer, Berlin, Heidelberg.

169. Antiga L. (2007). Generalizing vesselness with respect to dimensionality and shape. *Insight journal***, 3,** 1-14.

170. Liu S., Jones L. W., & Gu F. X. (2016). Nanotechnology and nanomaterials in ophthalmic drug delivery. In *Nano-Biomaterials for ophthalmic drug delivery* (pp. 83-109). Springer, Cham.

171. Himawan E. et al. (2019). Drug delivery to retinal photoreceptors. *Drug discovery today*.

172. Hosoya K. I., & Tomi M. (2008). Inner blood—retinal barrier: transport biology and methodology. In *Drug Absorption Studies* (pp. 321-338). Springer, Boston.

173. Patel M. R., Mandava N. K., Mitra A. K. (2013). Microdialysis in ocular drug development. In *Microdialysis in drug development* (pp. 197-222). Springer, New York.

174. Peng Y., Tang L. & Zhou Y. (2017). Subretinal injection: a review on the novel route of therapeutic delivery for vitreoretinal diseases. *Ophthalmic Research*, **58,** 217-226.

175. U. S. National Institutes of health Clinical Trials. Available from: https://clinicaltrials.gov/ct2/show/NCT00531024

176. Wang Y. et al. (2019). Intravenous treatment of choroidal neovascularization by photo-targeted nanoparticles. *Nature communications*, **10,** 1-9.

177. Kim J.H., Kim J.H., Kim K.W., Kim M.H. and Yu Y.S., (2009). Intravenously administered gold nanoparticles pass through the blood–retinal barrier depending on the particle size, and induce no retinal toxicity. *Nanotechnology*, **20,** 505101.

178. Kuskov A. N. et al. (2007). Amphiphilic poly-N-vinylpyrrolidone nanocarriers with incorporated model proteins. *Journal of physics: Condensed matter*, **19,** 205139.

179. Kuskov A. N. et al. (2018). Self-assembled amphiphilic poly-N-vinylpyrrolidone nanoparticles as carriers for hydrophobic drugs: Stability aspects. *Journal of applied polymer science*, **135,** 45637.

180. Villemson A. L., Kuskov A. N., Shtilman M. I., Galebskaya L. V., Ryumina E. V., & Larionova N. I. (2004). Interaction of polymer aggregates based on stearoyl-poly-N-vinylpyrrolidone with blood components. *Biochemistry (moscow)*, **69,** 621-628.

181. Tsatsakis A. et al. (2019). In vitro blood compatibility and in vitro cytotoxicity of amphiphilic poly-N-vinylpyrrolidone nanoparticles. *Food and chemical toxicology*, **127,** 42-52.

182. Zhang E. et al. (2020). Release kinetics of fluorescent dyes from PLGA nanoparticles in retinal blood vessels: in vivo monitoring and ex vivo localization. *European Journal of Pharmaceutics and Biopharmaceutics*.

183. Owens III D. E., & Peppas N. A. (2006). Opsonization, biodistribution, and pharmacokinetics of polymeric nanoparticles. *International journal of pharmaceutics*, **307,** 93-102.

184. Hawkins E. D., Hommel M., Turner M. L., Battye F. L., Markham J. F., & Hodgkin P. D. (2007). Measuring lymphocyte proliferation, survival and differentiation using CFSE time-series data. *Nature protocols*, **2,** 2057.

185. Giarratana M. C. et al. (2005). Ex vivo generation of fully mature human red blood cells from hematopoietic stem cells. *Nature biotechnology*, **23,** 69-74.

186. Staffend N. A., & Meisel R. L. (2011). DiOlistic labeling of neurons in tissue slices: a qualitative and quantitative analysis of methodological variations. *Frontiers in neuroanatomy*, **5,** 14.

187. Villa C. H., Anselmo A. C., Mitragotri S., & Muzykantov V. (2016). Red blood cells: Supercarriers for drugs, biologicals, and nanoparticles and inspiration for advanced delivery systems. *Advanced drug delivery reviews*, **106,** 88-103.

188. Parodi A. et al. (2013). Synthetic nanoparticles functionalized with biomimetic leukocyte membranes possess cell-like functions. *Nature nanotechnology*, **8,** 61-68.

189. Muzykantov V. R. (2010). Drug delivery by red blood cells: vascular carriers designed by mother nature. *Expert opinion on drug delivery*, **7,** 403-427.

190. Chu D., Dong X., Shi X., Zhang C., & Wang Z. (2018). Neutrophil-based drug delivery systems. *Advanced materials*, **30,** 1706245.

191. Fuchs Y., & Steller H. (2011). Programmed cell death in animal development and disease. *Cell*, **147,** 742-758.

192. Friedlander R. M. (2003). Apoptosis and caspases in neurodegenerative diseases. *New england journal of medicine*, **348,** 1365-1375.

193. Benowitz L. I., He Z., & Goldberg J. L. (2017). Reaching the brain: advances in optic nerve regeneration. *Experimental neurology*, **287,** 365-373.

194. Forrester J., & Peters A. A. (1967). Nerve fibers in the optic nerve of rat. *Nature*.

195. Yu S., Tanabe T., & Yoshimura N. (2006). A rat model of glaucoma induced by episcleral vein ligation. *Experimental eye research*, **83,** 758-770.

196. Almasieh M., Wilson A. M., Morquette B., Vargas J. L. C., & Di Polo A. (2012). The molecular basis of retinal ganglion cell death in glaucoma. *Progress in retinal and eye research*, **31,** 152-181.

197. Rousseau V., & Sabel B. A. (2001). Restoration of vision IV: role of compensatory soma swelling of surviving retinal ganglion cells in recovery of vision after optic nerve crush. *Restorative neurology and neuroscience*, **18,** 177-189.

198. Yin H., Kanasty R. L., Eltoukhy A. A., Vegas A. J., Dorkin J. R., & Anderson D. G. (2014). Non-viral vectors for gene-based therapy. *Nature reviews genetics*, **15,** 541-555.

199. Mullard A. (2011). Gene therapies advance towards finish line. *Nature review drug discovery* **10,** 719–720

200. Gavrilov K., & Saltzman W. M. (2012). Therapeutic siRNA: principles, challenges, and strategies. *The Yale journal of biology and medicine*, **85,** 187.

201. Whitehead K. A., Langer R., & Anderson D. G. (2009). Knocking down barriers: advances in siRNA delivery. *Nature reviews drug discovery*, **8,** 129-138.

202. Setten R. L., Rossi J. J., & Han S. P. (2019). The current state and future directions of RNAi-based therapeutics. *Nature reviews drug discovery*, **18,** 421-446.

203. Lee J. M., Yoon T. J., & Cho Y. S. (2013). Recent developments in nanoparticle-based siRNA delivery for cancer therapy. *BioMed research international*.

204. Morrison C. (2018). Alnylam prepares to land first RNAi drug approval. *Nature review drug discovery* **17,** 156–157.

205. Pardridge W. M. (2020). Blood-brain barrier and delivery of protein and gene therapeutics to brain. *Frontiers in aging neuroscience*, **11,** 373.

206. Kreuter J. (2014). Drug delivery to the central nervous system by polymeric nanoparticles: what do we know?. *Advanced drug delivery reviews*, **71,** 2-14.

207. Godse R., Singh K., Shrivastava A., & Shinde U. (2016). Polymeric nanoparticulate systems: A potential approach for ocular drug delivery. In *Nano-biomaterials for ophthalmic drug delivery* (pp. 351-387). Springer, Cham.

208. Standard Operation Protocol "SOP-Intravitreal Injection". Institute of Medical Psychology, Otto von Guericke University.

209. Sautter J., Schwartz M., Duvdevani R., & Sabel B. A. (1991). GM1 ganglioside treatment reduces visual deficits after graded crush of the rat optic nerve. *Brain research*, **565,** 23-33.

210. Standard Operation Protocol "SOP-Optic Nerve Crush". Institute of Medical Psychology, Otto von Guericke University.

211. Tang Z. et al. (2011). An optic nerve crush injury murine model to study retinal ganglion cell survival. *Journal of visualized experiments*, **50,** e2685.

212. Chen Y. H., Keiser M. S., & Davidson B. L. (2018). Viral vectors for gene transfer. *Current protocols in mouse biology*, **8,** e58.

213. Bender H. R., Kane S., & Zabel M. D. (2016). Delivery of therapeutic siRNA to the CNS using cationic and anionic liposomes. *Journal of visualized experiments*, **113,** e54106.

214. Schneider T., Becker A., Ringe K., Reinhold A., Firsching R., & Sabel B. A. (2008). Brain tumor therapy by combined vaccination and antisense oligonucleotide delivery with nanoparticles. *Journal of neuroimmunology*, **195,** 21-27.

215. Zhang J., Li X., & Huang L. (2014). Non-viral nanocarriers for siRNA delivery in breast cancer. *Journal of controlled release*, **190,** 440-450.

216. Lam J. K., Chow M. Y., Zhang Y., & Leung S. W. (2015). siRNA versus miRNA as therapeutics for gene silencing. *Molecular therapy-nucleic acids*, **4,** e252.

217. Dowdy S. F. (2017). Overcoming cellular barriers for RNA therapeutics. *Nature biotechnology*, **35,** 222.

218. Duan J. et al. (2009). Cationic polybutyl cyanoacrylate nanoparticles for DNA delivery. *BioMed research international*.

219. Wittrup A., & Lieberman J. (2015). Knocking down disease: a progress report on siRNA therapeutics. *Nature reviews genetics*, **16,** 543-552.

220. Gupta R. B. (2006). Fundamentals of Drug Nanoparticles. In *Nanoparticle Technology for Drug Delivery*. (pp. 1-20). Taylor & Francis Group, New York.

221. Layzer J. M., McCaffrey A. P., Tanner A. K., Huang Z. A. N., Kay M. A., & Sullenger B. A. (2004). In vivo activity of nuclease-resistant siRNAs. *Rna*, **10,** 766-771.

222. Bien A., Seidenbecher C. I., böckers T. M., Sabel B. A., & Kreutz M. R. (1999). Apoptotic versus necrotic characteristics of retinal ganglion cell death after partial optic nerve injury. *Journal of neurotrauma*, **16,** 153-163.

223. Rousseau V., Engelmann R., & Sabel B. A. (1999). Restoration of vision III: soma swelling dynamics predicts neuronal death or survival after optic nerve crush: in vivo. *Neuroreport*, **10,** 3387-3391.

224. Guzman-Aranguez A., Loma P., & Pintor J. (2013). Small-interfering RNAs (siRNAs) as a promising tool for ocular therapy. *British journal of pharmacology*, **170,** 730-747.

225. Tham Y. C., Li X., Wong T. Y., Quigley H. A., Aung T., & Cheng C. Y. (2014). Global prevalence of glaucoma and projections of glaucoma burden through 2040: a systematic review and meta-analysis. *Ophthalmology*, **121,** 2081-2090.

226. Flammer J., Konieczka K., & Flammer A. J. (2013). The primary vascular dysregulation syndrome: implications for eye diseases. *EPMA Journal*, **4,** 14.

227. Petros R. A., & DeSimone J. M. (2010). Strategies in the design of nanoparticles for therapeutic applications. *Nature reviews drug discovery*, **9,** 615-627.

228. Srikanth M., & Kessler J. A. (2012). Nanotechnology—novel therapeutics for CNS disorders. *Nature reviews neurology*, **8,** 307.

229. Kesselheim A. S., Hwang T. J., & Franklin J. M. (2015). Two decades of new drug development for central nervous system disorders. *Nature review drug discovery*, **14,** 815–816.

230. Doshi N., Zahr A. S., Bhaskar S., Lahann J., & Mitragotri S. (2009). Red blood cell-mimicking synthetic biomaterial particles. *Proceedings of the national academy of sciences,* **106,** 21495-21499.

231. Han X., Wang C., & Liu Z. (2018). Red blood cells as smart delivery systems. *Bioconjugate chemistry*, **29,** 852-860.

232. Saxena A., Mozumdar S., & Johri A. K. (2006). Ultra-low sized cross-linked polyvinylpyrrolidone nanoparticles as non-viral vectors for in vivo gene delivery. *Biomaterials*, **27,** 5596-5602.

233. Eisenstein M. (2019). Pharma's roller-coaster relationship with RNA therapies. *Nature*, **574,** S4-S6.

234. Janas M. M. et al. (2018). Selection of GalNAc-conjugated siRNAs with limited off-target-driven rat hepatotoxicity. *Nature communications*, **9,** 1-10.

235. Cheng C. J., Tietjen G. T., Saucier-Sawyer J. K., & Saltzman W. M. (2015). A holistic approach to targeting disease with polymeric nanoparticles. *Nature reviews drug discovery*, **14,** 239-247.

236. Hayreh S. S. (2020). Controversies on neuroprotection therapy in non-arteritic anterior ischaemic optic neuropathy. *British journal of ophthalmology*, **104,** 153-156.

237. Vigneswara V., & Ahmed, Z. (2016). Long-term neuroprotection of retinal ganglion cells by inhibiting caspase-2. *Cell death discovery*, **2**, 1-1.

238. Larner S. F., McKinsey D. M., Hayes R. L., & W. Wang K. K. (2005). Caspase 7: increased expression and activation after traumatic brain injury in rats. *Journal of neurochemistry*, **94**, 97-108

8. Ehrenerklärung

Ich versichere hiermit, dass ich die vorliegende Arbeit ohne unzulässige Hilfe Dritter und ohne Benutzung anderer als der angegebenen Hilfsmittel angefertigt habe; verwendete fremde und eigene Quellen sind als solche kenntlich gemacht.

Ich habe insbesondere nicht wissentlich:

• Ergebnisse erfunden oder widersprüchlich Ergebnisse verschwiegen,

• statistische Verfahren absichtlich missbraucht, um Daten in ungerechtfertigter Weise zu interpretieren, • fremde Ergebnisse oder Veröffentlichungen plagiiert,

• fremde Forschungsergebnisse verzerrt wiedergegeben.

Mir ist bekannt, dass Verstöße gegen das Urheberrecht Unterlassungs- und Schadensersatzansprüche des Urhebers sowie eine strafrechtliche Ahndung durch die Strafverfolgungsbehörden begründen kann.

Ich erkläre mich damit einverstanden, dass die Arbeit ggf. mit Mitteln der elektronischen Datenverarbeitung auf Plagiate überprüft werden kann.

Die Arbeit wurde bisher weder im Inland noch im Ausland in gleicher oder ähnlicher Form als Dissertation eingereicht und ist als Ganzes auch noch nicht veröffentlicht.

Ort, Datum

Untershrift